University of Alberta

SI - HCCI Mode Switching Optimization Using a Physics Based Model

by

Michael Neil Schleppe

A thesis submitted to the Faculty of Graduate Studies and Research in partial fulfillment of the requirements for the degree of

Master of Science

Department of Mechanical Engineering

Fall 2011
Edmonton, Alberta

Examining Committee

Dr. C Robert Koch, Mechanical Engineering

Dr. Jason Olfert, Mechanical Engineering

Dr. David Checkel, Mechanical Engineering

Dr. Vinay Prasad, Chemical and Materials Engineering

Abstract

High efficiency and low NO_x emissions make Homogeneous Charge Compression Ignition (HCCI) promising for use in internal combustion engines. Combining HCCI with Spark Ignition (SI) allows for extension of the engine's operating range.

A Physics-based Mode Switch Model (PMSM) of SI-HCCI mode switches has been developed, which combines a single zone physics-based SI model with a single zone detailed chemistry HCCI model. The PMSM predicts the shape of IMEP and CA50 SI-HCCI mode switch responses for a single cylinder natural gas engine.

Sensitivities of work output and combustion timing are calculated with respect to input variables and model parameters. A mode switch profile allowing SI-HCCI mode switches while holding engine torque constant is achieved using an optimization process that considers only conventional actuators of intake pressure and fuel injector pulse width. A similar optimization process is used to further improve mode switches using intake temperature adjustment.

Acknowledgements

It is my wish to acknowledge and thank professors Dr. Bob Koch and Dr. David Checkel for their supervision, technical support, and financial support throughout the writing of this thesis. Their assistance has made my experience extremely rewarding.

Thank you to my friends and colleagues, Ahmad, Ali, Dan, Dallin, Darren, Jason, Masoud, Rouzbeh, and Tyler, among others, for their support, expertise, and frequent intellectual discussions. Without you, completion of this work would not have been possible.

I must also express my extreme gratitude to my parents Vickilynne and John Schleppe, siblings Caitlyn and Adam Schleppe, my close friend Lucie Cornish, as well as my extended family and friends for their encouragement, extensive support, and patience as I pursue this degree.

Table of Contents

List of Figures

List of Tables

Nomenclature

Greek Symbols

α	Woschni Heat Transfer Correlation Coefficient [-]
α_{M}	Coefficient of Third Body (M) Effects on Reaction Rates [-]
γ	Ratio of Specific Heats [-]
η_{v}	Volumetric Efficiency [-]
θ	Crank Angle [degrees]
θ_{spark}	Crank Angle of Spark Initiation [degrees]
λ	Lambda [-]
$\nu'_{k,i}$	Forward Reaction Coefficient of the k^{th} Species of the i^{th} Reaction [-]
$\nu''_{k,i}$	Reverse Reaction Coefficient of the k^{th} Species of the i^{th} Reaction [-]
ρ_{w}	Density of the Cylinder Wall [kg/m^3]
ρ_{cyl}	Density of the Cylinder Mixture [kg/m^3]
τ	Inverse of Characteristic Time Scale of Temperature Rise [s^{-1}]
ϕ	Equivalence Ratio [-]
$\dot{\omega}_{k,i}$	Production Rate of the k^{th} Species of the i^{th} Reaction [mol/s]
Γ	Cylinder Temperature Coefficient [-]
$\Delta\theta_{\mathrm{b}}$	Burn Duration [degrees]

Symbols

a	Wiebe Function Coefficient [-]
c_1	Woschni Heat Transfer Coefficient [-]
c_2	Woschni Heat Transfer Coefficient [m/s K]
c_p	Mass Specific Heat Evaluated at Constant Pressure [kJ/kg K]
$c_\mathrm{p,w}$	Mass Specific Heat Capacity of Cylinder Wall [kJ/kg K]
$\bar{c}_\mathrm{p}$	Molar Specific Heat Evaluated at Constant Pressure [kJ/kmol K]
c_v	Mass Specific Heat Evaluated at Constant Volume [kJ/kg K]
$\bar{c}_\mathrm{v}$	Molar Specific Heat Evaluated at Constant Volume [kJ/kmol K]
f	Effective Valve Area Coefficient [-]
h	Woschni Convective Heat Transfer Coefficient [W/m^2 K]
h_k	Mass Specific Enthalpy of Species k [kJ/kg]
k_w	Thermal Conductivity of the Cylinder Wall [W/m K]
l_c	Connecting Rod Length [m]
m	Wiebe Function Coefficient [-]
$m_\mathrm{air,th}$	Theoretical Mass of Air in Cylinder [g]
m_b	Mass of Cylinder Contents Burnt [g]
$\dot{m}_\mathrm{b}$	Mass Rate of Cylinder Contents Burnt [g/s]

m_{cyl}	Mass of Cylinder Contents [g]
$\dot{m}_{\text{cyl}}$	Rate of Change in Mass of Cylinder Contents [g/s]
m_{f}	Mass of Fuel [mg]
m_{ivc}	Mass of Cylinder Contents at Intake Valve Close [g]
r_{c}	Crank Radius [cm]
s_k	Mass Specific Entropy of Species k [kJ/kg K]
t_{spark}	Time of Spark Initiation [s]
u_k	Mass Specific Internal Energy of Species k [kJ/kg]
x_k	Mole Fraction of Species k [-]
$[x_k]$	Molar Concentration of Species k [-]
y_{b}	Mass Fraction Burned [-]
$\dot{y}_{\text{b}}$	Rate of Change in Mass Fraction of Burnt Cylinder Contents [s^{-1}]
y_k	Mass Fraction of Species k [-]
$\dot{y}_k$	Rate of Change in Mass Fraction of Species k [s^{-1}]
A_{cyl}	Total Internal Surface Area of the Cylinder [cm^2]
A_{v}	Effective Valve Area [cm^2]
A_{w}	Approximate Cylinder Wall Area [cm^2]
B_{cyl}	Cylinder Bore [cm]

C_{D}	Valve Discharge Coefficient [-]
$\mathrm{COV}_{\mathrm{IMEP}}$	Covariance in IMEP [-]
D_{v}	Valve Seat Diameter [cm]
H_k	Enthalpy of Species k [kJ]
L	Cylinder Stroke Length [cm]
L_{cyl}	Instantaneous Cylinder Height [cm]
L_{v}	Valve Lift [cm]
L_{w}	Cylinder Wall Thickness [cm]
M_k	Molecular Mass of Species k [kg/kmol]
N_s	Engine Rotational Speed [rpm]
P_{cyl}	Cylinder Pressure [bar]
P_{exh}	Exhaust Pressure [bar]
P_{int}	Intake Pressure [bar]
P_{ivc}	Cylinder Pressure at Intake Valve Close [bar]
P_{o}	Upstream Pressure [bar]
P_{r}	Restriction Pressure [bar]
Q_{wall}	Heat Transfer from Cylinder Wall to Mixture [J]
$\dot{Q}_{\mathrm{wall}}$	Rate of Heat Transfer from Cylinder Wall to Mixture [W]

R_i	Mass Average Specific Gas Constant of Component i [kJ/kg K]
R_{u}	Universal Gas Constant [kJ/kmol K]
S_k	Entropy of Species k [kJ/K]
S_{p}	Mean Piston Speed [m/s]
T_{cool}	Coolant Temperature [K]
T_{cyl}	Cylinder Temperature [K]
$\dot{T}_{\mathrm{cyl}}$	Rate of Change in Cylinder Temperature [K/s]
T_{exh}	Exhaust Air Temperature [K]
T_{int}	Intake Air Temperature [K]
T_{ivc}	Cylinder Temperature at Intake Valve Closing [K]
T_{o}	Upstream Temperature [K]
T_{react}	Cylinder Temperature Threshold for Chemical Kinetics [K]
T_{wall}	Cylinder Wall Temperature [K]
V_{c}	Cylinder Clearance Volume [cm^3]
V_{cyl}	Cylinder Volume [cm^3]
$\dot{V}_{\mathrm{cyl}}$	Rate of Change in Cylinder Volume [cm^3/s]
V_{d}	Displacement Volume [cm^3]
V_{f}	Volume of Fuel Injected [cm^3]
V_{ivc}	Cylinder Volume at Intake Valve Close [cm^3]
V_{ivo}	Cylinder Volume at Intake Valve Open [cm^3]

Abbreviations

AFR	Air to Fuel Ratio
CA50	Crank Angle at 50% Fuel Burned, Relative to Top Dead Center [degrees]
CAD	Crank Angle Degrees
CI	Compression Ignition
CN	Combustion Noise
CNG	Compressed Natural Gas
CR	Volumetric Compression Ratio
EGR	Exhaust Gas Recirculation or Exhaust Gas Residual
EVC	Exhaust Valve Closing [degrees]
EVO	Exhaust Valve Opening [degrees]
FTM	Fast Thermal Management
HCCI	Homogeneous Charge Compression Ignition
HCCI-SI	HCCI to SI Mode Switch
HV	Heating Value per Mass of Cylinder Contents [kJ/kg]
IMEP	Indicated Mean Effective Pressure [bar]
IVC	Intake Valve Closing [degrees]
IVO	Intake Valve Opening [degrees]

LHV	Lower Heating Value [kJ/kg]
NG	Natural Gas
PMSM	Physics Based Mode Switch Model
PW	Fuel Injector Pulse Width [ms]
ROPR	Maximum Rate of Pressure Rise in the Cylinder [bar/CAD]
SI	Spark Ignition
SI-HCCI	SI to HCCI Mode Switch
SI-HCCI-SI	SI to HCCI to SI Mode Switch
Stabilize	Cycles from Mode Switch Initiation until ROPR $<$ 10 bar/CAD
TDC	Top Dead Center on the Compression Stroke
aTDC	After Top Dead Center on the Compression Stroke
bTDC	Before Top Dead Center on the Compression Stroke
TRG	Trapped Residual Gases
CO	Carbon Monoxide
CO_2	Carbon Dioxide
UHC	Unburned Hydrocarbons
HC	Hydrocarbons
N_2	Nitrogen
NO_x	Oxides of Nitrogen
O_2	Oxygen

Chapter 1

Introduction

Presently fossil fuels remain one of the planet's most relied upon sources of chemical energy. In order to drive a car, turn on a light bulb, fly an airplane, or cook a dinner, one needs to harness energy in one form and often convert it to another form in order to produce useful work. An internal combustion engine is an example of one such device, where the chemical energy stored in chemical fuels is converted by combustion to hot gas products, which are expanded in a turbine or piston cylinder device to produce mechanical energy. In turn this mechanical energy is used to move a vehicle, operate a piece of machinery, or is further converted to electrical energy by a generator.

As a source of chemical energy, fossil fuels have often been relied upon because of their availability, ease of use, and high energy densities in terms of volume and mass when compared to other energy forms, such as electrically charged batteries. Recently much concern has arisen over the use of fossil fuels as a primary energy source due to increasing difficulty of extraction, environmental damage caused by production and transport, and the greenhouse gas carbon dioxide (CO_2) that is emitted during production and use. In 2009, more than 73% of Canada's 690 Mt of CO_2 equivalent emissions originated from the combustion of fossil fuels (Canada, 2011). Due to current interest in reducing the greenhouse gases emitted into the

environment, alternative energy sources are being considered for use in applications that traditionally relied upon fossil fuels.

Several other forms of energy have been studied and successful conversion to mechanical and electrical energy has been demonstrated. Some of these alternative sources of energy include solar, wind, hydro, fuel cells, and biofuels. While many of these energy sources show promise in producing "stationary" power (Ristinen and Kraushaar, 2006), the fact remains that the storage and conversion processes of these energy sources typically have poor efficiency and/or energy density in terms of storage volume or mass, which makes them ineffective in automotive applications (Stone, 1999). As suitable alternative energy sources are developed for automotive applications, fossil fuel internal combustion engines continue to be made more efficient.

Traditionally, automotive internal combustion engines use two different forms or "modes" of combustion. One such mode is Spark Ignition (SI), where a mixture of fuel and air is inducted into the engine cylinder where it is then ignited by a spark after compression. SI combustion often results in high peak temperatures and pressures and relatively stable combustion. The high temperatures in SI engines can result in increased pollutant emissions, namely oxides of nitrogen (NO_x) (Heywood, 1988). The other combustion mode that is traditionally used in internal combustion engines is Compression Ignition (CI). Often embodied as a Diesel engine, a CI engine involves air being inducted into the cylinder where fuel is injected and ignition is the result of auto-ignition due to high temperatures and pressures in regions with appropriate air to fuel ratios (AFR). CI combustion is easily controlled through the use of fuel injection timing and can be characterized by lower combustion temperatures and higher efficiency (Stone, 1999). Unfortunately the lower combustion temperatures of a CI engine and pockets of rich AFR mixture can result in high emissions of harmful particulate matter and unburned

hydrocarbons (Stone, 1999).

Homogeneous charge compression ignition (HCCI) is another form of combustion in an internal combustion engine, where a homogeneous mixture of fuel and air is inducted into the engine cylinder and is auto-ignited by compression of the mixture. HCCI combustion is typically done using lean mixtures of fuel and air, which results in lower combustion temperatures and thus lower concentrations of NO_x in the exhaust (Dahl et al., 2008; Yao et al., 2009). HCCI combustion can be used without intake throttling and at high compression ratios, which results in higher efficiency and, by the nature of thermal efficiency, lower power specific emissions of CO_2 (Jun and Lida, 2004; Stanglmaier and Roberts, 1999). HCCI combustion has a strong dependance on intake temperature, intake pressure, compression ratio, fuel chemistry, and a number of other factors. The complex interaction of these factors makes HCCI combustion timing difficult to predict and control (Stanglmaier and Roberts, 1999). As a form of compression ignition, HCCI is able to take advantage of high compression ratio engines for increased efficiency. HCCI engine operation is normally limited by misfire at low loads and knock at high loads (Atkins, 2004; Jun and Lida, 2004).

Many studies have been devoted to the development and control of HCCI combustion, but it remains difficult to use HCCI combustion for a wide range of loads such as those expected at start-up, idle, and high load operation (Jun and Lida, 2004). HCCI use is especially difficult in automotive applications where frequent variations in load are expected. Some researches have looked into expanding the utility of HCCI combustion by using HCCI for mid-load operation and then switching to another form of combustion, such as SI or traditional CI, for high-load and low-load operation (Cairns and Blaxill, 2005; Wang et al., 2004; Yao et al., 2009). Switching between combustion modes can be difficult and costly in terms of load fluctuations and emissions. While it is possible to control SI to HCCI to SI mode

switching (SI-HCCI-SI) using advanced actuators such as variable valve timing, modifying fuel chemistry, and exhaust gas recirculation (EGR), implementation of these actuators can be expensive and at present somewhat impractical in production engines. For these reasons mode switching using conventional actuators is desirable. Mode switching between HCCI and SI combustion modes in a methane fueled internal combustion engine for a stationary natural gas (NG) engine using only intake air throttling and AFR has been investigated by (Boddez, 2011).

1.1 Research Objective

In this study an existing physics-based numerical engine model is further developed to describe the processes occurring during a mode switch from SI to HCCI combustion. The development of a physics-based mode switch model (PMSM) provides a virtual test bed for designing mode switching procedures and control systems that is inexpensive to use compared to a real engine. In addition the PMSM provides physical insight into engine cycle details that would be extremely difficult to measure on a real engine.

Mode switching between SI and HCCI combustion modes allows for the expansion of the engine's operating range into high and very low loads where the HCCI combustion would normally not be stable. Since HCCI combustion is an auto-ignition process that depends on the conditions in the cylinder to initiate combustion (Stanglmaier and Roberts, 1999), cycle to cycle coupling must be accounted for to obtain a smooth mode switch. The PMSM is used to provide information about internal processes occurring during a mode switch so that ideal mode switching input profiles can be created. Engine performance indicators that are estimated by the PMSM include indicated mean effective pressure (IMEP), which is a measure of the work done by the engine normalized by the displacement volume, and combustion timing, reported as the crank angle at which 50% of the

fuel has been consumed (CA50). The PMSM is unable to estimate the level of knock as this would require a more computationally intensive model. The quality of each mode switch is assessed in part by the mode switch performance criterion (MSPC) developed by (Boddez, 2011), which attempts to quantify the quality of a mode switch in terms of: smoothness in IMEP transition, duration of the mode switch, and level of knock.

The PMSM provides a platform that can be used in the understanding of mode switches and the development of optimized mode switching profiles. By using physics-based models, it is possible to closely look at the physical processes that cause a particular mode switch to be successful or unsuccessful. This study investigates actuating smooth mode switches using conventional actuators of intake air pressure and fueling rate. Further improvement of the mode switches by adding variable intake air temperature actuation is also investigated.

1.2 Thesis Outline

This thesis is organized into 6 chapters. Chapters 1 and 2 introduce readers to SI and HCCI combustion, and provide motivation for mode-switching by outlining previous studies and contributions to this area of research in a literature survey. Chapter 3 contains a summary of the PMSM. In Chapter 4 validation of the PMSM using data from an experimental test engine setup is shown. An analysis of input sensitivities and mode switch optimization using conventional actuators and intake air temperature is presented and discussed in Chapter 5. This thesis is concluded in Chapter 6, where future research directions and applications are discussed. Four appendices provide readers with additional information about the PMSM development, operating conditions, model parameters, and model program functions.

Chapter 2

Literature Survey

2.1 SI Combustion

Spark ignition is a combustion mode commonly used in internal combustion engines. A typical four stroke SI engine has an intake stroke, compression stroke, expansion stroke, and exhaust stroke. Usually the intake stroke involves a well mixed, close to stoichiometric, fuel and air mixture being inducted into the engine cylinder. This mixture is compressed in the cylinder by a piston and then at close to the minimum cylinder volume, or piston top dead center (TDC), the mixture is ignited by the discharge of a spark from a spark plug inserted into the cylinder. The resulting flame propagates from the ignition point at the spark plug through the engine cylinder until the fuel is consumed. Oxidation of the fuel results in a conversion of fuel and air reactants to products that exist at a much higher temperature than the reactants. This chemical conversion is characterized by a large heat release that causes an increase in mixture temperature and pressure. The cylinder then begins the expansion stroke where the hot gases expand, pushing the piston down, resulting in net work being produced (Heywood, 1988). Then the exhaust valve opens with the piston at the bottom of the cylinder and the remaining hot gases are exhausted to the atmosphere as the piston moves up.

As a result of the wide spread use of SI engines, they have been extensively

studied. Initial studies were often experimental in nature, where researchers would manually vary operating conditions to study SI operating range and performance characteristics. These studies often took a phenomenological view of the engine cycle, mapping parameters such as cylinder pressure, exhaust temperature, or observing combustion processes by employing optical cylinder heads and transparent cylinder walls. With advances in computer technology it has become increasingly practical to study SI engines using numerical models, the computers allowing researchers to simultaneously solve the several interdependent non-linear differential equations that describe SI engine physics (Yao et al., 2009).

2.1.1 SI Models

A simple form of SI engine model is the mean value model, where many of the complicated aspects of an SI engine cycle are lumped together into a simplified physically based model. Many examples of mean value engine models with varying levels of detail and accuracy exist including (Chevalier et al., 2000; Fekete et al., 1995; Hendricks, 1989; Hendricks and Vesterholm, 1992; Heywood, 1988; Ramos, 1989). One model offers a predictive look at SI engine performance characteristics by simulating a two zone system where the physics of the unburned and burned gases are considered separately (Bade Shrestha and Karim, 1999). (Coppin et al., 2010) uses a mean value engine model as the basis for a study on the effects of using gasoline-ethanol blends in an SI engine. Developments in computer technology have made it possible for more complicated engine models to be simulated. As early as 1986 a multidimensional fluid dynamic model was used to describe the combustion process in an SI engine (Amelio et al., 1986).

The mean value engine model has remained popular in recent years due to its simplicity and fast run times. While some mean value models lump many of the engine processes together, a detailed single zone model of the form presented in

(Heywood, 1988) and (Ramos, 1989), models engine processes on a crank angle degree basis. With these models each of the steps in an engine cycle or "strokes" are modeled separately using different sets of differential equations to describe the engine physics.

2.1.2 SI Engine Control

Combustion timing and load in an SI engine can be controlled by a number of actuators: spark timing, valve timing, fuel and air ratio, intake heating, supercharging, turbo-charging, fuel stratification, or recirculating external exhaust gases. Some methods for reducing harmful exhaust emissions and changing the engine power output involve detailed cylinder geometry design to increase turbulence and optimize flame propagation (Heywood, 1988). The primary focus of this study is optimization of mode switches from SI combustion through the use of conventional actuators, such as varying intake pressure with an electronic throttle valve and varying the AFR.

2.1.3 Benefits and Limitations of SI Combustion

The advantages of using a spark ignition engine are demonstrated by comparing an SI engine to its common alternative, the Diesel engine. Advantages include better power to weight ratios and reliable combustion timing (Heywood, 1988). High peak pressures created by the combustion of a well mixed stoichiometric air and fuel mixture at near constant volume results in high power output given the mass of the cylinder mixture. The power output of a spark ignition engine can be controlled by changing the amount of fuel and air that is inducted into the cylinder during the intake stroke. The fuel and air mixture in an SI engine is often premixed, resulting in relatively complete combustion with high hot gas temperatures leading to low emissions of particulate matter (PM) and unburned hydrocarbons (UHC).

Combustion in an SI engine is often optimized by creating in-cylinder turbulence, tuning the spark timing, and varying the amounts of both internal and external exhaust gas residuals (EGR).

With the benefits of SI combustion, in terms of power and ease of setting combustion timing, there are also some drawbacks to this type of combustion. The high load operation of SI engines is limited by a phenomenon known as knock. For an SI engine knock is defined as a portion of the cylinder mixture auto-igniting outside of the normal flame front (Stone, 1999). This auto-ignition results in a high frequency oscillation within the cylinder causing a loud"knocking" sound (Heywood, 1988; Stone, 1999). Other problems associated with engine knock include a large rise in peak cylinder pressure and a disruption of the boundary layer on the cylinder wall that causes greatly increased heat transfer rates. The tendency for knock to occur depends on the type of fuel used in the engine. The fuel octane number is a measure of the auto-ignition properties of a fuel; higher octane number fuels delay auto-ignition and can be used to reduce knock. Engine knock can cause significant damage to an engine and hinder its performance. Knock limits the maximum compression ratio that can be used in an SI engine, thus resulting in lower thermal efficiencies than could be achieved at higher compression ratios (Stone, 1999).

Another disadvantage of spark ignition engines is the NO_x emissions that are produced as a result of high temperature combustion both globally and in localized high temperature regions due to imperfect mixing (Heywood, 1988). Typical NO_x emissions of SI engines are on the order of 500 - 1000 ppm (Heywood, 1988) compared with NO_x emissions that are 10 to 40 times lower for HCCI combustion (Lavy et al., 2000). NO_x emissions can be limited by increasing the large scale turbulence in the cylinder, which improves the mixing of fuel and air, and by exhaust after-treatment in a catalytic converter.

SI engines also exhibit reduced performance and efficiency when operating at

part loads. As discussed above, to achieve part load in an SI engine the amount of fuel and air inducted into the cylinder is limited by throttling the intake mixture. The use of a throttle results in pumping losses in the system which ultimately leads to a reduction in overall efficiency.

2.1.4 Natural Gas SI

Natural gas (NG) as a fuel for SI combustion engines is promising in terms of knock resistance and reduced carbon dioxide emissions (Cho and He, 2007). Natural gas, which is primarily composed of methane, has an octane number close to 120 (Stone, 1999). For this reason natural gas can be used in SI engines with high compression ratios, resulting in higher thermodynamic efficiencies. Natural gas engines have the ability to run on lean fuel and air mixtures and with high levels of exhaust gas recirculation allowing for reduced emissions of NO_x and PM when compared to gasoline SI engines. One drawback of the natural gas SI engines is that compressed natural gas (primarily methane at 200 atm) has a fuel energy density of 8.1 MJ/L compared to gasoline's energy density of 31.9 MJ/L (Cengel and Boles, 2006). The low energy density of natural gas necessitates the use of high volume, high pressure, storage units accommodate the same fuel energy as a liquid fuel such as gasoline. Similarly, the low energy density of natural gas results in a low fuel and air mixture energy density, thus superchargers or bigger engine displacement volumes are required to meet high load demands for similar power outputs to gasoline SI engines. This can result in reduced overall engine efficiency when operating at higher loads (Cho and He, 2007). The need for a high volume or high pressure fuel storage unit for natural gas is a factor that limits its use in automotive applications. The 2011 price for natural gas is 3.39 $/GJ (Government of Alberta, 2011) compared to approximately 37.0 $/GJ for gasoline (AlbertaGasPrices.com, 2011; Cengel and Boles, 2006), making natural gas an attractive fuel for stationary

engine applications where natural gas storage and engine size is less of a concern.

2.2 HCCI Combustion

HCCI combustion is a form of compression ignition combustion that occurs in an internal combustion engine when a homogeneous mixture of fuel and air is compressed until cylinder conditions are favorable for auto-ignition of the mixture. One of the first observations of HCCI combustion was by (Onishi et al., 1979), known at that time as Active Thermo-Atmosphere Combustion (ATAC). (Onishi et al., 1979) observed that lean auto-ignition cycles in a two stroke engine without the use of a spark, formerly considered to be "run-on" cycles, could be reliably controlled in a small operating window. HCCI combustion in a four-stroke engine could be further controlled by the reintroduction of exhaust gas to the intake mixture (Najt and Foster, 1983). Before the 1990's few studies of HCCI combustion were conducted. In the 1990's a renewed interest in increasing engine efficiency and lowering NO_x emissions resulted in numerous studies on HCCI (Yao et al., 2009).

In HCCI combustion auto-ignition occurs at several points in the cylinder simultaneously, resulting in a fast reaction with short combustion duration characterized by a sharp rise in cylinder pressure (Berntsson and Denbratt, 2007b; Stanglmaier and Roberts, 1999). HCCI combustion is dependant on in-cylinder conditions and is therefore influenced by several variables including but not limited to: auto-ignition properties of the fuel, fuel concentration, residual amount, residual reactivity, mixture homogeneity, compression ratio, intake temperature, latent heat of vaporization of the fuel, engine temperature, and heat transfer to the engine (Stanglmaier and Roberts, 1999).

A need for high efficiency clean burning internal combustion engines has arisen as a result of legislation in both North America and in Europe, such as the Canadian Environmental Protection Act 1999 (CEPA 1999) regulating fuel quality and

emissions that can be produced by an engine, increased green house gas awareness, and high fuel prices. HCCI combustion exhibits high efficiency and low emissions, making it an excellent candidate for meeting these needs (Jun and Lida, 2004; Stanglmaier and Roberts, 1999). The main barriers to the use of HCCI combustion include control of the combustion phasing, extending the operating range, high unburned hydrocarbon and carbon monoxide (CO) emissions, operation during cold start, and homogeneous mixture preparation (Yao et al., 2009).

2.2.1 Benefits of HCCI Combustion

There are a number of benefits associated with the use of HCCI combustion in internal combustion engines. HCCI is a type of compression ignition and is therefore limited by knock in terms of rate of pressure rise rather than by auto-ignition properties like in SI combustion (Atkins, 2004). The lean mixture combustion at high compression ratios results in HCCI combustion having similar thermal efficiency to traditional CI engines, which is higher than efficiencies typically found in SI engines, especially at part loads (Jun and Lida, 2004; Stanglmaier and Roberts, 1999). The homogeneous nature of the combustion reaction, with the lean mixture simultaneously igniting throughout the entire cylinder, results in well distributed low temperature ignition points. The level of homogeneity in the mixture and the lower combustion temperatures in HCCI engines results in relatively lower NO_x emissions and PM emissions than in conventional CI engines and lower NO_x emissions than in SI engines (Dahl et al., 2008; Yao et al., 2009).

2.2.2 Limitations of HCCI Combustion

Despite the benefits of HCCI combustion, there are still a number of challenges that limit the use of HCCI combustion in production engines. As stated above, HCCI combustion depends on a number of interacting operating characteristics

that influence the chemical kinetics of the system. Combustion phasing in HCCI engines is difficult to control because of the absence of a direct ignition control such as a spark in SI combustion or fuel injection in Diesel combustion. Inability to control the combustion phasing in HCCI combustion can result in unstable combustion, which can lead to misfire, knock and unacceptable fluctuations in IMEP. As a result the operating range of HCCI combustion is narrow in most engines. For liquid fuels, fuel wall wetting and relatively low combustion gas temperatures observed in homogeneous auto-ignition leads to relatively large amounts of fuel left un-ignited in cylinder crevices and areas with high rates of heat transfer cooling the charge (Yao et al., 2009). These unburned hydrocarbons are often observed in emissions from HCCI engines (Christensen and Johansson, 1998). The low exhaust temperature of HCCI combustion can also result in difficulty treating unburned hydrocarbons using a catalyst (Shahbakhti et al., 2010). High load and high speed operation also presents problems for HCCI combustion. Load is increased in HCCI combustion by increasing the amount of fuel inducted into the cylinder. More fuel normally results in faster combustion chemistry and unacceptably high rates of pressure rise that can damage the engine (Atkins, 2004). Instabilities can exist at high speeds, where the rates of heat transfer and limited time for auto-ignition result in misfires occurring (Shibata et al., 2004).

Table 2.1 summarizes the performance of SI, conventional CI, and HCCI combustion modes in terms of the criteria discussed for each mode above. Values in Table 2.1 are approximate and the thermal efficiencies are calculated based on compression ratio, with a cut-off ratio of 1 for the CI modes, thus actual thermal efficiencies will likely be lower (Cengel and Boles, 2006). While a typical HCCI cycle will have a cut-off ratio close to 1, a typical CI cycle will have a cut-off ratio greater than 1 resulting in lower thermal efficiency (Cengel and Boles, 2006).

Table 2.1: Summary of Combustion Mode Benefits and Limitations (Atkins, 2004; Cengel and Boles, 2006; Lavy et al., 2000; Heywood, 1988; Shahbakhti et al., 2010; Stone, 1999)

Criteria	**SI**	**CI**	**HCCI**
Compression Ratio	8 - 10	17 - 23	17 - 23
Fuel Octane Rating	83 - 100	0 - 25	Based on Engine
Fuel Cetane Rating	< 40	40 - 55	Based on Engine
Typical Equivalence Ratio	1.0	0.6 - 0.8	0.4 - 0.7
NO_x (ppm)	500 - 1000	500 - 1000	10 - 100
Max IMEP (bar)	7 - 10	5 - 7.5	4 - 9
Max η_{th} (%)	52 - 55	63 - 67	63 - 67
Combustion Timing Control	Spark	Injection	None

2.3 Control of HCCI Combustion

Several strategies have been investigated, with varying levels of success, for controlling HCCI combustion and extending the load range. Most of these strategies can be divided into the broad categories of: mixture dilution, modifying fuel properties, fast thermal management, and in-cylinder direct fuel injection. Many studies investigating HCCI control employ more than one actuator due to the complicated and highly coupled nature of the HCCI combustion problem.

2.3.1 Control of HCCI using Mixture Dilution

One approach to HCCI combustion phasing control is to advance or retard combustion timing by diluting the cylinder mixture. (Najt and Foster, 1983) showed that HCCI combustion in a four stroke engine could be controlled by introducing recirculated exhaust gas into the cylinder intake mixture. (Christensen and Johansson, 1998) showed combustion timing to be slower with higher amounts of EGR. One way of introducing exhaust gases to a cylinder mixture is through external exhaust gas recirculation where the exhaust gases are physically re-routed to the intake and injected into the intake stream with the fresh air and fuel mixture. A second way

of re-introducing exhaust gases is through internal exhaust gas recirculation where the amount of exhaust gas residual in the cylinder is varied by changing the timing of the intake and exhaust valve's opening and closing events.

External exhaust gas recirculation has been investigated by (Atkins and Koch, 2005), (Christensen and Johansson, 2000), and (Morimoto et al., 2001). In these studies external cooled EGR was used to control combustion phasing and extend the load range of an HCCI engine. (Christensen and Johansson, 2000) observed that the upper load limit of a supercharged HCCI engine could be increased to an IMEP of 16 bar through the addition of approximately 50% EGR to the intake mixture, which retarded combustion and avoided knock. (Atkins and Koch, 2005) also observed that diluting the intake mixture using EGR is effective in retarding SOC timing. Similarly the introduction of EGR of around 62% resulted in increasing maximum gross efficiency to 51%, much higher than that which could be achieved in an SI engine. Similar results were found in (Morimoto et al., 2001) using a Natural Gas fueled engine, also concluding that the total hydrocarbon emissions were reduced at higher loads with the introduction of EGR. While external EGR is promising for load range and combustion phasing improvement, some drawbacks still exist. To allow for the recirculation of the exhaust gas into the intake mixture the exhaust manifold pressure has to be increased to a level over that of the intake manifold pressure. This pressure increase is often achieved by throttling the exhaust manifold, which can result in higher pumping losses and thus an overall lower net efficiency of the engine (Christensen and Johansson, 2000). Efficiency losses are also seen as a result of the need to cool the exhaust gases before re-induction to prevent early auto-ignition (Christensen and Johansson, 2000).

Internal exhaust gas recirculation is another promising method for achieving stable HCCI combustion. By changing the valve timing of the engine the amount of trapped residual gases (TRG) in the cylinder can be changed, thereby chang-

ing the temperature, pressure, and composition of the cylinder mixture at IVC. (Law et al., 2000) found that it was possible to change the amount of internal EGR by varying valve timing, which in turn allows for control of combustion phasing of HCCI combustion. (Milovanovic et al., 2004) studied the influence of a fully variable valve timing (FVVT) strategy on the control of a gasoline HCCI engine and found that EVC and IVO timing have the greatest impact on the ability to control HCCI combustion timing. EVO and IVC timing were found to have little effect on HCCI combustion phasing control. (Cairns and Blaxill, 2005) combined the concepts of internal and external EGR to extend the load range of a multi-cylinder gasoline HCCI engine while avoiding knock. It was also found that this combined EGR scheme could be used to facilitate a smooth transition between controlled auto-ignition (or HCCI) and SI modes, utilizing a hybrid combustion technique expanding the engine's operating range. A different take on FVVT control of HCCI combustion was seen in (Urata et al., 2004) where a combination of direct injection, FVVT with an electromagnetic valve train, and intake boost was used to control HCCI. (Urata et al., 2004) hypothesized that injecting a small amount of fuel during negative valve overlap would allow unburned hydrocarbons in the internal residual to react, which could facilitate compression ignition during the following cycle. While using internal EGR is promising for extending the load range and achieving the benefits of low NO_x operation in gasoline engines, the same cannot be said for natural gas HCCI engines. It was found that due to the energy requirements for NG auto-ignition, intake heating and high compression ratios are required to achieve auto-ignition in the NG HCCI engine (Yap et al., 2004). Internal EGR has potential to reduce the intake heating requirement for NG combustion, but because of the high compression ratios necessary to achieve auto-ignition the amount of internal EGR available for mixture dilution was significantly reduced (Yap et al., 2004). As well high combustion temperatures from NG

HCCI combustion can lead to significantly higher NO_x emissions when compared to a gasoline HCCI engines (Yap et al., 2004). (Kawasaki et al., 2006) addressed some of these problems by experimenting with the opening of the intake valve a small amount during the exhaust stroke. This "pilot opening" allows for exhaust gases to be pulled into the intake manifold, thus heating the intake mixture and increasing the total amount of internal EGR.

2.3.2 Control of HCCI by Changing Fuel Properties

Changing fuel properties of the cylinder mixture is a method that can be used for HCCI control (Atkins, 2004). The time and conditions needed for auto-ignition vary between fuels, so combustion timing can be controlled and the operating range can be expanded by varying the fuel properties in an HCCI engine. (Shibata et al., 2004) conducted a study on the effects of fuel properties on HCCI engine performance. In the study fuels with different octane numbers were used in a four cylinder engine. The resulting low temperature heat release (LTHR) and high temperature heat release (HTHR) values varied with fuel composition. The low temperature chemical kinetics during LTHR as well as the "negative temperature coefficient regime between LTHR and HTHR have been observed to have a large impact on HCCI combustion (Stanglmaier et al., 2001). (Berntsson and Denbratt, 2007a; Dec and Sjoberg, 2004) found that a large amount of fuel stratification can lead to retarded ignition timing, which provides an additional actuator for control; however, too much stratification can ultimately lead to unstable combustion.

Dual fuel usage is a method that can be used to actively vary the fuel octane number by mixing a fuel with a high octane number and a fuel with a low octane number to create a fuel mixture with an intermediate octane number. The effects of different primary reference fuel blends on HCCI operating range, start of combustion, burn duration, IMEP, indicated specific emissions, and indicated

specific fuel consumption were investigated by (Atkins and Koch, 2005) who found that by changing the fuel octane number the HCCI operating range could be expanded. (Lupul, 2008) showed that mode switching between SI and HCCI combustion modes can be controlled by varying octane number. (Stanglmaier et al., 2001) found that HCCI combustion timing could be controlled by mixing Fischer Tropsch (FT) Naptha with NG in an NG HCCI engine, allowing for optimization of efficiency and NO_x emissions at part loads. (Strandh et al., 2004) designed a PID controller and a model based linear quadratic Gaussian controller to establish cycle-by-cycle ignition timing control of a engine using blends of ethanol and a 50/50 mixture of n-heptane and ethanol. In an expanded study of HCCI control (Wilhelmsson et al., 2007) uses dual fuels, NG and n-heptane, and a variable geometry turbocharger to develop an operational scheme in a NG engine by adding the lowest possible boost pressure to reduce pumping losses and minimize NO_x emissions. (Saanum et al., 2008) found that HCCI control is possible using a mixture of hydrogen enriched NG and diesel fuel. Significant research exists on the addition of reformer gas to fuels of various compositions to control HCCI combustion, which is interesting because of the ability to produce reformer gas from other fuels, effectively eliminating the need for two separate fuel sources. Experimental work in this area has been completed by (Hosseini and Checkel, 2006, 2007b,a, 2008), and numerical work by (Kongsereeparp and Checkel, 2008a,b).

2.3.3 Control of HCCI using Fast Thermal Management

Fast Thermal Management (FTM) is a method of control that involves quickly changing the temperature of intake air to control combustion phasing. Some studies have suggested that HCCI combustion timing is sensitive to intake air temperature (Christensen and Johansson, 1998, 1999). (Haraldsson et al., 2004; Yang et al., 2002) suggested the use of recovered heat from exhaust gases to heat

one of two intake air streams. By using two air streams, one heated by exhaust gases and the other direct from atmosphere, each controlled with independent throttles, the temperature of the final intake air stream can be controlled by mixing the two streams (Haraldsson et al., 2004; Yang et al., 2002). Both studies observed the ability of the FTM system to control the combustion phasing of HCCI combustion. The study by (Yang et al., 2002) indicates that while FTM is effective at controlling combustion phasing in HCCI engines, the "thermal inertia" of the system makes cycle by cycle temperature adjustment difficult, which in turn complicates the control of HCCI combustion during transients (Yang et al., 2002). This lag in achieving the desired HCCI combustion phasing was also observed by (Haraldsson et al., 2004), although in that study FTM was presented as an acceptable alternative to using variable compression ratio in closed loop control of HCCI combustion.

2.3.4 Control of HCCI using Direct Injection

Injecting fuel into the cylinder at different stages of the engine cycle allows HCCI combustion timing to be advanced by improving mixture ignitability (Handford, 2009) or retarded by increasing fuel stratification (Su et al., 2007), creating the possibility of expanding the low and high load operating limits. (Handford, 2009) demonstrated the advance of combustion timing in a natural gas fueled HCCI engine by injecting n-heptane directly into the cylinder. (Urushihara et al., 2003) found that a small injection of fuel during the NVO interval and a second injection during the intake stroke resulted in internal fuel reformation, which improved the ignitability of the cylinder mixture. (Dec and Sjoberg, 2003) found that direct injection of fuel early in the intake stroke produced near identical results to a premixed charge. However, injection close to TDC improved the combustion efficiency of very low fuel load mixtures ($\phi < 0.2$). Numerical models by (Stralin et al., 2003; Su et al., 2007) found that fuel stratification caused by injection of fuel around

TDC resulted in pockets of rich fuel and air mixture, which promoted ignitability. Overall fuel stratification extended the combustion duration helping to avoid knock, thus extending the operating range of the engine. A numerical study by (Gong et al., 2002) showed that power density of an HCCI engine could be improved by the injection of a small amount of diesel fuel during the compression stroke of the engine. This pilot fuel injection also decreased the sensitivity of the HCCI combustion to intake conditions. Direct injection can be a good way to control HCCI combustion, but it depends heavily on the type of fuel and the timing of the direct injection. (Wagner et al., 2003) demonstrates that it would not be possible to use n-heptane as a port injection fuel for HCCI and instead a carefully timed n-heptane direct cylinder injection is used to avoid wall impingement and utilize the benefits of HCCI combustion. (Helmantel and Denbratt, 2004) uses a multiple injection scheme of n-heptane to allow for sufficient mixing to operate a conventional diesel common passenger rail car engine with HCCI combustion.

2.4 HCCI Engine Modeling

Many different types of HCCI models exist, with varying levels of complexity. The simplest form of HCCI model is a single zone mean value engine model with lumped chemistry approximating combustion as a one step reaction such as that used in (Shahbakhti and Koch, 2010), (Olsson et al., 2000), and (Roelle et al., 2004). To obtain a more accurate estimate of ignition timing for HCCI combustion a single zone model with detailed chemical kinetics is used, such as (Kirchen et al., 2007) or (Kongsereeparp, 2008). (Aleiferis et al., 2005) used a similar detailed chemistry model based on CHEMKIN II chemical kinetics algorithms, but without a heat transfer model, which decreased the accuracy of calculated ignition timing. The problem with a single zone combustion model is that it considers only one zone of perfectly homogenous mixture in the cylinder despite the fact that spatial vari-

ances in the AFR, temperature, and heat transfer rates can affect the resulting chemical kinetics and combustion duration. For this reason multi-zone models with detailed chemical kinetics have been developed to study HCCI combustion, such as (Tzanetakis et al., 2010) or (Kongsereeparp, 2008). To establish the effects of phenomenon such as fuel stratification, intake swirl, EGR distribution, and gas dynamics, a level of detail can be added to HCCI detailed chemistry models by considering three dimensional fluid dynamics using computational fluid dynamic models, such as (Wang et al., 2004) or (Tominaga et al., 2004). (Xu et al., 2005) compares the simulation of an HCCI engine using a single zone model with detailed chemical kinetics to a multi-zone model with detailed chemical kinetics and a 1D fluid flow model. If the mixture in the cylinder is somewhat uniform in nature then a single zone model is sufficient for calculating the auto-ignition timing (Xu et al., 2005). If fuel stratification or NVO is introduced a multi-zone model is required for an accurate description of the HCCI combustion process (Xu et al., 2005). These results are supported by (Kirchen et al., 2007) who found that a single zone model was sufficient for calculating ignition timing, but was not able to adequately predict post-ignition phenomena such as emissions, peak combustion pressure, or combustion duration. The variation in auto-ignition timing predictions between single zone and multi-zone models is largely dependent on the cylinder temperature distribution. (Xu et al., 2005) also found that the multi-zone model is more suited for comparing simulated data to experimental data, while the single-zone model is useful for rapid parametric studies such as those used for investigating the effect of fuel properties and operating conditions on the trends of engine combustion timing. The choice of a single zone model over a multi-zone model for this study is based largely on the much shorter computational time required to simulate a combustion cycle using a single zone detailed chemical kinetics model, as well as the single zone model's ability to adequately predict ignition timing (Kirchen et al., 2007). Where

the computational time of a single zone HCCI model with detailed chemistry in this study is approximately 30 seconds on a current PC, simulation of a multi-zone model with full thermodynamic coupling can take several hours (Kongsereeparp, 2008).

2.5 Natural Gas HCCI

Natural gas as a fuel offers a high mass energy density and low cost, and its gas phase makes preparation of a homogeneous mixture relatively easy. Due to auto-ignition properties natural gas requires high compression ratios in HCCI applications, which results in higher combustion efficiency, but also higher combustion temperatures and peak pressures. As an alternative to high compression ratios, intake heating can be used to promote auto-ignition of natural gas (Olsson et al., 2002). However, this also results in higher combustion temperatures, which can cause higher NO_x emissions. (Jun and Lida, 2004) investigated the operating conditions required for high efficiency, low CO emissions in a four-stroke NG HCCI engine. It was found, similar to results of studies of PRF fuels by (Atkins, 2004), that the HCCI operating region of a NG engine is restricted at low load by misfiring and high load by early combustion, causing engine knock (Jun and Lida, 2004). (Jun and Lida, 2004) also presents a common trade-off in NG HCCI combustion, the combustion efficiency is maximized and CO emissions are minimized when combustion peak temperatures are over 1500 K; however, when temperatures are over 1800 K NO_x starts to increase. Another limitation of NG HCCI combustion, presented earlier in section 2.3.1, is the limited ability to using internal EGR at high compression ratios, one of the principle methods for HCCI control. Some methods to control NG HCCI combustion include: suppling external EGR at the cost of some pumping losses, boosting intake pressure, and increasing intake temperature to allow the use of lower compression ratios. Unfortunately these methods of im-

proving NG HCCI combustion all contribute to overall cycle efficiency reduction. Dual fuels or additives such as reformer gas can be used to control NG HCCI combustion (Kongsereeparp and Checkel, 2008a), but this adds a high degree of complexity to the fueling system.

2.6 Mode Switching

Many of the studies of HCCI combustion presented above, including (Cairns and Blaxill, 2005), (Yao et al., 2009), and (Wang et al., 2005), suggest that switching between HCCI combustion mode at part load and SI or CI combustion mode at low and high loads, expands the load range of an HCCI engine. The part load benefits of HCCI, such as increased efficiency and ultra-low NO_x emission, are realized while the inherent problems with NG HCCI combustion are avoided at high loads and low loads through the use of another combustion mode. The choice of the alternative mode, SI or CI, depends on the type of engine and fuel that is being used for HCCI. Engines with low compression ratios or fuels with high octane numbers would be more suited to switching to SI combustion, whereas engines with high compression ratios and fuels with low octane numbers or high centane numbers, which already employ direct injection, may be more suited to switching to CI (diesel) combustion.

2.6.1 Experimental Mode-Switching

A number of studies have experimentally investigated mode switching to and from SI and HCCI modes. (Wang et al., 2005) takes a look at the effects of using SI and fuel stratification to control HCCI combustion with fuel injection. An engine operating in HCCI mode at low loads and part loads and in SI mode at higher loads is used to study the performance characteristics and emissions of each combustion mode, as well as the switches between the modes. (Wang et al., 2005) found that

HCCI combustion exhibited advantages over SI combustion mode in terms of lower NO_x emissions and lower indicated specific fuel consumption. It was also shown that during the transition between modes the use of spark assisted HCCI and direct fuel injection allowed the HCCI combustion to be controlled and stabilized (Wang et al., 2005). (Lupul, 2008) demonstrated mode switches on a single cylinder test engine with low ON fuels from SI mode to HCCI mode, demonstrating similar levels of CO and UHCs and much lower NO_x emissions in HCCI mode than in SI mode. A study by (Kuzuyama et al., 2007) involved three separate experiments with regards to HCCI operating range and HCCI-SI mode switching. In the first experiment methane fueled HCCI was achieved with some consistency without intake air heating through the use of external EGR and turbo-charging. At higher engine speeds stable combustion could be achieved by increasing the amount fuel in the mixture; however, this resulted in unacceptable levels of engine knock. Retarding combustion timing fixed the knock levels, but often resulted in misfire cycles. In the second experiment a CFD simulation showed that the presence of a local hot spot in the cylinder resulted in higher HCCI combustion stability with acceptable levels of combustion noise. The final experiment showed that mode switching between SI and HCCI, allowed stable transitions to be achieved with minimal misfires and acceptable knock with the use of variable intake pressure, fueling control, and variable valve timing during the switch. The variable valve timing focused primarily on EVC, which allowed for variation in the amount internal EGR (Kuzuyama et al., 2007).

Some studies have looked for strategies to improve the performance of engines switching between HCCI combustion and SI combustion modes using a number of increasingly complicated actuators. (Milovanovic et al., 2005) developed a strategy for mode switching by coordinating trapped residual gas rates, intake throttle position, fueling rates, and spark timing. These parameters are shown to have a large

impact on the quality of the transition from one mode to the next and therefore require different controlling parameters for different speeds and loads. While the transition from SI to HCCI was found to be smooth the reverse transition from HCCI to SI was found to result in some misfires. Weak and unstable combustion was often observed during the mode transitions resulting in higher levels of knock compared to steady state SI and HCCI combustion.

(Tian et al., 2007) experimentally investigated SI-HCCI mode switching by adjusting valve timing to achieve negative valve overlap and implementing a gasoline direct injection strategy. A smooth transition was realized in one cycle, the entire process including throttle action spanned 10 cycles. The mode switch was also modeled using a numerical model coupled with BOOST and CHEMKIN software to optimize fuel injection strategies during the switch. A similar study by (Kakuya et al., 2008) investigated strategies for mode switching from SI to HCCI. The strategy involved closely controlling the AFR and the internal EGR by coordinating valve timing and intake throttle position, in addition to an advance in spark timing and double fuel injection to stabilize combustion. Mode switches performed with only one actuator could not produce switches without fluctuations. (Wu et al., 2010) conducted a study with the objective of investigating load fluctuations during the mode switch and developing a control method to minimize the fluctuations. Experimental investigation showed that a slow change in intake manifold air pressure causes AFR and TRG fluctuations during the switch, which in turn results in load fluctuations. Cylinder to cylinder differences in AFR and TRG prompt the need for individual cylinder injection and valve timing control. Results on the test engine showed that through careful optimization of VVT, throttle angle, and fueling, a smooth mode switch with little variance in IMEP over the transition could be achieved (Wu et al., 2010).

Some experimental work has also gone into investigating the types of hybrid

combustion that occur when the spark is extended past the mode switch actuation to avoid misfire in the first few HCCI cycles. (Chen et al., 2011) developed a strategy to allow for the operation of an HCCI-SI multi-mode engine over the entire operating range of the engine by varying the amount of internal and external EGR. Outside of the range of normal HCCI operation thermal and mechanical stability was achieved by using a hybrid spark induced (assisted) compression ignition (SICI) combustion with large amounts of EGR (15 - 40 %). A similar study by (Wang et al., 2009) investigated the use of SICI combustion as a method of controlling and extending the operating range of HCCI combustion. The first part involved an optical study of the combustion process, which showed a spark induced flame that resulted in increased temperature and pressure, which in turn induced the main auto-ignition. Further studies showed that for a gasoline engine the SICI combustion clearly showed a two-stage heat release and resulted in lower NO_x emissions and higher thermal efficiency than that observed in SI combustion (Wang et al., 2009).

Mode switching between SI and HCCI combustion modes can be achieved through the implementation of complicated actuators such as variable valve timing and direct fuel injection. For HCCI combustion and mode switching to be viable on production engines it would be useful to be able to perform SI-HCCI-SI mode switches using only conventional actuators such as intake air throttling, fueling rate, and fuel injection timing. (Boddez, 2011) conducted an experimental study of SI-HCCI-SI mode switches on a cooperative fuel research (CFR) test engine. The development of a mode switching strategy using the actuators of intake throttle angle, fueling rate, and fuel injection timing was investigated. Mode switches in this study are evaluated in part using a mode switch performance criterion (MSPC) developed by Boddez to describe the fluctuation in IMEP, relative knock level, and length of transition between steady state SI and HCCI (Boddez, 2011).

2.6.2 Numerical Mode-Switching Models

Narrow operating regions and complicated control systems can make it difficult to experimentally investigate the physics of a combustion mode switch. The use of numerical models can speed up and simplify the process of investigating mode switches provided that some deviation from experimental values is tolerated. (Ohyama, 2000) used a physics-based model of an ultra-lean combustion (HCCI) engine to develop engine control systems for AFR, knock intensity, and to avoid misfires.

Modes switches are often numerically studied with the use of physics-based mean value models, which sacrifice accuracy for the ability to investigate variations in ignition timing and IMEP during mode switches with reasonable computational intensity. Fast models are required to facilitate mode switch optimization and control system development over several dynamically linked cycles. (Roelle et al., 2004) presents a multi-mode multi-cycle model of a mode switch from SI to HCCI. This model captures early ignition and low work production after the mode switch as well as presents some suggestions for ways to improve the mode switch and ultimately achieve constant power and speed through the transition. The model includes a bulk flow model for the intake and exhaust strokes, a single zone model of in cylinder processes, a simple convective heat transfer correlation, and Wiebe and Arrhenius rate equations to describe the combustion processes for the SI and HCCI modes respectively. The hot residual gases from SI combustion complicate the transition by causing early ignition in the first HCCI cycle (Roelle et al., 2004). (Roelle et al., 2004) suggested that the model be used to help tune valve timings for a smooth SI-HCCI transition. A similar model by (Shaver et al., 2006) includes an exhaust manifold model to help capture dynamics caused by exhaust gas reinduction. (Roelle et al., 2006) describes a dynamic model of HCCI combustion from works (Roelle et al., 2004) and (Shaver et al., 2006), which includes a discrete cycle by cycle wall temperature model to capture cylinder wall temperature dynamics

during changes in operating parameters.

It is possible to develop a more complicated model of mode switches that would provide greater depth of understanding for the underlying physics at the expense of computational time. A series of papers by (Etheridge et al., 2010a,b) use a stochastic reactor model to simulate the transition from SI to HCCI combustion modes, providing a more detailed look at the chemical kinetics of the engine cycles. This model is coupled with GT-Power, a commercial simulation tool used for modeling intake and exhaust strokes that allows for dynamics coupling of cycles. The model is calibrated to match experimental steady state SI and HCCI operating conditions respectively. Mode switching is achieved by changing cam profiles and phasing to create negative valve overlap, adjusting the throttle, advancing the spark timing, and using pilot injection. Both experimentally obtained and modeled results are presented to show HCCI combustion stability during the mode switch to be highly dependant on the effects of the spark in the first HCCI cycles. The first HCCI cycles were observed by (Etheridge et al., 2010b) to be a combination of flame propagation and compression ignition, known in other studies as SICI combustion (Wang et al., 2009). In an attempt to improve computational times for the detailed reaction model of the SI-HCCI mode switches, the same authors created look-up tables for the simulation results to establish a model with the benefits of detailed chemistry calculations that would be able to run in a fraction of the time (Etheridge et al., 2010b). This fast model was used for mode transition optimization and resulted in smoother transitions from SI to HCCI combustion modes and reduced NO_x emissions (Etheridge et al., 2010b).

2.7 Mode Switching in this Thesis

This thesis involves the development of physics-based numerical engine models for the SI and HCCI combustion regimes, similar in concept to those developed by

(Roelle et al., 2004) and (Shaver et al., 2006). The SI model, developed for this study, considers the entire engine cycle. The cylinder contents are modeled as a single zone with lumped parameters and combustion is modeled with a Wiebe function. Many of the differential equations used to describe the SI cycle are based on (Heywood, 1988) and (Ramos, 1989). This single zone SI model is used as the basis for the SI portion of the mode switch model. Contrary to the models developed in (Roelle et al., 2004) and (Shaver et al., 2006), the HCCI model used in this study is a single zone HCCI model with detailed chemical kinetics, providing a more accurate estimate of auto-ignition timing than can be found using an Arrhenius rate equation threshold. The HCCI model has been adapted for dynamic computation from the single zone HCCI model developed in (Kongsereeparp, 2008). The SI model and HCCI model, both validated for steady state operation, are then combined to create a dynamic SI-HCCI mode switching model. Dynamics of the engine cycles are established through the use of an exhaust model that feeds the state of the engine residual gases forward to the input of the next cycle and a discrete cycle by cycle wall temperature model, modified from the work of (Roelle et al., 2006), to simulate the cylinder wall temperature changes during a mode switch. The resulting model requires less than 30 seconds per cycle on a 3.00 GHz computer to simulate a mode transition from SI to HCCI and provides a useful tool to conduct mode switch optimization.

Chapter 3

SI-HCCI Engine Model

A numerical model that is capable of simulating the process of switching an internal combustion engine from a steady state SI combustion mode to a steady state HCCI combustion mode is described in this chapter. The goal of the model is to capture trends in IMEP and combustion timing, including misfires. The experimental operating conditions described in Chapter 4 for the mode switches will be used to validate the model. The model is a balance between providing detailed information about physical processes occurring and acceptable computer execution time of 30 minutes for a mode switch.

To meet these objectives a numerical model has been developed using MATLAB code to describe the processes occurring during a mode switch from SI to HCCI mode in a CFR engine. The HCCI model is a detailed chemical kinetics single zone model based on (Kongsereeparp, 2008), but modified for this study. The SI combustion model is a detailed single zone phenomenological model that for consistency has a parallel structure to the HCCI engine model. The SI and HCCI models are linked dynamically through the mode switches by considering the cycle to cycle change in wall temperature, intake pressure, exhaust gas temperature, and fuel injection rate to create the physics-based mode switch model (PMSM). The SI and HCCI models are subdivided into the following model components:

intake, compression, ignition, heat release and expansion, and exhaust. The model equations require that parameters, constants, and coefficients (listed in Appendix C) be defined. In addition, the operating conditions that are used for running and parameterizing the model are listed in Appendix B.

Figure 3.1 schematically shows how the SI and HCCI models have been divided into sub-models. Figure 3.2 is a schematic of the single zone model; mass flow is defined as positive when flowing into the system, heat transfer is defined as positive when transferred into the system, and work is defined as positive when work is done by the system.

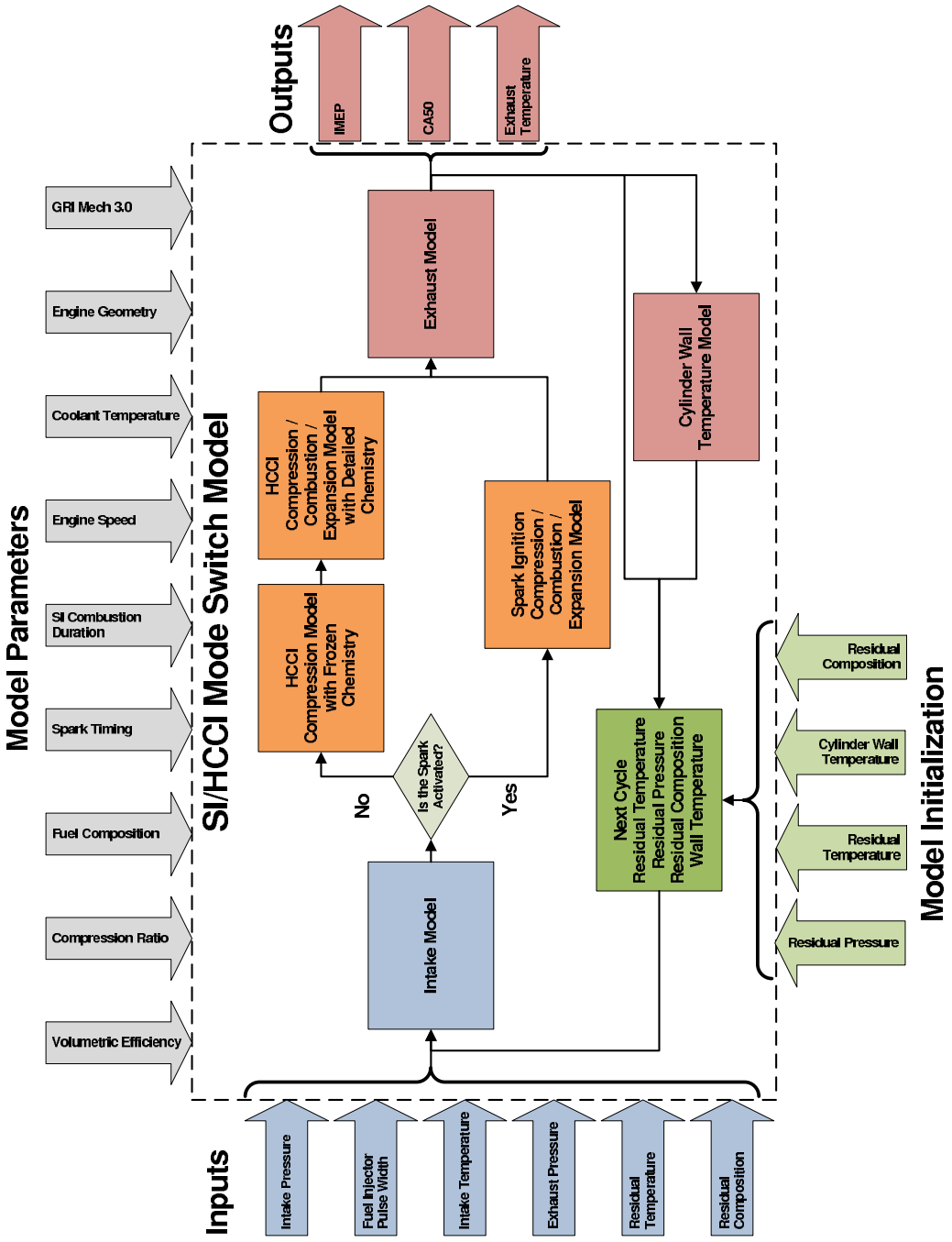

Figure 3.1: Schematic of SI-HCCI Numerical Mode Switch Model

3.1 Main Model Assumptions

The engine is modeled as a disk shaped single zone combustion chamber, assuming no blow-by. Gases in the system are considered to be homogeneous; the thermodynamic properties change with respect to time but are uniform in space throughout the mixture. Temperature, pressure, volume, and composition of the system gases are related through the ideal gas law. Heat transfer is not considered in the intake or exhaust manifolds, and intake and exhaust pressures are assumed to be constant over a complete engine cycle. Intake mixture and residual gas mixing during the intake stroke is modeled using the first law of thermodynamics as mixing between a uniform fuel and fresh air intake mixture and uniform exhaust gas residuals remaining in the cylinder. Combustion in the SI model is assumed to proceed according to the Wiebe function (Ramos, 1989), with fuel and air reacting in a single step reaction to complete combustion products. The HCCI model assumes frozen chemistry below 600 K similar to (Kongsereeparp, 2008), with reactions only proceeding above this threshold. Chemical reactions are described according to GRI-Mech 3.0 reaction mechanism (Smith et al., 1999) and thermodynamic properties are allowed to vary with temperature according to the GRI-Mech thermochemistry (Smith et al., 1999), which is based on the NASA-Lewis (McBride et al., 1993) and Technion (Burcat and McBride, 1993) standard databases. Basic convective heat transfer between cylinder gases and the cylinder wall is considered and modeled using a modified Woschni function (Chang et al., 2004). The engine rotational speed is assumed to be constant during and between engine cycles.

3.2 Intake Model

The engine intake system is modeled with ordinary differential equations that describe many of the physical processes taking place during the intake stroke. These

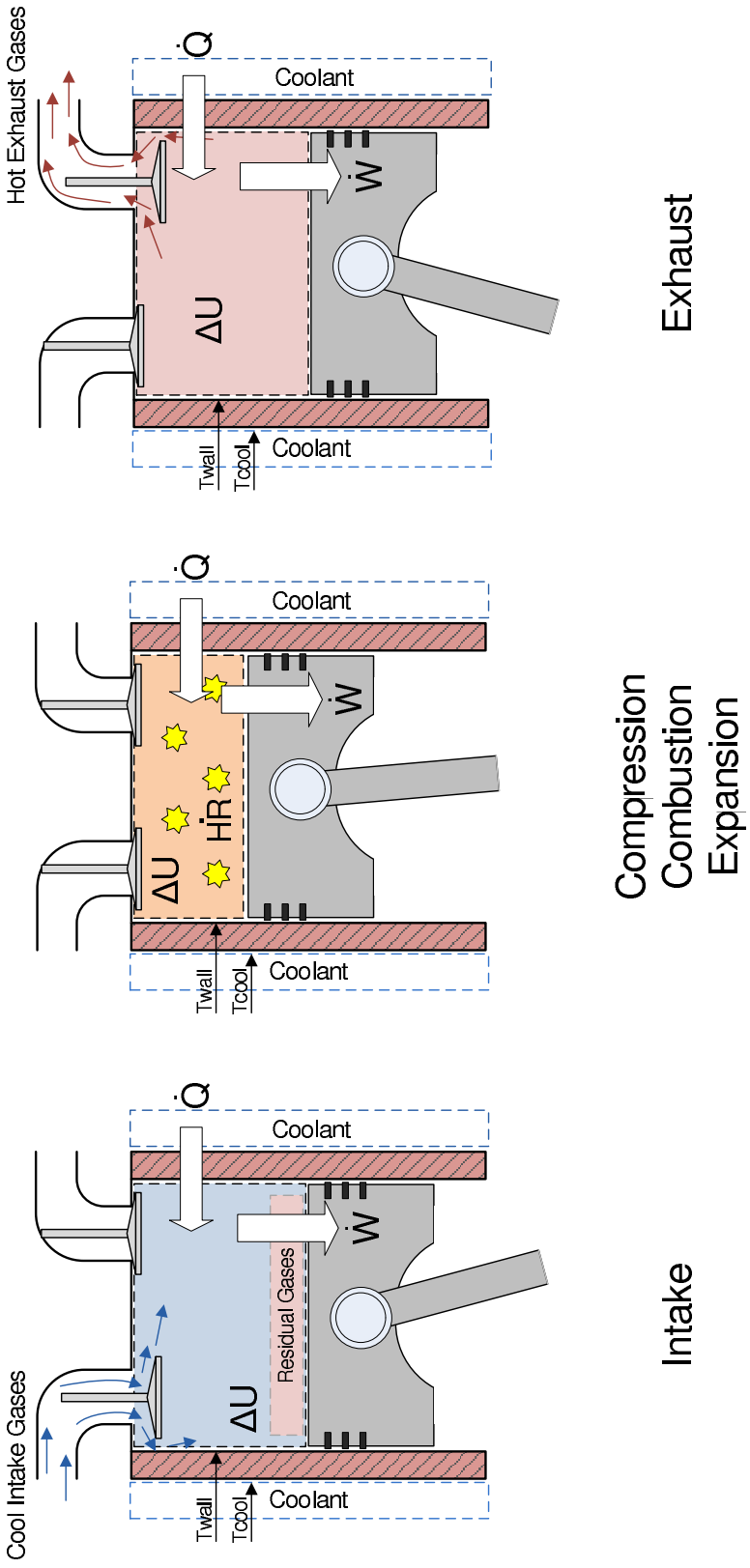

Figure 3.2: Schematic of Single Zone Model Work, Heat, and Mass Transfer

equations describe the mass flux past the intake valve into the engine cylinder, the change in temperature, pressure, and composition as a result of mixing between intake and residual gases, heat transfer to the cylinder walls, and change in cylinder volume. The intake stroke is modeled from the IVO to IVC.

Intake pressure is assumed to be constant during each cycle and is taken as the experimentally determined pressure at IVC. In a typical engine, pulsations in the intake manifold can result in significant pressure fluctuations (Chang et al., 2004). However, the experimental engine setup has a 210 L buffer tank that limits these pulsations, so for the purpose of the intake model the pressure is assumed to be constant. The intake manifold temperature is modeled as constant, neglecting any heat loss to the manifold walls. The intake charge is modeled as a homogeneous mixture of air and fuel at a composition that is determined by the mass of fuel injected and the mass of air inducted into the cylinder for one cycle. No wall wetting or evaporative cooling is considered, because the fuel used in both the model and the experimental setups is natural gas, a gaseous mixture of methane and ethane with some carbon dioxide, nitrogen, and often other species present. The cooling effect of mixing hot intake air with cooler fuel is considered. Intake and exhaust valve overlap is minimal in the CFR engine and has therefore not been considered in this study. Flows are considered in and out of the cylinder through the intake valve and are modeled as homogeneous charges of either intake or cylinder composition depending on the direction of flow.

3.2.1 Charge Composition

The intake charge composition is approximated using the amount of fuel injected into the intake manifold and the corresponding theoretical mass of intake air. Fuel is port injected into the CFR engine and the amount is specified in terms of a pulse width (PW) supplied to the fuel injector. (Boddez, 2011) has characterized

the mass of fuel injected into the intake manifold as

$$m_{\mathrm{f}} = 1.414 \times \mathrm{PW} - 2.375 \tag{3.1}$$

where m_{f} is the mass of fuel in mg injected into the intake manifold and PW is the fuel injector pulse width in ms. This model assumes that the mass of fuel injected is linearly related to the fuel injector pulse width over the pulse width range of 10 - 17 ms (Boddez, 2011). Coefficients and constants in equation 3.1 are determined in the characterization carried out by (Boddez, 2011).

The theoretical mass of air inducted into the cylinder during each cycle, assuming that the ideal gas law ($pV = mRT$) holds for fresh air entering the cylinder, is calculated using

$$m_{\mathrm{air,th}} = \frac{P_{\mathrm{int}} \left(V_{\mathrm{d}} - V_{\mathrm{f}}\right) \eta_{\mathrm{v}}}{R_{\mathrm{air}}\, T_{\mathrm{int}}} \tag{3.2}$$

where $m_{\mathrm{air,th}}$ is the theoretical mass of air inducted into the cylinder, P_{int} is the intake air pressure, V_{d} is the cylinder displacement volume, V_{f} is the volume of fuel calculated using the ideal gas law and m_{f}, η_{v} is the volumetric efficiency, R_{air} is the specific gas constant for air, and T_{int} is the intake air temperature. This model assumes that the residual gases occupy the clearance volume of the cylinder, the fuel occupies a volume determined using the mass of fuel, and the intake air occupies the remaining cylinder volume. The volumes of air and fuel are scaled by the volumetric efficiency term, which is related to engine speed, intake pressure, and intake temperature. Volumetric efficiency is tuned for the simulation and is approximated from experimental results. In the experimental results two intake manifold configurations are used. Volumetric efficiency is higher for the larger intake manifold, lower for the smaller intake manifold, and is tuned accordingly. Values for volumetric efficiency can be found in Appendix C.

The "theoretical" mass of air in Equation 3.2 is considered together with the mass of fuel that has been injected to establish an intake charge composition. Later it will be shown that this approximation compares well to experimental results for the conditions used in this study.

The mass and state of exhaust gas residual (EGR) in the cylinder from the previous cycle also needs to be determined. For a first approximation the EGR temperature and pressure are taken as exhaust values and the composition is assumed to be the complete combustion products associated with the intake charge composition (Kongsereeparp, 2008). In subsequent cycles the EGR composition, temperature, and pressure are determined from the exhaust solution for the previous cycle.

The ideal gas law is assumed to hold for residual exhaust gases and approximate mass of EGR in the cylinder at IVO is calcualted using

$$m_{\mathrm{r}} = \frac{V_{\mathrm{ivo}}\, P_{\mathrm{exh}}\, M_{\mathrm{r}}}{R_{\mathrm{u}}\, T_{\mathrm{exh}}} \tag{3.3}$$

where m_{r} is the mass of the exhaust gas residual, V_{ivo} is the cylinder volume at intake valve open, M_{r} is the approximate molar mass of the exhaust gas residual based on the available composition data, R_{u} is the universal gas constant, and T_{exh} is the exhaust temperature.

3.2.2 Valve Mass Flux

Mass flux through the valves into and out of the cylinder is modeled using a differential equation describing the mass flux of a compressible fluid flowing isentropically through an orifice (Ramos, 1989). This model assumes that the gas flows are homogeneous and the thermodynamic properties of the mixture are the mass averaged properties of the individual species at a single bulk temperature value. The intake valve is modeled as an orifice with changing area that is described by

the experimentally determined intake valve lift profile, and a discharge coefficient (C_{d}) as determined on a flow bench (Kongsereeparp, 2008), which can be found in Appendix C.

An effective valve area is used to determine intake mass flux and is,

$$A_{\mathrm{v}} = f\,\pi\,D_{\mathrm{v}}\,L_{\mathrm{v}} \tag{3.4}$$

where A_{v} is the effective valve area determined by f, which has a value of 1 for the exhaust valve and 0.5 for the intake valve to account for shrouding on half of the valve's circumference, valve seat diameter D_{v}, and the experimentally determined valve lift L_{v}. The mass flow rate through the intake valve is calculated using the following equations.

It has to be established whether the flow through the valve is choked or un-choked flow. This is determined from (Heywood, 1988) using,

$$\left(\frac{P_{\mathrm{r}}}{P_{\mathrm{o}}}\right) \leq \left(\frac{2}{(\gamma+1)}\right)^{\frac{\gamma}{(\gamma-1)}}, \tag{3.5}$$

which when evaluated to be true the flow is considered choked and therefore does not depend on the downstream pressure. Where P_{r} is the pressure at the restriction (cylinder pressure during intake, exhaust manifold pressure during exhaust), P_{o} is the upstream pressure (intake manifold pressure during intake, cylinder pressure during exhaust), and γ is the upstream ratio of specific heats (intake manifold conditions during intake, cylinder conditions exhaust). For choked flow the following equation describes the mass flux through the intake valve into the cylinder (Ramos, 1989). The mass flux through the valve for un-chocked flow is

$$\dot{m}_{\mathrm{cyl}} = \frac{C_{\mathrm{D}}\,A_{\mathrm{v}}\,P_{\mathrm{o}}}{\sqrt{R_{\mathrm{o}}\,T_{\mathrm{o}}}}\left(\frac{P_{\mathrm{r}}}{P_{\mathrm{o}}}\right)\left(\frac{2\,\gamma}{\gamma-1}\left[1-(\frac{P_{\mathrm{r}}}{P_{\mathrm{o}}})^{\frac{(\gamma-1)}{\gamma}}\right]\right)^{\frac{1}{2}} \tag{3.6}$$

where $\dot{m}_{\mathrm{cyl}}$ is the mass flux into or out of the cylinder, R_{o} is the specific gas

constant of the upstream gases, and T_o is the temperature of the upstream gases. The mass flux through the valve for chocked flow is

$$\dot{m}_{cyl} = \frac{C_D\, A_v\, P_o}{\sqrt{R_o\, T_o}} \sqrt{\gamma} \left(\frac{2}{\gamma + 1} \right)^{\frac{(\gamma+1)}{2(\gamma-1)}} . \tag{3.7}$$

For the intake model the upstream conditions are taken as intake manifold conditions and downstream conditions are taken as cylinder conditions. For the exhaust model the upstream conditions are taken as cylinder conditions and downstream conditions are taken as exhaust manifold conditions. It is assumed that no heat transfer occurs to or from the intake/exhaust manifolds or the valves during the intake and exhaust strokes. Heat transfer to the cylinder walls is still considered for these models.

3.2.3 Cylinder Volume

The instantaneous cylinder volume can be described in terms of crank angle degrees by considering engine geometry (Heywood, 1988) using the equation

$$V_{cyl} = V_c + \left(\frac{V_c\,(CR - 1)}{2} \right) \left(\frac{l_c}{r_c} + 1 - \cos\theta - \sqrt{\left(\frac{l_c}{r_c} \right)^2 - \sin^2\theta} \right) \tag{3.8}$$

where V_{cyl} is the volume of the engine cylinder at crank angle θ, V_c is the engine clearance volume, CR is the volumetric compression ratio, l_c is the connecting rod length, and r_c is the crank radius. The instantaneous rate of change in cylinder volume can be determined by taking the derivative of the instantaneous volume with respect to crank angle. The time derivative of the cylinder volume is calculated as

$$
\begin{aligned}
Z_1 &= \mathrm{CR} - 1 \\
Z_2 &= -2\,(\sin\theta\ \cos\theta)\left(\left(\frac{l_\mathrm{c}}{r_\mathrm{c}}\right)^2 - \sin^2\theta\right)^{-\frac{1}{2}} \\
\dot{V}_\mathrm{cyl} &= \frac{V_\mathrm{c}\,Z_1}{2}\left(\sin\theta - \frac{Z_2}{2}\right)\left(\frac{2\,\pi\,(6\,N_s)}{360}\right)
\end{aligned}
\tag{3.9}
$$

where $\dot{V}_\mathrm{cyl}$ is the time derivative of the cylinder volume and N_s is the engine rotational speed in rpm. Both the SI and HCCI models assume constant engine speed, the validity of this assumption is discussed in Chapter 4. Crank angle degrees (CAD), θ, are determined based on cycle time and engine speed, and are indexed to 360 CAD at compression TDC. Z_1 and Z_2 are temporary variables defined only for Equation 3.9.

3.2.4 Heat Transfer

Heat transfer to the engine cylinder walls has been described by (Woschni, 1967), where a single correlation was developed describing the rate of heat transfer from a compression ignition engine cylinder. This correlation has since been modified by several authors for various engine geometries and combustion modes; some of these modifications are described in (Stone, 1999). (Chang et al., 2004) suggested an improved Woschni correlation for an HCCI engine. This heat transfer model considers only simple convective heat transfer and does not consider radiative heat transfer from hot cylinder gases.

The form of the Woschni correlation suggested by (Chang et al., 2004) for use in HCCI engines is

$$V_{\text{tuned}} = c_1\, 2\, L\, \frac{N_{\text{s}}}{60} + \frac{c_2}{6}\, V_{\text{d}} \left(\frac{T_{\text{ivc}}}{P_{\text{ivc}} V_{\text{ivc}}} \right) \left(P_{\text{cyl}}\, 10^5 - P_{\text{ivc}} \left(\frac{V_{\text{ivc}}}{V_{\text{cyl}}} \right)^{\gamma} \right)$$

$$h = \alpha\, P_{\text{cyl}}^{0.8}\, L_{\text{cyl}}^{-0.2}\, T_{\text{cyl}}^{-0.73}\, (V_{\text{tuned}})^{0.8} \tag{3.10}$$

where h is the Woschni heat transfer coefficient with units of W/m^{2}K, P_{cyl} is the cylinder pressure in bar, T_{cyl} is the cylinder mixture temperature in K, L_{cyl} is the instantaneous cylinder height in m, N_{s} is the engine rotational speed in rpm, and c_1 (2.28), c_2 (0 m/sK), and α (64.972) are coefficients for the Woschni correlation that are tuned for the engine. T_{ivc} in K, P_{ivc} in Pa, and V_{ivc} in m^3 serve as the reference temperature, pressure, and volume taken at IVC as required for the Woschni correlation. Motored pressure has been approximated for an isentropic system as $P_{\text{motoring}} = P_{\text{ivc}} \left(\frac{V_{\text{ivc}}}{V_{\text{cyl}}} \right)^{\gamma}$ (Soyhan et al., 2009).

The characteristic length is represented by L_{cyl}, the instantaneous cylinder height, rather than the cylinder bore, B_{cyl} as suggested in the original correlation. The justification for changing the characteristic length is that by using instantaneous cylinder height the correlation captures a changing characteristic length that tends to vary inversely proportional to the heat transfer. Also the temperature exponent has been determined in (Chang et al., 2004) to be -0.73 rather than -0.53 for HCCI and the convection due to combustion velocity term has been reduced by a factor of 6 due to the lack of a discernable flame front in HCCI combustion. For HCCI combustion the modified correlation Equation 3.10 is used, where $\alpha = 64.97$ during compression, $\alpha = 259.89$ during expansion, $c_1 = 2.28$, $c_2 = 0$ m/sK before ignition, and $c_2 = 0.00324$ m/sK after ignition (Ramos, 1989). Additional model parameters are listed in Appendix C.

The correlation used in the PMSM for heat transfer from the cylinder walls when in SI mode is given in the following equation and is based on the original

Woschni correlation. The cylinder bore has been substituted for the instantaneous cylinder height as the characteristic length as suggested in (Chang et al., 2004). The Woschni heat transfer coefficient for heat transfer to the cylinder walls in the SI model is calculated using

$$\begin{aligned} V_{\text{mot}} &= c_1\, 2\, L\, \frac{N_{\text{s}}}{60} \\ V_{\text{comb}} &= c_2\, V_{\text{d}} \left(\frac{T_{\text{ivc}}}{P_{\text{ivc}}\, V_{\text{ivc}}} \right) \left(P_{\text{cyl}}\, 10^5 - P_{\text{ivc}} \left(\frac{V_{\text{ivc}}}{V_{\text{cyl}}} \right)^{\gamma} \right) \\ h &= \alpha\, P_{\text{cyl}}^{0.8}\, L_{\text{cyl}}^{-0.2}\, T_{\text{cyl}}^{-0.53}\, (V_{\text{mot}} + V_{\text{comb}})^{0.8} \end{aligned} \tag{3.11}$$

where for the SI model $\alpha = 129.94$ (Woschni, 1967), $c_1 = 2.28$, $c_2 = 0$ m/sK before ignition, and $c_2 = 0.00324$ m/sK after ignition (Ramos, 1989).

The cylinder surface area for heat transfer and instantaneous global cylinder wall heat transfer from the cylinder walls to the cylinder mixture are described using

$$\begin{aligned} A_{\text{cyl}} &= \frac{2\pi\, B_{\text{cyl}}^2}{4} + \pi\, B_{\text{cyl}}\, L_{\text{cyl}} \\ \dot{Q}_{\text{wall}} &= h\, A_{\text{cyl}}\, (T_{\text{wall}} - T_{\text{cyl}}) \end{aligned} \tag{3.12}$$

where A_{cyl} is the instantaneous cylinder wall area exposed to the gases in m^2, B_{cyl} is the cylinder bore in m, $\dot{Q}_{\text{wall}}$ is the rate of heat transfer from the cylinder walls to the mixture in W, and T_{wall} is the cylinder wall temperature in K.

The coefficient α in the SI model is the original value suggested by (Woschni, 1967) for SI combustion and is tuned in both compression and expansion for HCCI combustion. The initial value of α for SI combustion is found to be adequate, the HCCI value started at the value recommended by Woschni for a compression

ignition engine and is modified by a correction factor to account for differences in engine geometry and the high pressures predicted by a single zone model. Ideal values of α for HCCI combustion were found to be $0.5\,\alpha_{\text{woschni}}$ for compression and $2\,\alpha_{\text{woschni}}$ for expansion. The higher value of heat transfer during expansion is to compensate for the over-prediction in peak pressure as a result of using a single zone model. There is a large variation between different methods for estimating both mean and instantaneous heat transfer, but these differences are small because the heat transfer coefficient only minimally affects engine performance predictions (Stone, 1999). All model parameters are listed in Appendices B and C.

3.2.5 Cylinder Composition

As the intake gases enter the cylinder and mix with the exhaust gas residual the composition of the cylinder mixture changes. The change in composition is described using

$$\dot{y}_k = \frac{\dot{m}_{\text{cyl}}}{m_{\text{cyl}}}(y_{k,\text{int}} - y_{k,\text{cyl}}), \tag{3.13}$$

derived from the continuity equation, where $\dot{y}_k$ is the rate of change of the mass fraction of the k^{th} species in the cylinder mixture, $y_{k,\text{int}}$ is the mass fraction of the k^{th} species in the intake flow, and $y_{k,\text{cyl}}$ is the mass fraction of the k^{th} species in the cylinder. Here 6 species are considered for the SI model and include CH_4, C_2H_6, O_2, N_2, CO_2, and H_2O. The HCCI model considers any of the 53 species from the GRI-Mech 3.0 mechanism that are present in the cylinder or intake gases.

3.2.6 Cylinder Temperature

The change in temperature of the cylinder mixture during the intake can be described using the first law of thermodynamics for an unsteady flow system. An equation that determines the rate of change of temperature for an intake process

in terms of mixing between the EGR and intake charge, work done on the mixture by changing cylinder volume, heat transfer from the cylinder walls, and changing homogeneous mixture composition is given in (Heywood, 1988).

$$
\begin{aligned}
Z_1 &= \left(\sum_{k=1}^{K} \dot{y}_k \, h_k + R_{\text{cyl}} \, T_{\text{cyl}} \sum_{k=1}^{K} \dot{y}_k \, y_k \right) \\
Z_2 &= -\frac{\dot{m}_{\text{cyl}}}{m_{\text{cyl}}} \, (h_{\text{cyl}} - R_{\text{cyl}} \, T_{\text{cyl}}) \\
Z_3 &= \frac{1}{m_{\text{cyl}}} (\dot{m}_{\text{cyl}} \, h_{\text{flow}} - P_{\text{cyl}} \, \dot{V}_{\text{cyl}} + \dot{Q}_{\text{wall}}) \\
Z_4 &= c_{\text{v,cyl}} \\
\dot{T}_{\text{cyl}} &= \frac{(Z_1 + Z_2 + Z_3)}{Z_4}
\end{aligned}
\tag{3.14}
$$

Where $\dot{T}_{\text{cyl}}$ is the rate of change in cylinder temperature, K is the number of species present in the cylinder (limited to reactants and products in the SI model, but extended to intermediate species for the HCCI model), h_k is the mass specific enthalpy of species k, R_{cyl} is the mass average specific gas constant for the cylinder gases, h_{flow} is the mass specific enthalpy of the gases entering or leaving the cylinder, and $c_{\text{v,cyl}}$ is the mass average specific heat evaluated at constant volume for the cylinder gases. A detailed derivation of Equation 3.14 from the equation given in (Heywood, 1988) to the form given above is the subject of Appendix A. Z_1, Z_2, Z_3, and Z_4 are temporary variables defined only for Equation 3.14.

3.2.7 Thermodynamic Properties

The thermodynamic properties used to determine the rate of change in cylinder mixture temperature are found using the thermodynamic coefficients in NASA polynomial format for the species present in the cylinder during the intake stroke (Smith et al., 1999).

The following three equations allow the calculation of basic thermodynamic properties,

$$\frac{C^{\circ}_{\mathrm{p},k}}{R_{\mathrm{u}}} = a_{1k} + a_{2k}\,T + a_{3k}\,T^2 + a_{4k}\,T^3 + a_{5k}\,T^4 \tag{3.15a}$$

$$\frac{H^{\circ}_{k}}{R_{\mathrm{u}}\,T} = a_{1k} + \frac{a_{2k}}{2}\,T + \frac{a_{3k}}{3}\,T^2 + \frac{a_{4k}}{4}\,T^3 + \frac{a_{5k}}{5}\,T^4 + \frac{a_{6k}}{6} \tag{3.15b}$$

$$\frac{S^{\circ}_{k}}{R_{\mathrm{u}}\,T} = a_{1k}\,\ln T + \sum_{n=2}^{\mathrm{N}} \frac{a_{nk}\,T^{n-1}}{n-1} + a_{\mathrm{N}+2,k} \tag{3.15c}$$

where $C^{\circ}_{\mathrm{p},k}$ is the specific heat of species k evaluated at constant pressure, H°_{k} is the enthalpy of species k, S°_{k} is the entropy of species k, $\mathrm{N} = 5$, and T is the species temperature in Kelvin. Coefficients a_{1k} to $a_{\mathrm{N}+2,k}$ are thermodynamic coefficients in NASA polynomial format from (Smith et al., 1999).

3.2.8 Cylinder Pressure

The rate of change in cylinder pressure is determined from the ideal gas law for the cylinder contents, $PV = mRT$. Neglecting the instantaneous change in the specific gas constant due to mixing, the instantaneous derivative of the cylinder pressure with respect to cylinder mass, temperature, and volume of the cylinder contents is calculated using

$$\dot{P}_{\mathrm{cyl}} = P_{\mathrm{cyl}} \left(\frac{\dot{T}_{\mathrm{cyl}}}{T_{\mathrm{cyl}}} + \frac{\dot{m}_{\mathrm{cyl}}}{m_{\mathrm{cyl}}} - \frac{\dot{V}_{\mathrm{cyl}}}{V_{\mathrm{cyl}}} \right) \tag{3.16}$$

where $\dot{P}_{\mathrm{cyl}}$ is the time derivative of the cylinder pressure.

3.3 Compression Model

The compression process is modeled from the intake valve close (IVC) event until TDC or ignition occurs, whichever comes first. The cylinder gases are assumed

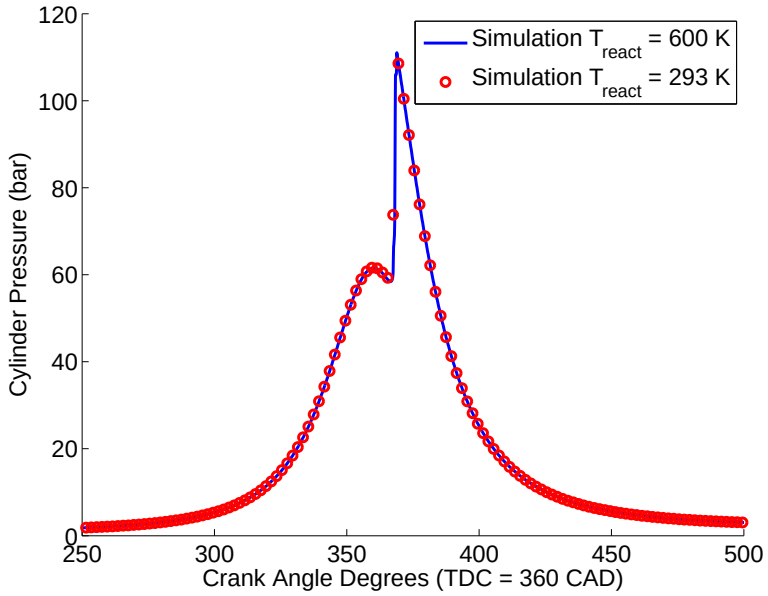

Figure 3.3: Simulated Pressure Traces of the HCCI Model with Frozen Kinetics Temperature Thresholds of 600 K and 293 K

to be a homogeneous mixture of intake products and exhaust gas residual that occupy a single zone defined by the cylinder volume. For the SI model it is assumed that the mixture is frozen, such that no chemical reactions takes place during the compression stroke until the spark ignites the mixture. The HCCI model assumes a frozen mixture at temperatures less than 600 K, while above 600 K the detailed chemical reaction calculations are initiated. The assumption of a frozen mixture for HCCI at temperatures lower than 600 K reduces the computational time by approximately 10 % while not greatly impacting the calculated values as shown in Figure 3.3. Figure 3.3 shows the pressure trace of a simulated HCCI cycle where kinetics are considered at all temperatures over 293 K compared to the pressure trace of a simulated HCCI cycle where kinetics are considered at all temperatures over 600 K. There is no significant difference in the pressure traces of the two simulations.

Changes in volume are tracked using Equations 3.8 and 3.9 described in the above section. Similarly, the Woschni heat transfer correlation used for the in-

take model, Equations 3.10 and 3.11, are again used to describe the heat transfer from the cylinder gases to the cylinder walls during compression for HCCI and SI combustion respectively.

The change in temperature during the compression stroke is described by Equation 3.14. Some terms in equation 3.14 are not relevant due to the closed system assumption so the resulting rate equation for temperature is

$$\dot{T}_{\text{cyl}} = \frac{-P_{\text{cyl}}\,\dot{V}_{\text{cyl}} + \dot{Q}_{\text{wall}}}{m_{\text{cyl}}\,c_{\text{v,cyl}}}. \tag{3.17}$$

Once the temperature rate of change is known, a differential form of the ideal gas law is used to describe the rate of change in cylinder pressure during compression assuming constant cylinder mass (ie. no blow-by) and gas properties. The pressure rate equation is

$$\dot{P}_{\text{cyl}} = P_{\text{cyl}}\left(\frac{\dot{T}_{\text{cyl}}}{T_{\text{cyl}}} - \frac{\dot{V}_{\text{cyl}}}{V_{\text{cyl}}}\right) \tag{3.18}$$

and describes the rate of change in cylinder pressure during the compression stroke for both the SI model and the HCCI model before the chemical kinetics start being considered ($T_{\text{cyl}} > 600$ K).

3.4 Ignition, Heat Release, and Expansion

The ignition, heat release, and expansion models span from the start of combustion or TDC, whichever comes first, to the exhaust valve open (EVO) event. For this part of the engine cycle the SI and HCCI models differ considerably due to the different modes of combustion occurring in each.

3.4.1 Spark Ignition - Heat Release and Expansion

Start of combustion in the spark ignition model occurs when the spark plug is used to ignite the cylinder mixture. The heat release is described by letting the lower heating value (LHV) represent the energy released per kilogram of fuel and approximating the rate of conversion from reactants to products using a modified Wiebe function (Ramos, 1989).

3.4.1.1 Heat Release

The lower heating value of the fuel composition used in the simulation is calculated using,

$$\mathrm{LHV} = \frac{\left(\sum_{k=1}^{K} x_k \bar{h}_k\right)_{\mathrm{Reactants}} - \left(\sum_{k=1}^{K} x_k \bar{h}_k\right)_{Products}}{\left(\sum_{k=1}^{K} x_k M_k\right)_{\mathrm{Fuel}}} \tag{3.19}$$

where LHV is the lower heating value of the fuel and air mixture, x_k is the mole fraction of species k, $\bar{h}_k$ is the standard molar enthalpy of species k evaluated from the GRI-Mech thermodynamics (Smith et al., 1999) at room temperature, and M_k is the molecular mass of species k. It is assumed that the reactants are only fuel and fresh air, with a mixture proportion equal to that of the intake mixture, and assumes that the combustion reaction results in complete combustion products. The heating value (HV) is calculated in terms of the mass of cylinder contents from the LHV using

$$\mathrm{HV} = \mathrm{LHV}\frac{m_{\mathrm{f}}}{m_{\mathrm{cyl}}}. \tag{3.20}$$

The differential form of the Wiebe function,

$$\dot{y}_{\mathrm{b}} = \exp\left(-a\left(\frac{\theta-\theta_{\mathrm{spark}}}{\Delta\theta_{\mathrm{b}}}\right)^{m+1}\right)\left(\frac{(m+1)a}{\Delta\theta_{\mathrm{b}}}\right)\left(\frac{\theta-\theta_{\mathrm{spark}}}{\Delta\theta_{\mathrm{b}}}\right)^{m}, \tag{3.21}$$

is used to express the rate at which the cylinder contents are burned and heat is released. In Equation 3.21 $\dot{y}_{\mathrm{b}}$ is the mass fraction rate of burnt cylinder contents, a and m are shape constants for the Wiebe function, θ is the instantaneous crank angle degree from the start of cycle reference time (0 CAD), θ_{spark} is the crank angle degree at which the spark ignites the cylinder mixture, and $\Delta\theta_{\mathrm{b}}$ is the burn duration in crank angle degrees. Shape constants a and m are set to $a = 5$ and $m = 2$ (Ramos, 1989). Values of θ_{spark} and $\Delta\theta_{\mathrm{b}}$ are tuned parameters based on matching simulated pressure traces to experimental pressure traces at the steady state SI operating point outlined in Appendix B. The tuned value of θ_{spark} is found to be 1 CAD aTDC (0.0860 s) compared to an approximate experimental crank angle of 3 CAD aTDC (0.0864 s) a difference of less than a percent relative to the cycle time.

The mass fraction rate of burnt cylinder contents can be converted to mass rate of burnt cylinder contents by using

$$\dot{m}_{\mathrm{b}} = \dot{y}_{\mathrm{b}}\, m_{\mathrm{cyl}}, \tag{3.22}$$

where $\dot{m}_{\mathrm{b}}$ is the mass rate of burnt cylinder contents. Using Equation 3.22, the heat release rate is calculated in

$$\dot{\mathrm{HR}} = \dot{m}_{\mathrm{b}}\,\mathrm{HV}, \tag{3.23}$$

where $\dot{\mathrm{HR}}$ is the instantaneous rate of heat release from chemical to sensible enthalpy.

3.4.1.2 Cylinder Composition

During combustion the conversion of reactants to complete combustion products are tracked with the following series of rate equations. Since air is assumed to be mixed with natural gas and complete combustion products from lean combustion in the SI model, the cylinder composition consists of CH_4, C_2H_6, O_2, N_2, CO_2, and H_2O. The equations for calculating conversion rates of the cylinder species are

$$\dot{y}_{CH_4} = -y_{CH_4,\text{ivc}}\,\dot{y}_b \tag{3.24a}$$

$$\dot{y}_{C_2H_6} = -y_{C_2H_6,\text{ivc}}\,\dot{y}_b \tag{3.24b}$$

$$\dot{y}_{O_2} = \left(\frac{2\,\dot{y}_{CH_4}}{M_{CH_4}} + \frac{3.5\,\dot{y}_{C_2H_6}}{M_{C_2H_6}} M_{O_2}\right) \tag{3.24c}$$

$$\dot{y}_{N_2} = 0 \tag{3.24d}$$

$$\dot{y}_{CO_2} = -\left(\frac{\dot{y}_{CH_4}}{M_{CH_4}} + \frac{2\,\dot{y}_{C_2H_6}}{M_{C_2H_6}} M_{CO_2}\right) \tag{3.24e}$$

$$\dot{y}_{H_2O} = -\left(\frac{2\,\dot{y}_{CH_4}}{M_{CH_4}} + \frac{3\,\dot{y}_{C_2H_6}}{M_{C_2H_6}} M_{H_2O}\right) \tag{3.24f}$$

where $\dot{y}_k$, y_k, M_k, are the instantaneous rate of change equations to species mass fraction, cylinder mixture mass fraction, and molecular weight respectively for species k, where 6 species are considered for the SI model including CH_4, C_2H_6, O_2, N_2, CO_2, and H_2O.

3.4.1.3 Cylinder Temperature

Heat release from combustion and changing cylinder composition result in the addition of two terms to Equation 3.17. The resulting equation for rate of change in cylinder temperature during heat release and expansion is

$$
\begin{aligned}
Z_1 &= \left(\sum_{k=0}^{K} \dot{y}_k \, c_{\mathrm{v},k} \, T_{\mathrm{cyl}} \right) \\
Z_2 &= \frac{1}{m_{\mathrm{cyl}}} (\dot{\mathrm{HR}} - P_{\mathrm{cyl}} \, \dot{V}_{\mathrm{cyl}} + \dot{Q}_{\mathrm{wall}}) \\
Z_3 &= c_{\mathrm{v,cyl}} \\
\dot{T}_{\mathrm{cyl}} &= \frac{(Z_1 + Z_2)}{Z_3}
\end{aligned}
\tag{3.25}
$$

where $c_{\mathrm{v},k}$ is the mass specific heat defined at constant volume for the k^{th} species. Z_1, Z_2, and Z_3 are temporary variables defined only for Equation 3.25.

3.4.1.4 Cylinder Pressure, Volume, and Heat Transfer

Rate equations for in-cylinder pressure and volume are the same as those used during the compression stroke, which are Equations 3.18 and 3.9 respectively.

The heat transfer correlation also remains the same through combustion and expansion. During combustion in the engine the heat transfer correlation constant c_2 changes from 0 to 0.00324 m/sK. The term c_2 in the heat transfer correlation allows for the consideration of additional forced convective heat transfer as a result of combustion in the engine cylinder (Woschni, 1967).

3.4.2 HCCI - Heat Release and Expansion

The start of combustion is achieved in the HCCI engine model when the rates of reaction reach a value significant enough to result in combustion reactions occurring. These rates of reaction are highly sensitive to temperature, and are calculated using the GRI-Mech 3.0 mechanism (Smith et al., 1999). This single zone model has been extensively validated in the work of Kongsereeparp (Kongsereeparp, 2008) and is shown to have good correlation with the start of combustion timing of an HCCI

engine. The crank angle degree resolved pressure trace of the HCCI model does not exactly match the experimental results, but this is a result of the assumption of a single reaction zone (Kongsereeparp, 2008; Kirchen et al., 2007). A single zone HCCI model under-predicts the combustion duration and thus the rate of pressure rise is significantly higher in the model than shown experimentally (Kirchen et al., 2007). In reality the reaction rates of different zones in the combustion chamber would vary slightly due to gradients in temperature, composition, and heat transfer resulting in an overall lower rate of pressure rise (Kongsereeparp, 2008).

3.4.2.1 Cylinder Reactions

The following equations describe the rate of change in cylinder species as the combustion reaction progresses, developed from (Kongsereeparp, 2008). The HCCI model differs from the SI model in that intermediate species are tracked through a multi-step combustion reaction.

A general elementary reaction is described by

$$\sum_{k=1}^{K} \nu_{k,i}^{'} X_k \Longleftrightarrow \sum_{k=1}^{K} \nu_{k,i}^{''} \mathrm{X}_k \tag{3.26}$$

where $\nu_{k,i}^{'}$ and $\nu_{k,i}^{''}$ are forward and reverse reaction coefficients for species k in reaction i, and X_k is species k. The species production rates are

$$\dot{\omega}_{k,i} = \left(\sum \alpha_{\mathrm{M}} \left[x_k\right]\right) \left(\nu_{k,i}^{''} - \nu_{k,i}^{'}\right) \left(k_{f,i} \prod_{k=1}^{K} \left[x_k\right]^{\nu_{k,i}^{'}} - k_{r,i} \prod_{k=1}^{K} \left[x_k\right]^{\nu_{k,i}^{''}}\right) \tag{3.27}$$

where $\dot{\omega}_{k,i}$ is the production rate of the k^{th} species of reaction i, α_{M} is a coefficient for considering third body effects of reaction rates, $[x_k]$ is the molar concentration of the k^{th} species, $k_{f,i}$ is the forward reaction rate of reaction i, and $k_{r,i}$ is the reverse reaction rate of reaction i. The the rate of change in cylinder mass

fraction of species k is calculated using

$$\dot{y}_k = \frac{\dot{\omega}_k \, M_k}{\rho_{cyl}} \tag{3.28}$$

where M_k is the molar mass of the k^{th} species and ρ_{cyl} is the density of the cylinder mixture, defined as $\rho_{\text{cyl}} = \frac{m_{\text{cyl}}}{V_{\text{cyl}}}$. Thermodynamic values are determined in the same method as they were for SI combustion using the GRI-Mech thermodynamics package (Smith et al., 1999).

3.4.2.2 Cylinder Temperature

Once the rate of change in cylinder composition for the reaction species is known, the rate of change in cylinder temperature can be determined from the first law of thermodynamics for a reacting mixture in a closed system. The equation for the rate of change in cylinder temperature is

$$\dot{T}_{\text{cyl}} = -\frac{1}{\rho \, \bar{c}_{\text{v,cyl}}} \sum_{i=1}^{\text{N}} (u_i \, \dot{\omega}_i \, M_i) - \frac{R_{\text{u}} \, T_{\text{cyl}} \times \sum_{i=1}^{\text{N}} [x_i]}{m_{\text{cyl}} \, \bar{c}_{\text{v,cyl}}} \dot{V}_{\text{cyl}} + \frac{1}{m_{\text{cyl}} \, \bar{c}_{\text{v,cyl}}} \dot{Q}_{\text{wall}} \tag{3.29}$$

where $\bar{c}_{\text{v,cyl}}$ is the molar specific heat of the cylinder mixture evaluated at constant volume, N is the total number of species, equal to 53 when using the GRI-Mech 3.0 reaction mechanism, and M_i is the molecular weight of species i.

(Kongsereeparp, 2008) addresses the fact that non-perfectly stirred mixtures can have significant effects on HCCI combustion timing. The initial temperature at IVC, calculated by assuming ideally mixed cylinder contents, is often higher than the actual temperature at IVC. For this reason the actual cylinder temperature will rise faster than the ideally calculated cylinder temperature in Equation 3.29

(Kongsereeparp, 2008). The rate of temperature change is described by

$$\dot{T}_{\text{int}} = \frac{m_{\text{cyl}}\,\bar{c}_{\text{p}}}{m_{\text{int}}\,\bar{c}_{\text{p,int}}}\dot{T}_{\text{cyl}} + \tau\,(T_{\text{cyl}} - T_{\text{int}}) - \Gamma\left(\frac{m_{\text{cyl}}\,\bar{c}_{\text{p}} - m_{\text{int}}\,\bar{c}_{\text{p,int}}}{m_{\text{int}}\,\bar{c}_{\text{p,int}}}\right)\dot{T}_{\text{cyl}} \tag{3.30}$$

$$\begin{aligned}\dot{T}_{\text{cyl}} = &-\frac{1}{\rho_{\text{cyl}}\,\bar{c}_{\text{v,cyl}}}\sum_{i=1}^{\text{N}}(u_i\,\dot{\omega}_i\,M_i) - \frac{R_{\text{u}}\,T_{\text{cyl}}\times\sum_{i=1}^{\text{N}}[x_i]}{m_{\text{cyl}}\,\bar{c}_{\text{v,cyl}}}\dot{V}_{\text{cyl}} \\ &+\frac{1}{m_{\text{cyl}}\,\bar{c}_{\text{v,cyl}}}\left(\dot{Q}_{\text{wall}} - \tau\times m_{\text{int}}\,\bar{c}_{\text{p,int}}\,(T_{\text{cyl}} - T_{\text{int}})\right)\end{aligned} \tag{3.31}$$

where τ is the inverse of a characteristic time scale of the relative temperature rise, defined in (Kongsereeparp, 2008) to be 34 while T_{cyl} is less than T_{int} after which time the value of τ becomes zero. The subscript "int" means "of intake mixtures" and is representative of the system starting from IVC at a temperature equal to the intake air temperature. Γ in Equation 3.30 sets the rate of temperature rise of T_{int} equal to that of T_{cyl} when the temperatures are equal, thus this term is not included in Equation 3.31. By considering the enthalpy exchange of the mixtures in the cylinder, the Equation 3.31 replaces Equation 3.29 (Kongsereeparp, 2008).

3.4.2.3 Cylinder Pressure, Volume, and Heat Transfer

The cylinder pressure and volume instantaneous rate equations are determined in the same way that they are during the compression stroke using Equations 3.18 and 3.9 respectively.

The heat transfer correlation remains the same as in Equation 3.31 throughout combustion and expansion for HCCI. With the initiation of combustion in the engine the heat transfer correlation coefficient c_2 is set to 0.00324 m/sK and α is set to 259.89. Heat transfer model parameters are defined in Appendix C.

3.5 Exhaust Model

The exhaust stroke of the engine returns to a similar structure for both spark ignition and HCCI models. This model is computed from EVO to IVO of the next cycle. The exhaust model is very similar to the intake model except that: the flow of gases is reversed to be out of the cylinder, the heat transfer is greater due to higher gas temperatures, exhaust manifold pressure is assumed to be constant, and it is assumed that the mixture composition is no longer changing.

3.5.1 Exhaust Mass Flux

Mass flux from the cylinder through the exhaust valve is described by Equations 3.4 to 3.7, the only difference being that upstream and restriction conditions are taken as the cylinder and exhaust conditions respectively. The exhaust valve is not shrouded in the CFR engine so the variable f in Equation 3.4 is assigned a value of 1.

3.5.2 Cylinder Temperature

The instantaneous rate of change in temperature during the exhaust stroke is

$$\begin{aligned} Z_1 &= -\frac{\dot{m}_{\text{cyl}}}{m_{\text{cyl}}}\,(h_{\text{cyl}} - R_{\text{cyl}}\,T_{\text{cyl}}) \\ Z_2 &= \frac{1}{m_{\text{cyl}}}(\dot{m}_{\text{cyl}}\,h_{\text{flow}} - P_{\text{cyl}}\,\dot{V}_{\text{cyl}} + \dot{Q}_{\text{wall}}) \\ Z_3 &= c_{\text{v,cyl}} \\ \dot{T}_{\text{cyl}} &= \frac{(Z_1 + Z_2)}{Z_3} \end{aligned} \tag{3.32}$$

and is similar to Equation 3.14 derived for the intake stroke. Z_1, Z_2, and Z_3 are temporary variables defined only for Equation 3.25. The only difference between

Equation 3.32 and Equation 3.14 is that the cylinder composition is assumed to be unchanging during the exhaust stroke, thus eliminating the mass fraction rate terms ($\dot{y}_k$) from the equation. In Equation 3.32, $\dot{m}_{\text{cyl}}$ is a negative value indicating the cylinder gas mass flow rate through the exhaust valve is out of the cylinder, and h_{flow} is the enthalpy of the cylinder gases.

3.5.3 Cylinder Volume, Pressure, and Heat Transfer

The rate of change in both volume and pressure are modeled the same for the exhaust stroke as for the intake stroke described in Equations 3.9 and 3.16 respectively. Heat transfer to the cylinder walls is also described by the same equations as those used for the expansion model in both SI and HCCI combustion modes.

3.6 Cycle to Cycle Models

For the PMSM to be able to simulate a mode switch between SI and HCCI combustion modes the SI and HCCI engine models need to be dynamically linked. To do this the PMSM includes a cylinder wall temperature model and thermodynamic coupling.

3.6.1 Cylinder Wall Temperature Model

The wall temperature of the engine cylinder is important for HCCI combustion timing, as wall temperatures can affect heat transfer rates and combustion phasing. The time scale of the change in wall temperature is such that wall surface temperature dynamics are considered on a cycle by cycles basis using the following equations based on (Roelle et al., 2006). Conductive heat transfer through the cylinder wall is assumed and is modeled as a resistive heat transfer system. The outside cylinder wall temperature is assumed equal to the temperature of the coolant and the inside cylinder wall temperate is determined as T_{wall} in the following equations.

The formula used for calculating the approximate wall area, including cylinder head and piston, when the piston is at TDC is

$$A_{\mathrm{w}} = \frac{2\,\pi}{4} B_{\mathrm{cyl}}^2 + \frac{4\,V_{\mathrm{c}}}{B_{\mathrm{cyl}}} \tag{3.33}$$

With the approximate wall area and values for heat transfer, a new cylinder wall temperature is calculated using

$$Q_{\mathrm{wall}} = \int_{t_{\mathrm{o}}}^{t_{\mathrm{cyc}}+t_{\mathrm{o}}} \dot{Q}_{\mathrm{wall}}\,\mathrm{d}t \tag{3.34a}$$

$$R_{\mathrm{w}} = \frac{L_{\mathrm{w}}}{k_{\mathrm{w}}\,A_{\mathrm{w}}\,t_{\mathrm{cyc}}}$$

$$C_{\mathrm{w}} = \frac{\rho_{\mathrm{w}}\,A_{\mathrm{w}}\,L_{\mathrm{w}}\,c_{\mathrm{p,w}}}{2}$$

$$T_{\mathrm{wall}}(i+1) = T_{\mathrm{cool}} + \left(1 - \frac{1}{R_{\mathrm{w}}\,C_{\mathrm{w}}}\right)\left(T_{\mathrm{wall}}(i) - T_{\mathrm{cool}}\right) - \frac{Q_{\mathrm{wall}}}{C_{\mathrm{w}}} \tag{3.34b}$$

where i is the past cycle number, T_{cool} is the engine coolant temperature, Q_{wall} is the bulk heat transfer during the cycle, L_{w} is the wall thickness, k_{w} is cylinder wall thermal conductivity, A_{w} is the contact area between the wall and hot gases, t_{cyc} is the time it takes to complete one engine cycle defined in the equation $t_{\mathrm{cyc}} = \frac{120}{N_{\mathrm{s}}}$, ρ_{w} is the density of the cylinder wall material, and $c_{\mathrm{p,w}}$ is the heat capacity of the cylinder wall material. The contact area A_{w} is assumed equal to the exposed side wall area when the piston is at TDC as most of the heat transfer takes place during combustion when the cylinder volume is at or close to a minimum. Material constants are from (Incropera and DeWitt, 2002) for plain carbon steel and are listed amongst the model parameters in Appendix C.

3.6.2 Thermodynamic Coupling

Engine cycles are also linked by the exhaust gas residual that remains in the cylinder at IVO after the exhaust stroke from the previous cycle. The temperature and composition of the residual mass can impact the temperature of the cylinder mixture at IVC. HCCI combustion is highly dependant on the pressure and temperature history of the cycle and thus different temperatures and pressures at IVC impact the peak pressure, temperature, and combustion timing of the engine cycle (Stanglmaier and Roberts, 1999). The end thermodynamic state of the exhaust mixture from the previous cycle (at IVO) is used as the initial conditions for the next cycle. The initial residual mass of the system is estimated using the ideal gas law in Equation 3.3.

3.6.3 Mode Switch Evaluation

(Boddez, 2011) presents a method for quantitatively evaluating the quality of a mode switch on an experimental basis. The Mode Switch Performance Criterion (MSPC) considers weighted values for mode switch duration, smoothness in IMEP transition, and knock to describe the success of a given mode switch. MSPC is calculated as follows:

$$\sigma_{\text{IMEP trans}} = \sqrt{\frac{1}{\text{Duration}} \sum_{i=1}^{\text{Duration}} \left(\text{IMEP}_{\text{actual}} - \text{IMEP}_{\text{target}}\right)^2} \tag{3.35}$$

$$\mu_{\text{IMEP trans}} = \frac{\text{IMEP}_{\text{actual}} - \text{IMEP}_{\text{final}}}{2} \tag{3.36}$$

$$\text{COV}_{\text{IMEP trans}} = \frac{\sigma_{\text{IMEP trans}}}{\mu_{\text{IMEP trans}}} \tag{3.37}$$

$$\text{MSPC} = \text{Duration} + \frac{1}{2}\left(\frac{\text{COV}_{\text{IMEP trans}}}{0.05} - 1\right)_{\text{COV}_{\text{IMEP trans}} > 0.05} + 5\left(\sum_{i=1}^{\text{Stabilize}} \frac{\text{ROPR}_i}{10} - 1\right)_{\text{ROPR}_i > 10} \tag{3.38}$$

Duration describes the number of cycles in the mode switch, calculated for the experimental results from the cycle where the mode switch is first commanded to the first cycle where the covariance in IMEP drops below a value of 0.05. For the PMSM simulated results a covariance threshold of 0.02 is used instead as it provides a more comparable analysis between the experimental and simulated results. $\text{COV}_{\text{IMEP trans}}$ is the covariance of the IMEP calculated over the mode switch used to describe the smoothness of the mode switch and included while the magnitude is over 0.05 for the experimental data and 0.02 for the simulated results. $\text{IMEP}_{\text{target}}$ is calculated by linearly interpolating the cycle value of IMEP between the steady state SI IMEP value before the mode switch and the steady state HCCI IMEP value after the mode switch. "Stabilize" is the number of cycles that it takes for ROPR to drop below a magnitude of 10 bar/CAD. The knock parameter is based on the maximum rate of pressure rise, which is included if it has a magnitude over 10 bar/CAD. The knock parameter is not applicable for the simulated results because the higher rate of pressure rise due to the single zone model assumptions confounds the rate of pressure rise as a performance indicator. A detailed analysis of MSPC as a mode switch performance indicator is given in (Boddez, 2011).

3.7 Model Summary

A physics-based multi-zone model (PMSM) has been developed to simulate mode switches between SI and HCCI combustion modes on a single cylinder engine. The PMSM is based on a single zone phenomenological SI model developed for this

study and a single zone HCCI model with detailed chemical kinetics, adapted from (Kongsereeparp, 2008). It is assumed that the engine speed remains constant through the cycles, no blow-by occurs, temperature, pressure, volume, and composition of the gas mixture are related by the ideal gas law, and heat transfer to the cylinder walls is convective heat transfer. The intake and exhaust manifold temperatures and pressure are assumed to be constant throughout the engine cycles. Heat release is described by a Wiebe function in the SI model and by chemical kinetics based on the GRI-Mech 3.0 (Smith et al., 1999) mechanism for HCCI. Figure 3.4 summarizes the model equations of the PMSM for each stroke of simulated engine operation. Model parameters are listed in Appendix C. A stiff ordinary differential equation solver, ODE15s, is used in MATLAB® to numerically solve the differential equation models.

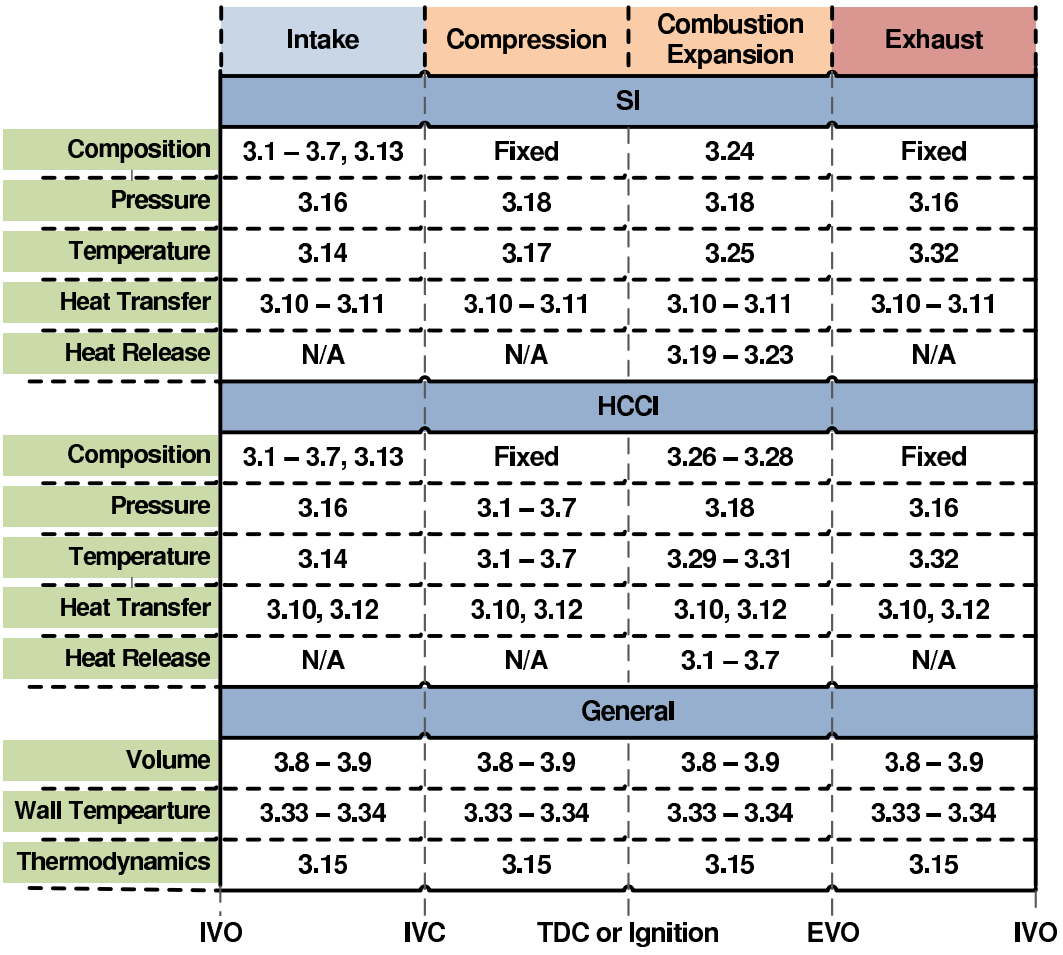

Figure 3.4: PMSM Model Equation Summary. Numbers in the Table Denote Equation Numbers.

Chapter 4

Model Parametrization and Validation

4.1 Experimental Apparatus

A Waukesha Co-operative Fuels Research (CFR) engine capable of operating in both SI and HCCI modes has been modified to run mode switches between SI and HCCI. Modifications have been made to the engine for studies by many individuals, including by not limited to (Atkins, 2004), (Hosseini, 2008), (Handford, 2009), and (Boddez, 2011).

The Waukesha CFR engine depicted in Figure 4.1 was originally designed for determining the octane numbers of fuels by testing the fuels' knock limits. The CFR engine is designed to withstand high levels of knock, making it extremely useful for testing combustion modes at knock levels that could be harmful to a normal engine.

4.1.1 Engine Components

The following table outlines the components that comprise the University of Alberta's CFR test engine setup. Numbers in the table correspond with the engine schematic in Figure 4.2. Table 4.1, Table 4.4, Figure 4.1, Figure 4.2, and Figure 4.3 are adapted with permission from the work of (Boddez, 2011).

Table 4.1: Components used in Experimental Setup. Adapted from (Boddez, 2011)

Item	**Description**	**Manufacturer**	**Model**
1	Air Pressure Regulator	Lincoln	600008
2	Air Mass Flow Meter	TSI	42350101
3	Pressure Relief Valve	Conbraco Ind.	13-202 (10 psi)
4	Bypass Valve	-	1" NPT
5	210L Buffer Tank	-	-
6	Electronic Throttle	Woodward	8404-2019 (1" L-Series)
7	3 kW Electric Heater	-	-
8	CNG Fuel Injector	Ford	F5TE-B5A
9	Needle Valve	Swagelok	1/4"
10	Condenser Coils	In-House Design	-
11	CFR Engine	Waukesha	Optical Research Head
12	Spark Plug	NGK	BR8HS-10
13	EGR Loop	-	1" pipe
14	EGR Control Valve	Swagelok	SS-12NRF8-G
15	Gate Valve	WOG	2" 200
16	Needle Valve	Swagelok	1/4"
17	Condensing Coils	In-House Design	1/4" Swagelok Tubing
18	CNG Mass Flow Meter	Omega	FMA-A2117
19	3.5L Buffer Tank	-	-

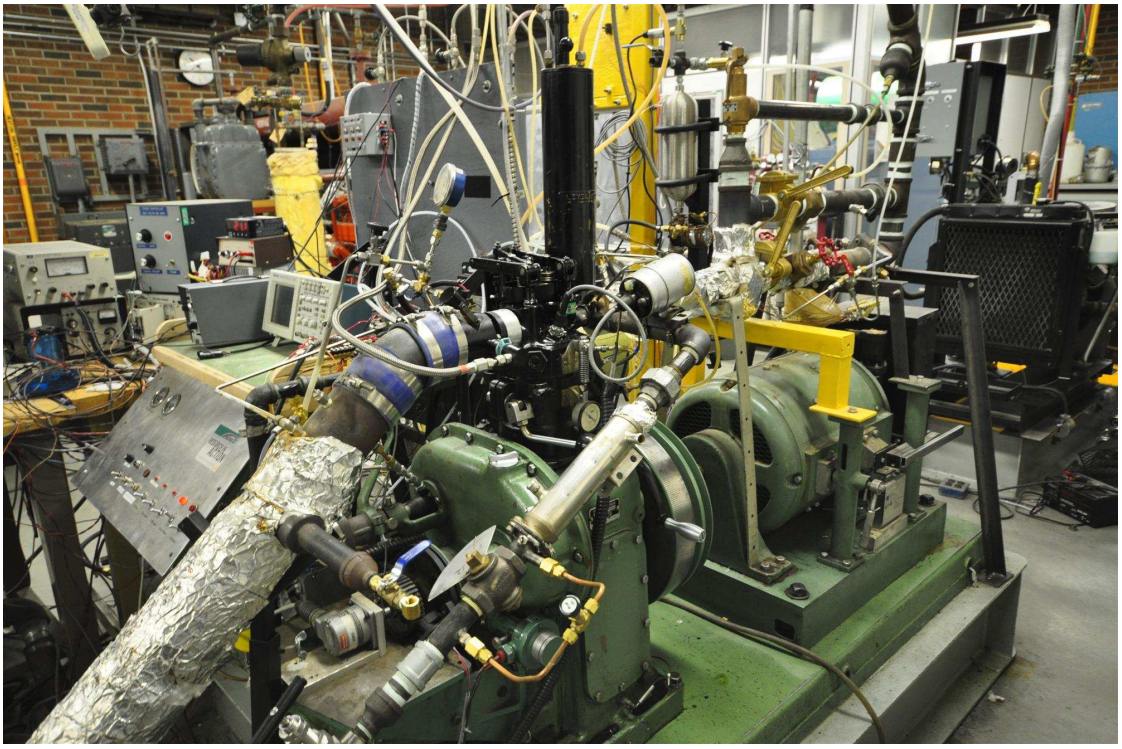

Figure 4.1: CFR Engine Test Setup. Adapted from (Boddez, 2011)

4.1.2 Engine Specifications

The engine is a single cylinder Waukesha CFR engine with an optical head installed to allow for in-cylinder instrumentation. The intake air pressure is boosted with the use of a high capacity building air compressor and is pumped into the intake system where a 210 L buffer tank is used to help minimize pulsations. The air moves through the intake manifold, which has a capacity of approximately 10 L in the large configuration, and is heated by an electric resistive heater as it moves through the manifold. Intake pressure is controlled by the Woodward electronic throttle valve, which has a modified sleeve to reduce the orifice diameter from 1" to 5/8" to help achieve the necessary pressure reductions required for low load SI operation. In the early tests by (Boddez, 2011) the intake manifold volume was approximately 10 L. The volume was later reduced to approximately 0.5 L by moving the throttle downstream of the intake heater, item 7 in Figure 4.2.

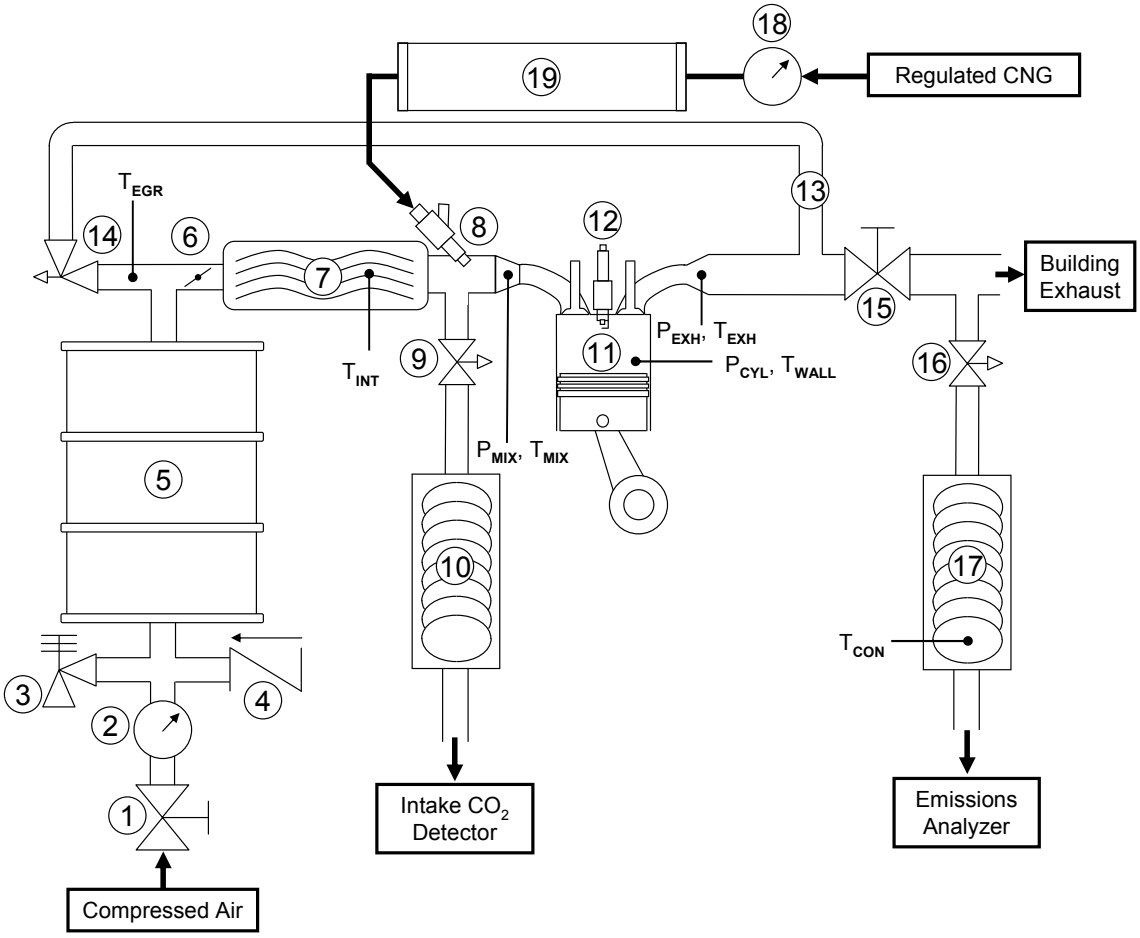

Figure 4.2: Experimental CFR Engine Setup Schematic. Adapted from (Boddez, 2011) with permission

Table 4.2: CFR Engine Geometry

Component	**Description**
Piston	Flat Top
Combustion Chamber	Disk Shape
Bore	8.255 cm (3.250")
Stroke	11.43 cm (4.500")
Connecting Rod Length	25.40 cm (10.0")
Cylinder Wall Thickness	0.792 cm (0.312")
Clearance Volume	Variable
Displacement Volume	0.612 L (37.33 in^3)

Table 4.3: Intake and Exhaust Valve Timing Relative to Piston Top Dead Center

Valve Event	**Timing**
IVO	350° bTDC
IVC	146° bTDC
EVO	140° aTDC
EVC	375° aTDC

Reduction of the intake manifold volume allows for more immediate control of the intake air pressure during the intake stroke.

The single cylinder, 4 stroke, test engine has dimensions provided in Table 4.2. The optical head is outfitted with a Kistler 6043A piezoelectric pressure transducer that is used to measure in-cylinder pressure as well as a NGK BR8HS-10 spark plug, which provides the spark for the SI combustion mode. The engine is cooled by water coolant that maintains a temperature close to 100 °C throughout the tests.

Exhaust temperature and pressure are measured in the exhaust manifold with the use of a thermocouple and pressure transducer. The timing of the intake and exhaust valves is outlined in Table 4.3.

Near constant engine speed is achieved with the use of a large fly-wheel and an active dynamometer attached to the crank shaft of the engine.

4.1.3 Engine Data Analysis

A detailed on-board data analysis and engine control program was developed by (Boddez, 2011) and provides cycle by cycle updates on engine performance parameters that can then be fed into control systems. The specific equipment and modifications made to the CFR engine setup are outlined in (Boddez, 2011). The engine program is responsible for regulating throttle position to obtain desired intake pressure through use of a PI controller, specifying fuel injection pulse width, controlling spark activation, and logging data from the various thermocouples, pressure transducers, gas analyzers, and crank shaft encoder. The logged data is then processed in real time to obtain cycle-by-cycle values for engine performance parameters such as IMEP, CA50, efficiency, and rate of pressure rise. This processed data is stored for further post-processing. Figure 4.3 schematically shows the engine control scheme and data analysis system.

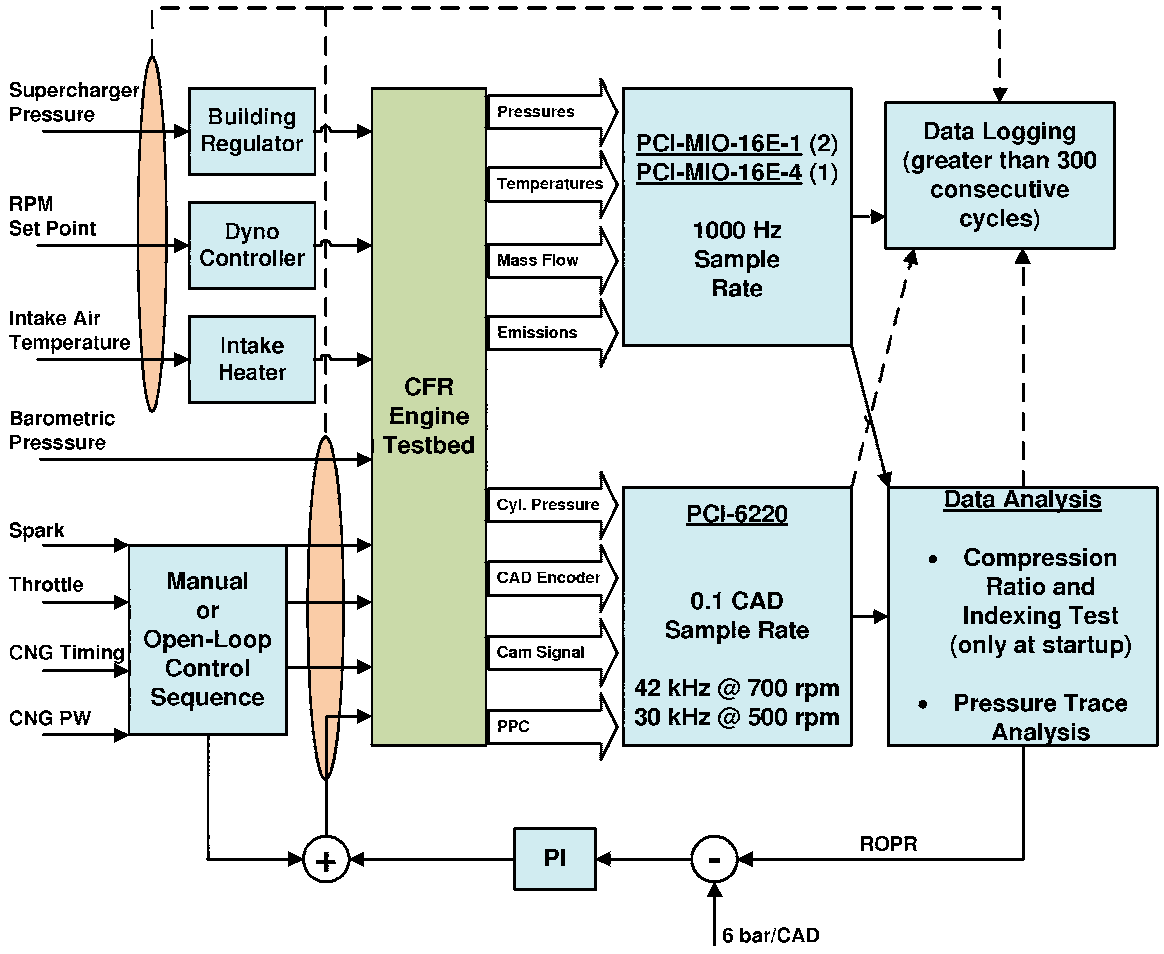

Figure 4.3: Engine Control Schematic. Adapted from (Boddez, 2011) with permission

Table 4.4: Uncertainty at 95% Confidence for Values Presented in Mode-Switching Data Plots. Adapted from (Boddez, 2011) with permission

Parameter	**Uncertainty**
Average Intake Pressure	0.027 bar
P_{IVC}	0.027 bar
CNG PW	-
CNG Timing	1.1 CAD
IMEP	0.06 bar
CA50	0.83 CAD
ROPR	0.03 bar/CAD
Equivalence Ratio	12%

The uncertainties in many of the measurements throughout a mode switch, as calculated by (Boddez, 2011), are reproduced with permission in Table 4.4.

4.2 Model Parametrization

The model parametrization is based on steady state SI and HCCI operating conditions outlined in Tables B.4 and B.5 of Appendix B. The volumetric efficiency (η_v) is tuned for both the afore mentioned operating point with large intake manifold configuration and small intake manifold operating conditions outlined in Tables B.6 and B.7. Engine speed is assumed to be constant at 700 rpm. Figure 4.4 shows the experimental engine speed through a mode switch consistent with operating conditions in Tables B.4 and B.5 of Appendix B. In this and following sections, cycles are labeled in figures with either SI or HCCI followed by a number. SI indicates a spark ignition cycle and HCCI indicates a homogeneous charge compression ignition cycle, occurring the number of cycles indicated in the label number from the initial mode switch actuation. In SI - HCCI mode switches SI 0 is the last SI cycle and HCCI 1 is the first HCCI cycle. In HCCI - SI cycles HCCI 0 is the last HCCI cycle and SI 1 is the first SI cycle.

As can be seen in Figure 4.4 the experimental engine speed first undershoots

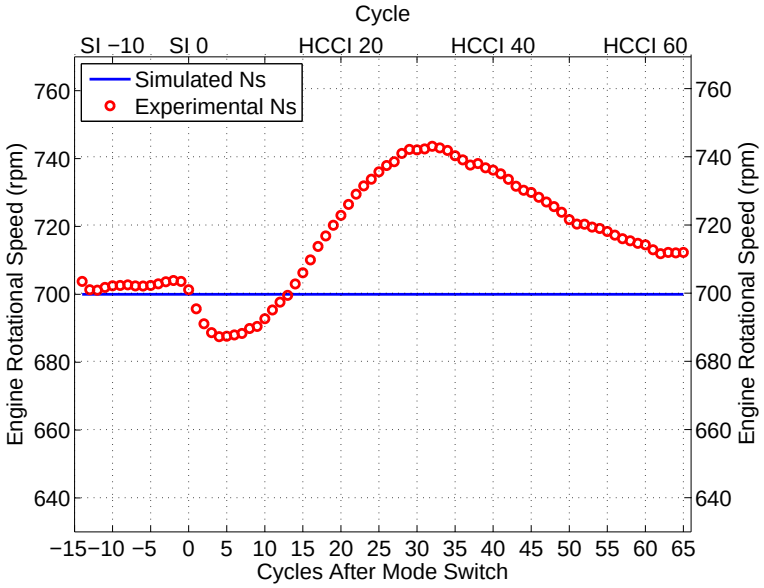

Figure 4.4: Simulated and Experimental Engine Rotational Speeds over a SI - HCCI Mode Switch

the set point value of 700 rpm by a little over 2 %, after which the dynamometer corrects the engine speed resulting in an overshoot of just over 6 %. The assumption of a constant 700 rpm engine rotational speed does not capture all of the dynamics during the mode switch, but exact prediction of the engine speed resulting from control by the active dynamometer would not be possible and thus constant engine speed is assumed. The sensitivity analysis in Section 5.1 further discusses the validity of a constant engine speed assumption.

4.2.1 Intake Model

Intake pressure is assumed constant at the experimentally determined value, and fresh intake air temperature is assumed constant since changes in intake temperature occur on a time scale that is much longer than a single engine cycle. The PMSM intake model is explained in detail in Section 3.2. Table 4.5 shows the simulated and experimental values for conditions at IVC.

The data in Table 4.5 is the average of 50 cycles that have been simulated in

Table 4.5: Intake Valve Close Conditions for SI Model and SI Experimental Data

	SI Model	**SI Experimental**	**Difference (%)**
m_{ivc}(g)	284	283	0.6
P_{ivc}(bar)	0.58	0.53	8.0
ϕ	0.843	0.819	2.9

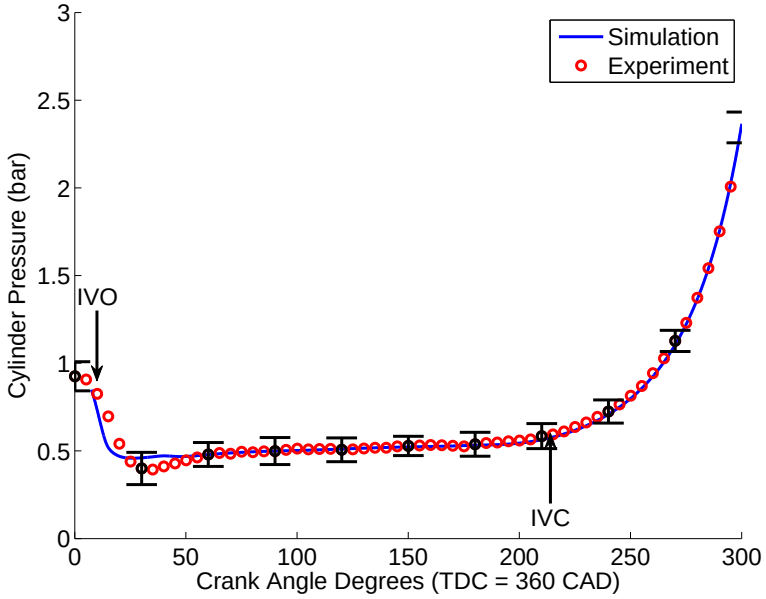

Figure 4.5: SI Intake Pressure - Simulated and Experimental

spark ignition mode after a 30 cycle period that allows the wall temperature and exhaust temperature to stabilize from the initial values used in the model. From Table 4.5 one can see that the SI model closely tracks the experimental results at these conditions.

The simulated and experimental pressure traces are compared in Figure 4.5. Error bars on the figures in this chapter represent two standard deviations in the experimental data over 50 cycles from the same experimental run and operating conditions. Figure 4.5 shows that the model closely tracks the experimental pressure trace during the intake stroke. The pressure fluctuations observed in the experimental results during the intake stroke is a product of residual exhaust gases pulsing into the intake manifold as the intake valve opens. The PMSM does not ac-

Table 4.6: Intake Valve Close Conditions for HCCI Model and HCCI Experimental Data

	HCCI Model	**HCCI Experimental**	**Difference (%)**
m_{ivc}(g)	666	657	1.4
P_{ivc}(bar)	1.32	1.21	9.7
ϕ	0.440	0.455	-3.2

count for pulsations in the system and thus some of the cylinder pressure dynamics are not captured during the intake stroke. Other discrepancies between the experimental and simulated results exist because of converting the cylinder pressure trace from gauge pressure to absolute pressure. This conversion, or 'pegging', is required due to the pressure sensor being a piezoelectric based sensor that measures relative pressure. The pegging is done by assigning data points during the intake stroke, between 160-165 CAD, to P_{ivc} as measured experimentally in the intake manifold. All remaining data points in the cycle are moved up or down by the same relative amount as the intake data points are moved. A detailed explanation of how P_{ivc} is measured can be found in (Boddez, 2011). The PMSM successfully approximates the experimental data within the experimental uncertainty range of two standard deviations. Approximation of the equivalence ratio within 2.9 % and intake mass at IVC within 0.6 % is achieved by tuning the volumetric efficiency term used to approximate the intake charge composition as outlined in equation 3.2.

Table 4.6 shows the modeled and experimental conditions at IVC averaged over 30 cycles for steady state HCCI combustion. The biggest difference from the SI to HCCI intake models is the value of volumetric efficiency. The HCCI model is similarly tuned using volumetric efficiency, which is approximated as higher when running in HCCI mode than in SI mode. Table 4.6 shows that the conditions at IVC from the HCCI model are similar to the experimental values. The differences in intake charge mass, equivalence ratio, and IVC pressure are similar to those observed when modeling the engine in SI mode.

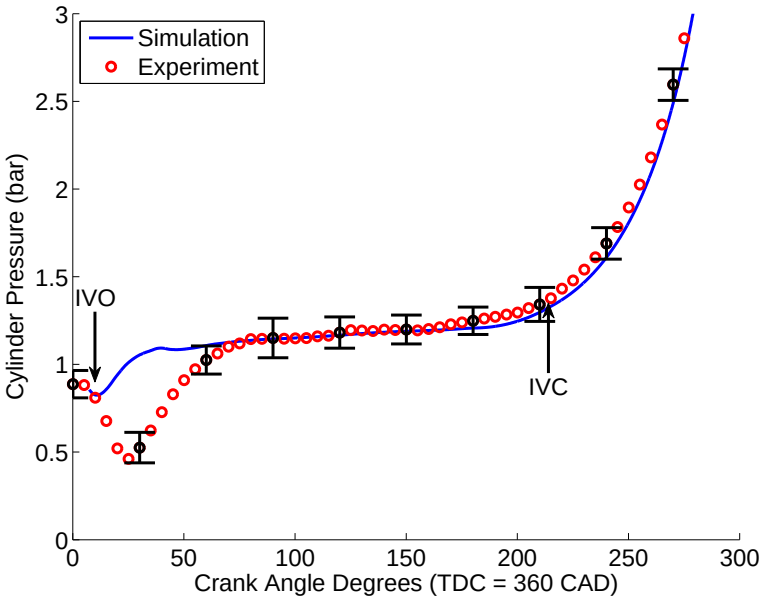

Figure 4.6: HCCI Intake Pressure - Simulated and Experimental

The intake pressure trace from steady state experimental HCCI operation is compared in Figure 4.6 with the HCCI simulation results. The simulated HCCI pressure trace in Figure 4.6 matches the experimental results with similar accuracy to that found for the SI model, with the simulated pressure trace lying within experimental uncertainty regions for most of the intake stroke. Similar accuracy between the SI and HCCI models is to be expected because the models operate on the same differential equations and many of the same basic assumptions despite the fact that they were developed separately. The largest difference between the model and experimental pressure traces is evident early in the intake stroke. Pulsations in the intake system are likely the cause of discrepancies between the modeled and experimental results, since the PMSM assumes constant intake pressure and does not consider pulsations in the system. Some discrepancies exist between the simulated and experimental data in the intake pressure traces, but HCCI combustion is highly influenced by the cylinder conditions at IVC. Since the simulation accurately predicts cylinder pressure, temperature, and composition at IVC, differences between the experimental and simulated intake pressure traces early in the stroke

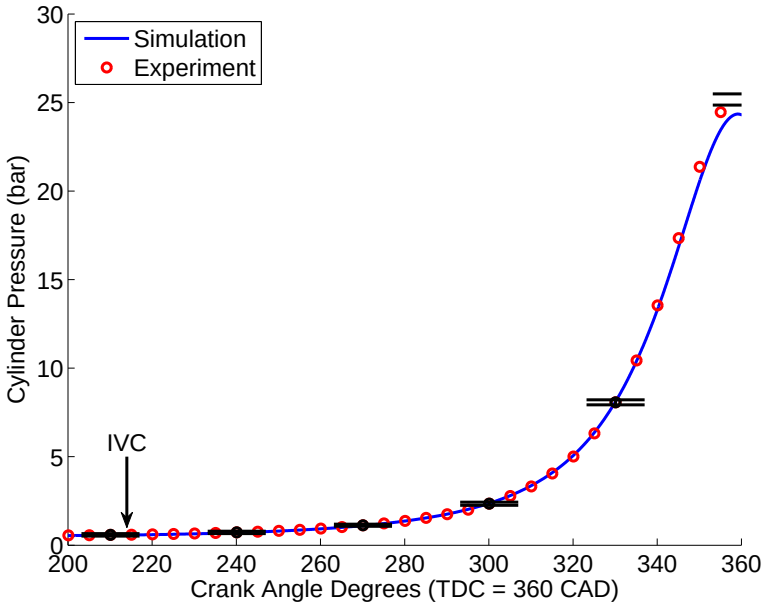

Figure 4.7: SI Compression Pressure - Simulated and Experimental

will not affect the compression model.

4.2.2 Compression Model

The compression model is used from IVC until ignition or TDC (360 CAD), whichever comes first. The model summary in Chapter 3 for the compression model describes in detail the processes that occur during the compression stroke of the engine. During this stroke, the pressure is highly dependant on the changing volume of the cylinder and thus the engine rotational speed and compression ratio. At the same time the pressure is also dependant on changing temperature as a result of boundary work and heat transfer from the cylinder walls. Figures 4.7 and 4.8 show the experimental and simulated pressure traces of SI and HCCI respectively from IVC until TDC.

In both cases, the simulated pressure traces closely match the experimental values through most of the curve. Near TDC (360 CAD) the simulated results diverge somewhat from the experimental data, possibly due to the equations not fully capturing the engine physics or the model parameters being slightly mismatched

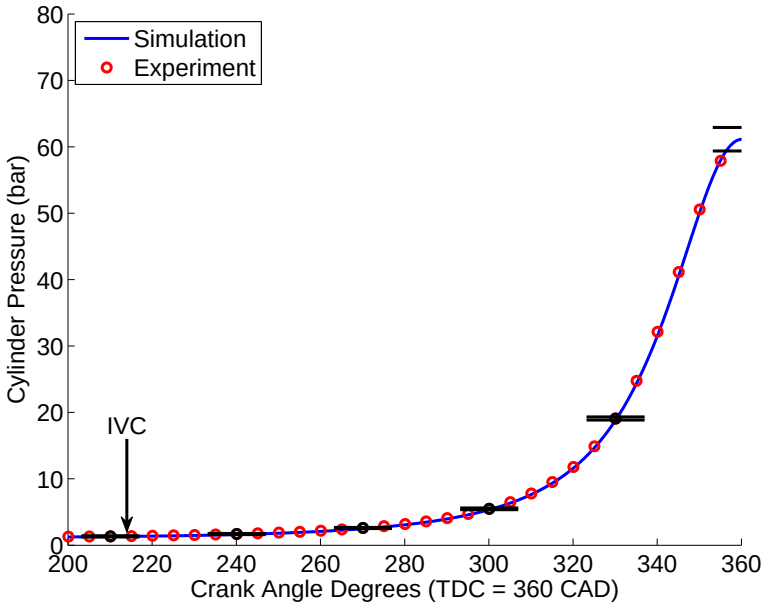

Figure 4.8: HCCI Compression Pressure - Simulated and Experimental

for the experimental data. Compression ratio is slightly higher in the simulated systems than calculated experimentally to allow for better pressure trace matching and to promote ignition in the HCCI model. The heat transfer coefficients in equations 3.10 and 3.11 are adjusted slightly from those values initially specified in (Woschni, 1967) to help match the pressure traces and account for differences in engine geometry and in-cylinder gas motion. The model parameters are listed in Appendix C.

4.2.3 Ignition, Heat Release, and Expansion Model

The ignition, combustion and heat release, and expansion phases are very different between the SI and HCCI model so they are validated separately.

4.2.3.1 Spark Ignition Combustion

The SI combustion process and heat release is described by a modified Wiebe function (Ramos, 1989). Spark timing and burn duration are specified in the Wiebe function, which describes the combustion process by providing a model for

mass fraction of mixture burnt. The mass fraction of mixture burnt is used to calculate an incremental amount of heat released using the lower heating value and to update the conversion of reactants to products, which are assumed to be complete products for the SI model. The spark timing and burn duration are chosen by hand using an optimization process where 110 SI cycles are simulated with spark timing ranging from -5 to 5 degrees after top dead center (aTDC) with a step value of 1 CAD and combustion duration ranging from 40 to 85 CAD with a step value of 5 CAD for each spark timing value. Each parameter is varied individually to produce a pressure trace that is then matched to the experimental pressure trace. The optimal spark timing and combustion duration are defined as those that minimize the sum of square errors of the simulated pressure trace compared to the experimental pressure trace evaluated at each $\frac{1}{10}$ of a crank angle degree. The simulated case with the best fit to the experimental pressure trace has a spark time of 1 CAD aTDC and a combustion duration of 60 CAD. The operating conditions and model parameters do not change substantially for SI cycles in the simulation runs because of the narrow operating range of SI at high intake temperatures on the CFR test engine. Operating conditions for SI cycles are outlined in detail in Appendix B. The optimized combustion and expansion pressure trace for SI is shown in Figure 4.9.

As can be seen in Figure 4.9 the simulated results match the experimental results with similar accuracy to that seen in the compression model. The heat transfer correlation in the SI model does have a large impact on the shape and magnitude of the simulated pressure trace. However, in this case the original correlation suggested by (Woschni, 1967) with some modifications from (Chang et al., 2004) was found to be sufficient and was not altered. The optimization process for choosing spark timing and combustion duration appears to be sufficient given the large amount of variation in the experimental pressure traces in the heat release

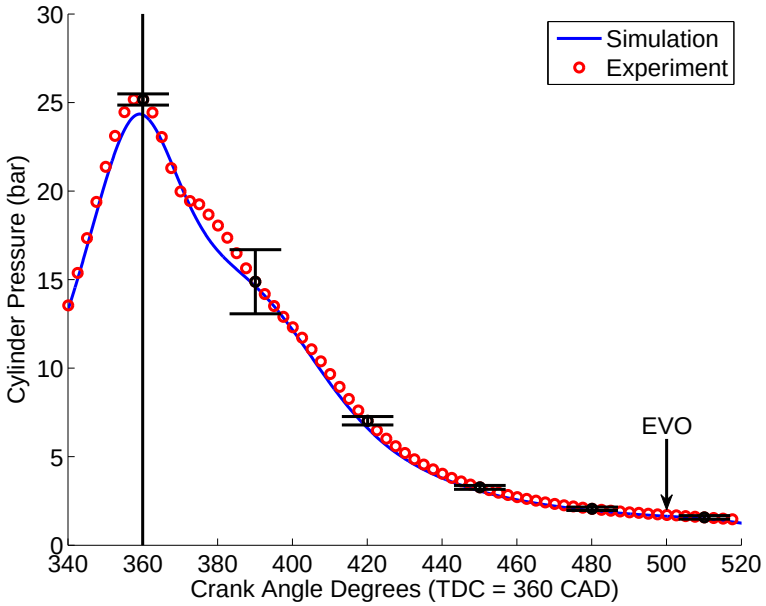

Figure 4.9: Optimal SI Combustion and Expansion Pressure - Simulated and Experimental

region represented by the two standard deviation experimental uncertainty bars shown in Figure 4.9.

4.2.3.2 HCCI Combustion

The HCCI combustion process is governed by the detail chemistry of the single zone model. Once a high enough temperature is achieved ignition occurs, which is the rapid increase in the rates of reaction for the elementary reactions modeled using the GRI-Mech 3.0 reaction mechanism (Smith et al., 1999). The combustion process continues until the reactants are consumed, temperature is reduced as a result of heat loss, and the cylinder volume expands, resulting in the reduction of reaction rates to a point where they are once again insignificant.

Figure 4.10 shows the pressure trace from the simulated and experimental HCCI combustion and expansion zones. What can be seen in Figure 4.10 is that the simulation predicts ignition timing of approximately 367 CAD compared to 361 CAD determined experimentally. The predicted CA50 timing is closer with the simulation

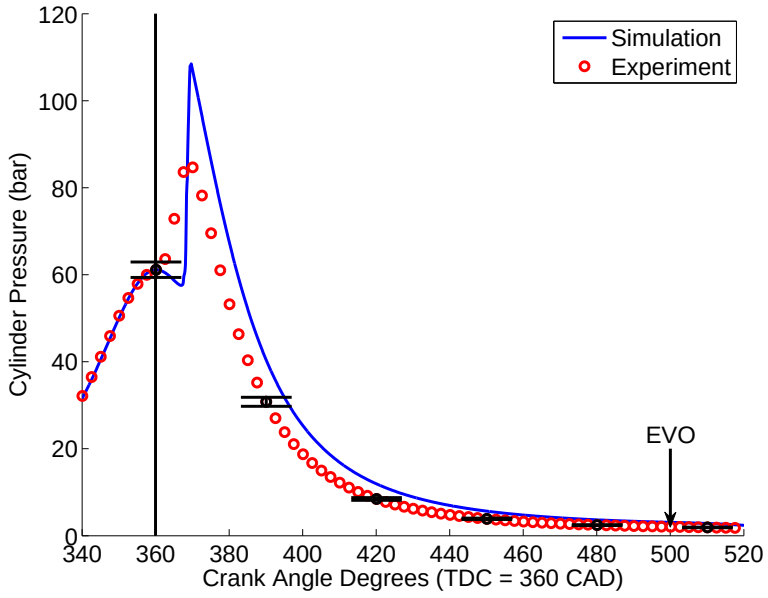

Figure 4.10: HCCI Combustion and Expansion Pressure - Simulated and Experimental

predicting 8.7 CAD aTDC compared to an experimental value of 3.9 CAD aTDC. The simulated pressure trace also differs from the experimental pressure trace. In a single zone model it is assumed that ignition occurs simultaneously throughout the entire cylinder, resulting in prediction of a short combustion duration and thus a much faster pressure rise and peak pressure than observed experimentally. While, a multi-zone model would more accurately represent the pressure trace, the single zone model captures the ignition timing of the mixture with reasonable accuracy and can be simulated in less than 2 % of time that it would take to simulate a full multi-zone model (Kongsereeparp, 2008). The high peak pressure as a result of the fast combustion chemistry also leads to a much higher IMEP and efficiency from the simulation than what is observed experimentally. The heat transfer rate during expansion is tuned to a value that is twice as high as the original value suggested in (Woschni, 1967) to compensate for the high peak pressure and increase the simulation's ability to predict exhaust conditions such as T_{exh}. Model parameters are listed in Appendix C.

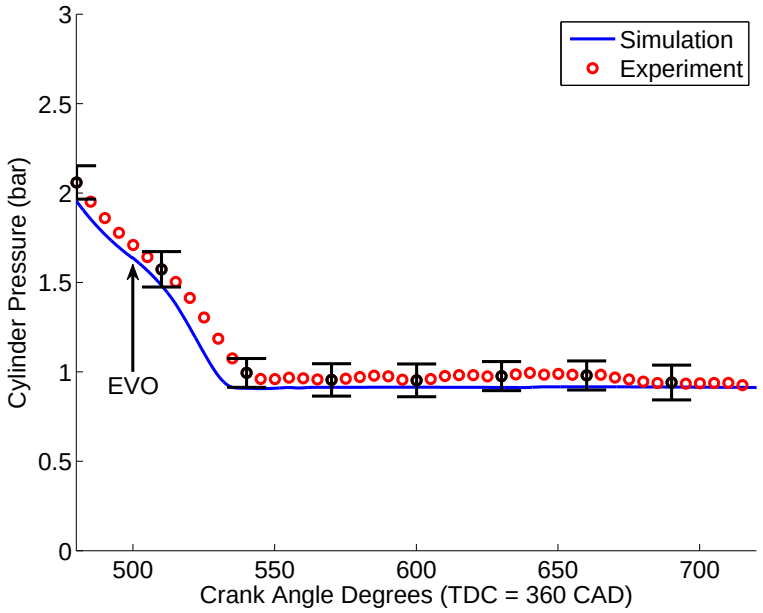

Figure 4.11: SI Exhaust Pressure - Simulated and Experimental

4.2.4 Exhaust Model

The exhaust stroke model spans from EVO to IVO and depends on the pressure and temperature history from the expansion models. Figures 4.11 and 4.12 show exhaust pressure traces of simulated data compared to experimental data for the SI and HCCI models respectively.

As can be seen in Figures 4.11 and 4.12, the simulated pressure traces have a similar shape to the experimental pressure traces. Differences between experimental results and simulated results can be largely attributed to the cycle pressure history before the EVO event. In the SI model, the differences are likely the result of using the Wiebe function to describe the heat release, and the fact that only a single zone is considered. Similarly, differences in the HCCI pressure trace between modeled and experimental results is attributed to the high overshoot in pressure that occurs due to the use of a single zone model. For the most part, simulated results fall within two standard deviations of the experimental results later in the cycle. The use of multiple zones and a detailed look at mass flows and heat transfer

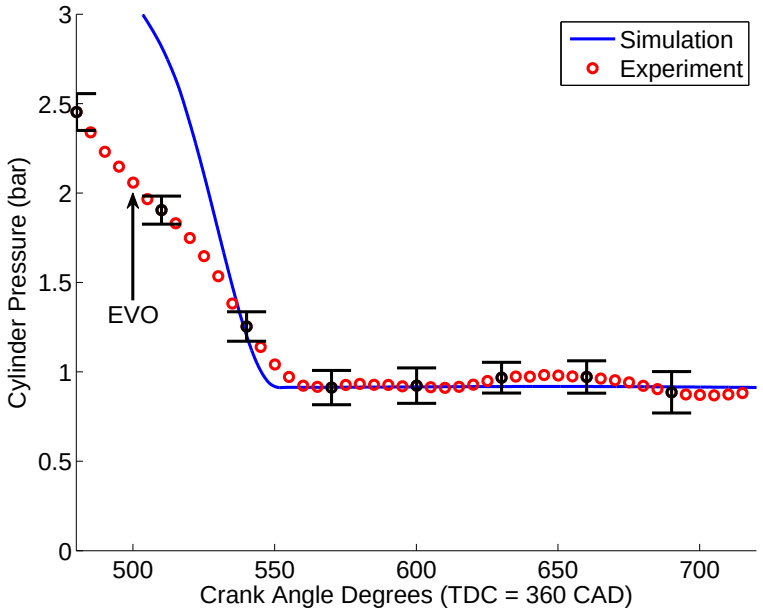

Figure 4.12: HCCI Exhaust Pressure - Simulated and Experimental

Table 4.7: Exhaust Valve Open Conditions for SI Model and SI Experimental Data

	SI Model	**SI Experimental**	**Difference (%)**
T_{exh}(K)	771	699	10.2
P_{exh}(bar)	0.913	0.913	0.1
T_{wall}(K)	395	N/A	N/A

rates between zones could improve this model (Kongsereeparp, 2008), but would result in a model that is more computationally intensive than required for this study. Similar to the intake model, the exhaust model assumes flow only through the exhaust valve.

Tables 4.7 and 4.8 summarize the simulated and experimental exhaust conditions for the SI and HCCI cycle models respectively and compare the results with experimental values.

The exhaust pressure in the simulation is specified to be the same as the experimental exhaust manifold pressure and constant through all cycles. The small error observed between experimental and simulated exhaust pressure values exists because of small cycle to cycle variances in experimental results. The exhaust tem-

Table 4.8: Exhaust Valve Open Conditions for HCCI Model and HCCI Experimental Data

	HCCI Model	**HCCI Experimental**	**Difference (%)**
T_{exh}(K)	645	562	14.7
P_{exh}(bar)	0.913	0.915	0.2
T_{wall}(K)	383	N/A	N/A

perature is over predicted in the SI model by about 10 % and in the HCCI model by about 15 %, perhaps as a result of the pressure overshoot from the single zone model in the HCCI model, and differences between specified and experimental spark and combustion duration values in the SI model. The temperature variations are relatively small when considering the number of assumptions that have been made leading up to the exhaust models. The cylinder wall temperature is also tabulated, and is higher in SI combustion than in HCCI combustion by about 12 K, which is expected because of the lower combustion temperatures in HCCI combustion. There is no experimental cylinder wall temperature measurement available.

4.3 Cycle Validation

The full cycle experimental and simulated pressure traces from the operating points defined in Tables B.4 and B.5 of Appendix B are shown in Figures 4.13 and 4.14 respectively. These operating conditions are used for parametrization of the models.

Figure 4.13 shows the simulated SI pressure trace over the full cycle closely matches the experimental pressure trace. Figure 4.14 shows the simulated HCCI pressure trace over the full cycle is similar to the experimental pressure trace, with deviation expected after ignition because of the greater rate of pressure rise calculated by the single zone model after ignition.

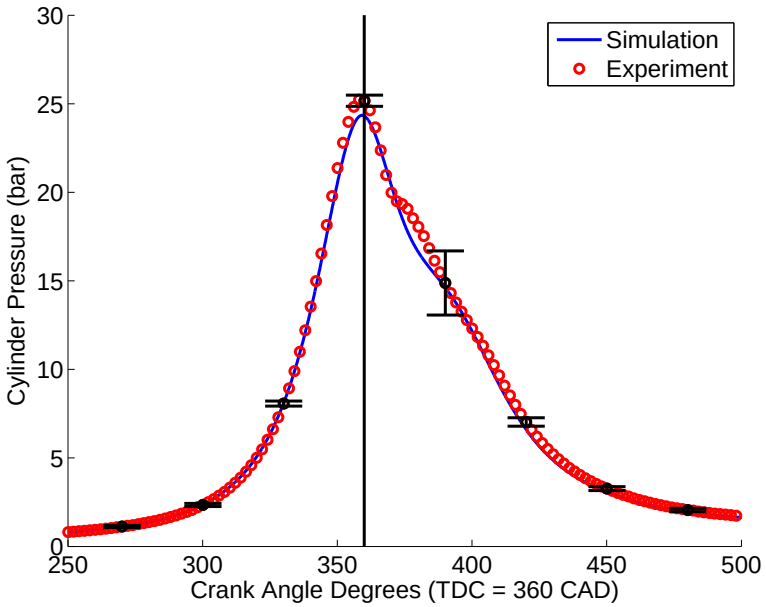

Figure 4.13: SI Full Cycle Pressure at the Operating Point Defined in Table B.4 - Simulated and Experimental

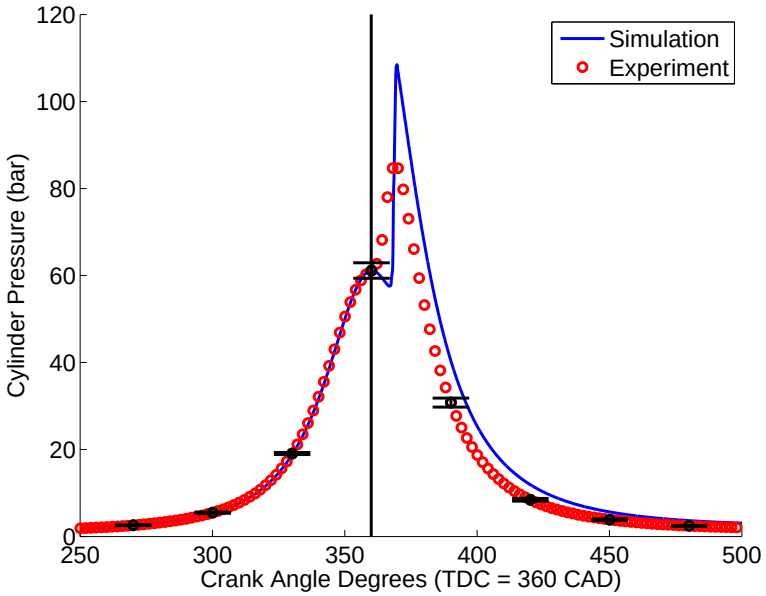

Figure 4.14: HCCI Full Cycle Pressure Traces at the Operating Point Defined in Table B.5 - Simulated and Experimental

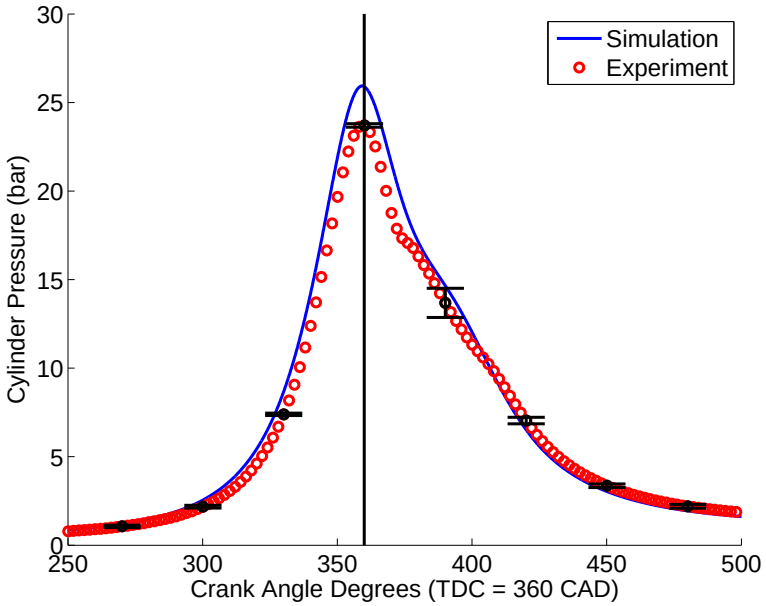

Figure 4.15: SI Full Cycle Pressure Traces at the Operating Point Defined in Table B.10 - Simulated and Experimental

4.3.1 Cycle Cross Validation

The SI and HCCI engine cycle models are cross validated by comparing simulated results to a slightly different set of operating conditions as outlined in Tables B.10 and B.11 of Appendix B, allowing only the inputs and the volumetric efficiency to change for the smaller intake manifold configuration. The pressure traces of the entire cycle for both SI and HCCI simulations are compared to experimental values in Figures 4.15 and 4.16 respectively.

Figure 4.15 shows a good matching of the simulated SI pressure trace to the experimental pressure trace. There is some variation in peak pressure because of the assumption of an "ideal" single zone engine with homogeneous mixture and approximated heat transfer. The pressure rise due to combustion of the mixture is also difficult to match exactly. Combustion heat release approximated by the Wiebe function results in a reasonable match of pressure traces. The model matches experimental results almost as well as in Figure 4.13, although the estimate of peak pressure is less accurate. For a more accurate analysis the model would require

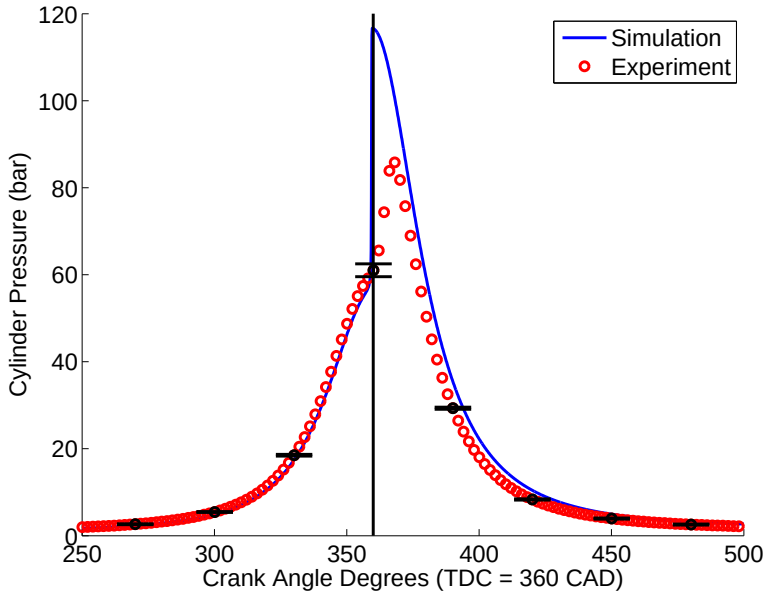

Figure 4.16: HCCI Full Cycle Pressure Traces at the Operating Point Defined in Table B.11 - Simulated and Experimental

detailed chemistry and multiple zones, which for a segregated solver model with several zones could take the computational time from 30 seconds per cycle to 2 hours per cycle and as much as 9 hours per cycle when using a fully coupled multi-zone model (Kongsereeparp, 2008), eliminating the ability to run this model quickly and try a number of mode switch strategies.

The HCCI pressure traces in Figure 4.16 show a higher level of variability between experimental and simulated results than seen in the SI pressure traces or the HCCI pressure traces of Figure 4.14. The use of a single zone model for simulating HCCI combustion has a greater impact on the shape of the pressure curve than when simulating SI combustion because the prediction of simultaneous mixture ignition throughout the combustion chamber results in an overshoot in peak pressure. Figure 4.16 shows that the combustion timing is approximated within 6 CAD. This information is important for simulating a mode switch as it helps to indicate whether there is a possibility of knock occurring due to early ignition.

4.4 Mode Switch Validation

With both the SI and HCCI models validated for steady state operation, the models are combined to create the PMSM. To validate the PMSM over a mode switch the experimental results of (Boddez, 2011) are used for four different mode switch profiles: a step increase in intake pressure, first order increase in intake pressure, an HCCI-SI mode switch with a gradual decrease in pressure, and a mode switch optimized for both fueling rate and intake pressure profile.

For each of the validation runs, experimentally determined intake pressures, exhaust pressure, intake temperatures, exhaust temperatures, fueling profiles, and spark profiles, are input to the simulation to show how closely the model tracks the experimental values during the mode switch. The mode switch figures show IMEP (bar) and fuel injector pulse width (ms) on the left vertical axis, intake pressure (bar) on the right vertical axis, cycles after the mode switch on the bottom axis, and the modeled cycle on the top axis. Fuel injector pulse width (ms) and intake pressure (bar) are indicated on the figures as they are direct inputs for the experimental engine. Cycle 0 after the mode switch denotes the first cycle where inputs change to begin a mode switch. In SI-HCCI mode switches cycle SI 0 is the last cycle where the spark is activated and in HCCI-SI mode switches cycle HCCI 0 is the last cycle before the spark is re-activated.

4.4.1 Intake Pressure - Step Increase

In this test the electronic throttle valve is opened wide in a single step actuation to increase the air pressure to the cylinder facilitating a mode switch between steady state SI operation and steady state HCCI operation. No model parameters are changed during the validation. The intake pressures and fuel injector pulse widths for each cycle are provided as inputs to the simulation from the experimental results. Conditions for these operating points are outline in Tables B.4 and B.5 of

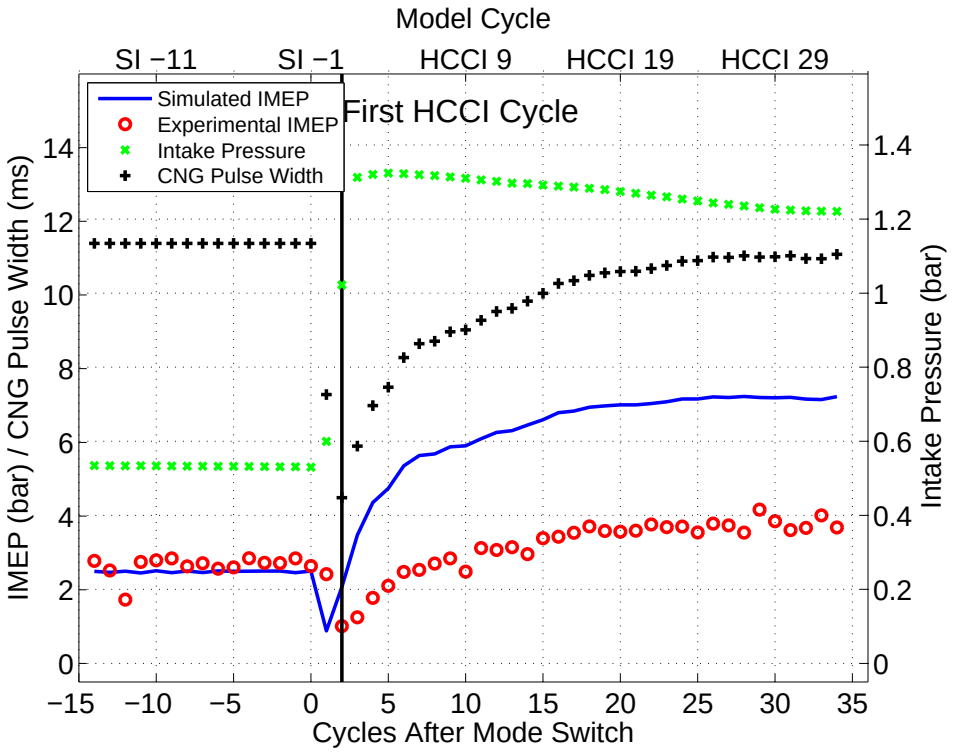

Figure 4.17: SI - HCCI Mode Switch - Step Increase in Intake Pressure 1 - Cycle IMEP - $T_{\text{int}} = 383.15$ K, Large Intake Manifold. $\text{MSPC}_{\text{sim}} = 47.5$, $\text{MSPC}_{\text{exp}} = 51.1$.

Appendix B. At the same time fueling rate is adjusted to a lower value to facilitate obtaining a lean fuel and air mixture, as well as to avoid knock in the first HCCI cycles. Figures 4.17 and 4.18 show the experimental IMEP and ignition timing, represented by CA50 throughout a mode switch compared to simulated values so as to assess the accuracy of the model.

Figure 4.17 shows how IMEP changes as a function of engine cycle during a mode switch initiated by a step increase in intake pressure. This set of experimental results is chosen because it has the lowest "MSPC" value (best performance) of the tests that utilize a step increase in intake pressure due to relatively constant experimental IMEP.

The simulated HCCI cycle IMEP values are much higher than those found experimentally. This can be explained by reviewing the single cycle HCCI validation. The much higher peak pressure predicted by the single zone HCCI model as a re-

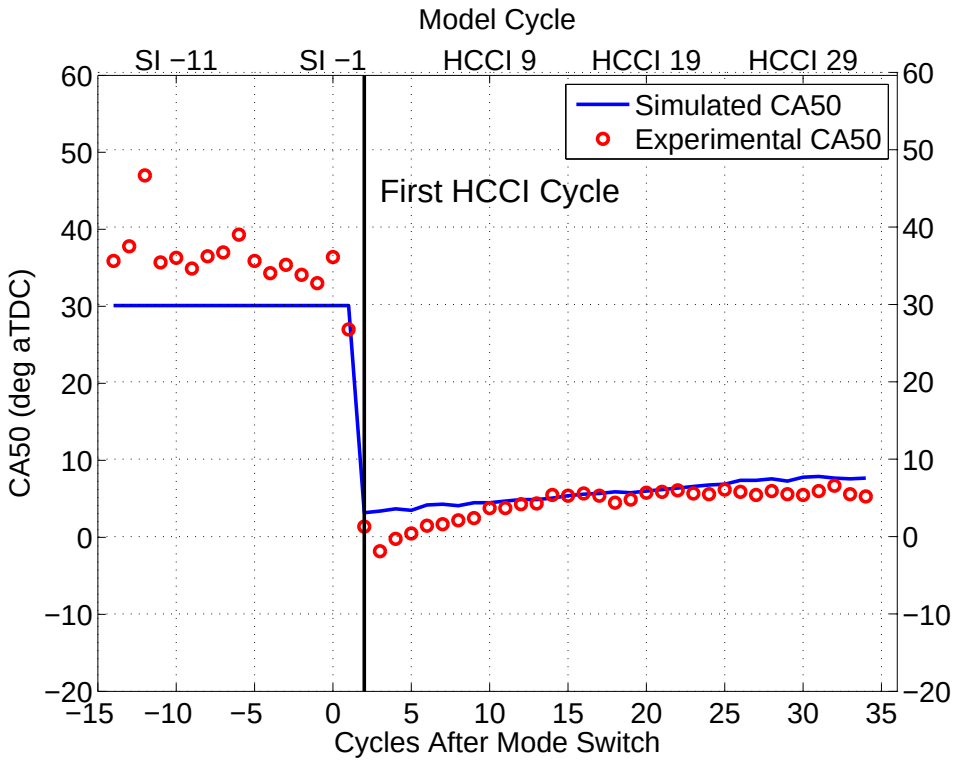

Figure 4.18: SI - HCCI Mode Switch - Step Increase in Intake Pressure 1 - Cycle CA50 - $T_{\text{int}} = 383.15$ K, Large Intake Manifold. $\text{MSPC}_{\text{sim}} = 47.5$, $\text{MSPC}_{\text{exp}} = 51.1$.

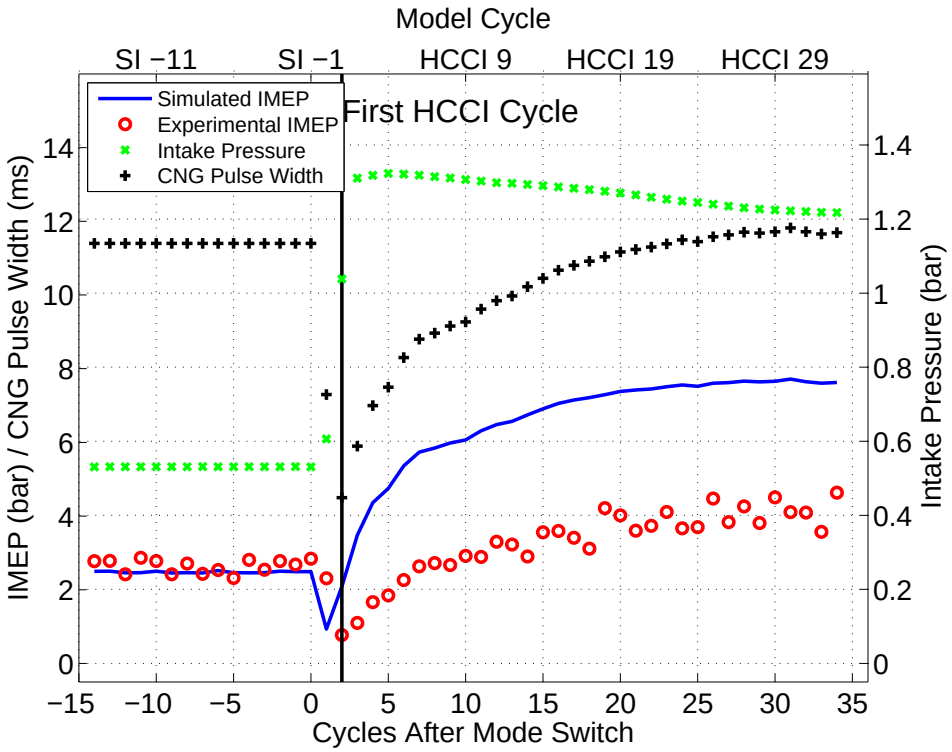

Figure 4.19: SI - HCCI Mode Switch - Step Increase in Intake Pressure 2 - Cycle IMEP - $T_{\text{int}} = 383.15$ K, Large Intake Manifold. $\text{MSPC}_{\text{sim}} = 48.9$, $\text{MSPC}_{\text{exp}} = 79.5$

sult of the fast chemistry results in a higher IMEP. The trend in IMEP through the mode switch is generally the same between experimental and simulated results, which is important when considering a mode switch. In cycle SI 0 the spark is still activated while the intake pressure is increased and the fuel injection rate is decreased resulting in a dip in IMEP, which is more evident in the simulated cycle than in the experimental results. The following cycle, HCCI 1, the spark is deactivated, the intake pressure is raised, and the fuel injection rate is further decreased resulting in HCCI combustion. In the following HCCI cycles the combustion timing retards and the IMEP climbs as the fuel injection rate is increased and the intake pressure is decreased to the steady state value.

Figures 4.19 and 4.20 show the experimental and simulated results of a mode switch the highest "MSPC" value (worst performance) of the experimental results of mode switches initiated by a step increase in intake pressure. The simulated

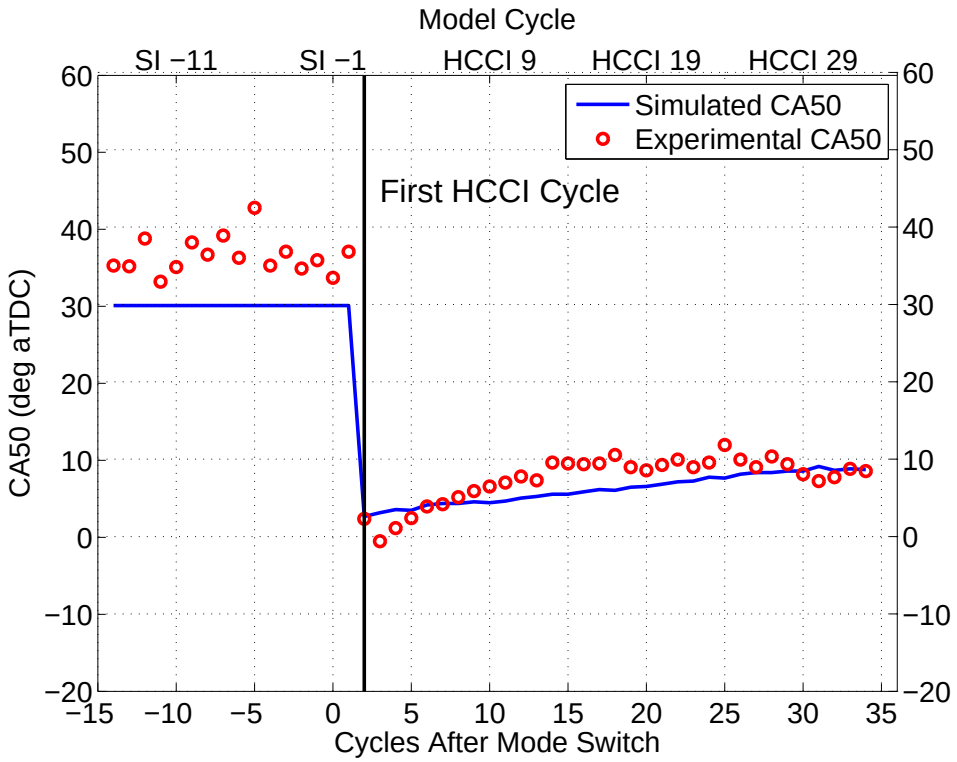

Figure 4.20: SI - HCCI Mode Switch - Step Increase in Intake Pressure 2 - Cycle CA50 - $T_{\text{int}} = 383.15$ K, Large Intake Manifold. $\text{MSPC}_{\text{sim}} = 48.9$, $\text{MSPC}_{\text{exp}} = 79.5$

Table 4.9: MSPC - Step Increases in Intake Pressure

	Sim 1	**Exp 1**	**Sim 2**	**Exp 2**
Duration	19	16	20	34
Smoothness	28.5	33.4	28.9	45.6
Knock	N/A	0	N/A	0
MSPC	47.5	49.4	48.9	79.6

results for CA50 show that the model is able to predict early combustion cycles in the HCCI cycles immediately following the mode switch.

The main difference between the two tests is that, in the second test, instability in the experimental results during the HCCI cycles directly following the mode switch results in an increased mode switch duration and poor performance in the area of IMEP smoothness. In the first test, the fueling rate in the later HCCI cycles is lower than in the second test, as is the CA50 timing. Later CA50 timing in the HCCI cycles of the second test may indicate that these cycles are operating closer to the misfire limit where combustion is more sensitive to the initial cylinder conditions and thus less stable. Less variability at these conditions is seen in the simulated data, because many of the factors in the experimental results that may result in instabilities, such as local hot spots, fuel stratification, and knock, are not modeled. To assist in quantifying the quality of a mode switch the MSPC is used. Table 4.9 outlines the performance of the two mode switches presented in this section and compares the MSPC values of the experimental results with those of the simulated results.

Table 4.9 indicates for the experimental results that the second mode switch has a higher MSPC and is therefore worse than the first mode switch. Differences in MSPC between the two experimental runs result from the prolonged duration in the second experimental mode switch and high variability in IMEP in the HCCI cycles. This variability may be the result of the HCCI cycles operating in proximity to the misfire limit or in-cylinder inhomogeneities that are not captured by the

PMSM. Almost no difference is seen in the MSPC value between the first and second simulated mode switches because the model is not able to capture the same level of variability in IMEP that is seen in the experimental HCCI cycles.

4.4.2 Intake Pressure - First - Order Increase

Another method of achieving a mode switch between SI and HCCI mode is to change the intake pressure from the SI operating point to the higher pressure at the HCCI operating point as a first order increase. Figures 4.21 and 4.22 compare the simulated and experimental results for two different first order pressure increase mode switches. The intake temperature for this test is higher by 6 K than for the step pressure increase initiated mode switches, at 389 K. The higher intake temperature promotes stable HCCI combustion, but makes it more difficult to avoid knock in SI combustion. The intake manifold volume is approximately 0.5 L for these tests so intake pressure response is faster than for the large manifold setup. SI and HCCI operating conditions are listed in Tables B.6 and B.7 of Appendix B.

The mode switch depicted in Figures 4.21 and 4.22 was chosen from the experimental results as the first-order increase case with the lowest MSPC. Figure 4.22 shows that the simulated results for CA50 do not track the experimental results as well as they did in the first tests. This is a result of the intake temperature being higher in this set of tests than in the step increase in pressure tests, and thus the necessity for later spark timing in the experimental SI cycles for IMEP stability and to avoid knock. As the simulated spark timing is kept constant, this change in CA50 for the SI cycles is not captured.

Differences between simulated and experimental CA50 values in the HCCI cycle are of a smaller magnitude and are more likely the result of the PMSM structure not capturing all of the complicated physics of the HCCI cycles.

The cycle based time response of the IMEP and CA50 in Figures **??** and 4.22

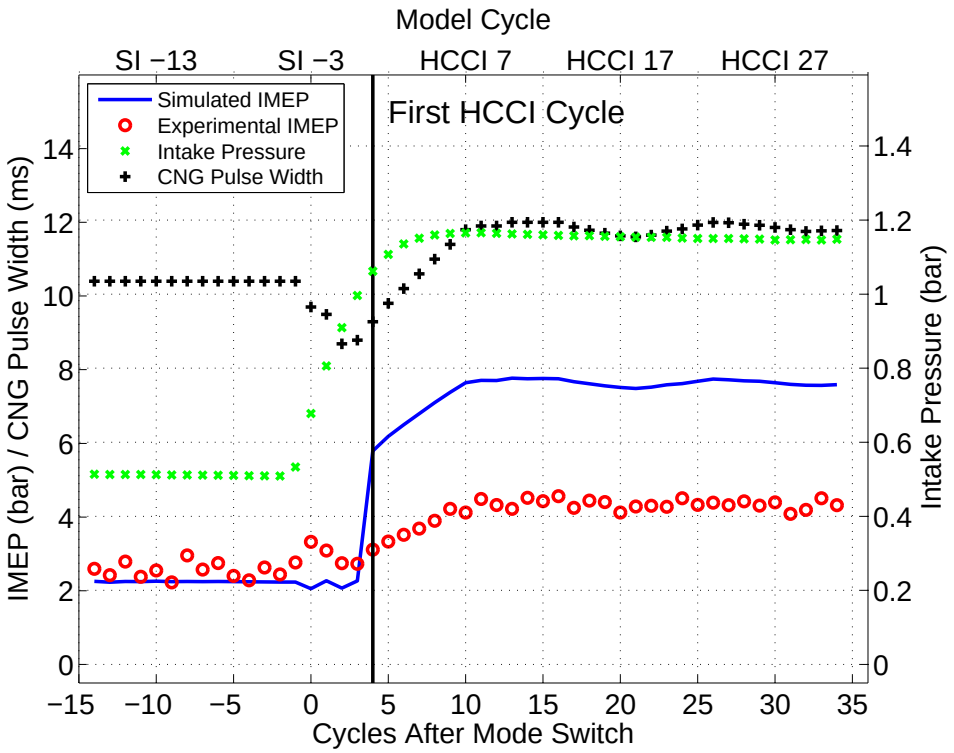

Figure 4.21: SI - HCCI Mode Switch - First Order Increase in Intake Pressure 1 - Cycle IMEP - $T_{\text{int}} = 389.15$ K, Small Intake Manifold. $\text{MSPC}_{\text{sim}} = 47.5$, $\text{MSPC}_{\text{exp}} = 19.2$

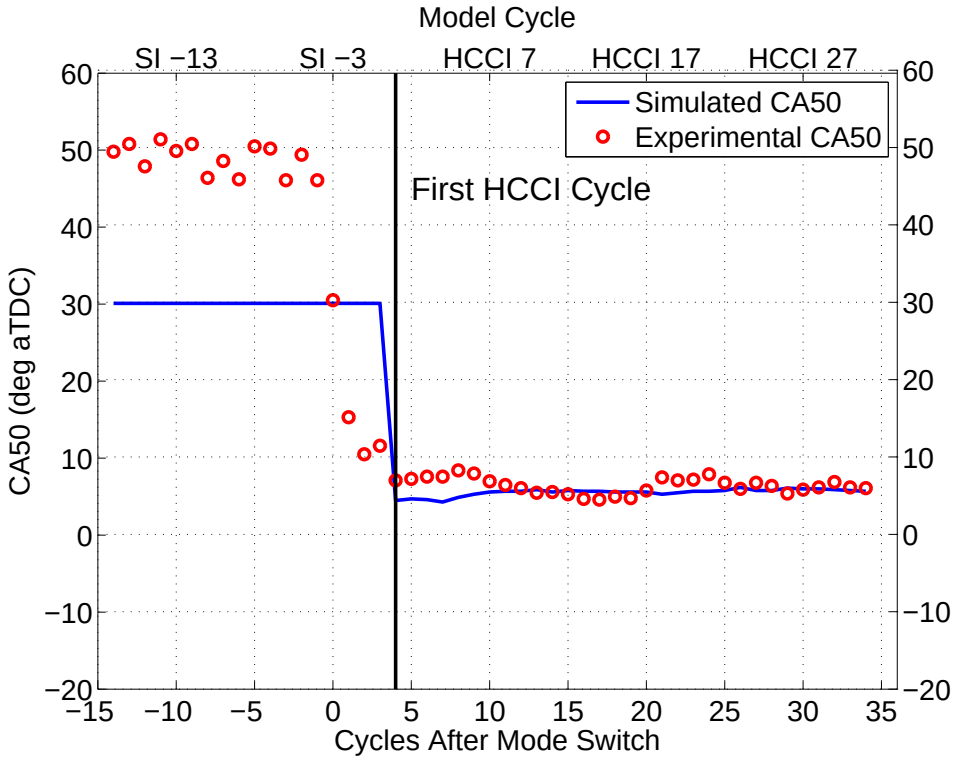

Figure 4.22: SI - HCCI Mode Switch - First Order Increase in Intake Pressure 1 - Cycle CA50 - $T_{\text{int}} = 389.15$ K, Small Intake Manifold. $\text{MSPC}_{\text{sim}} = 47.5$, $\text{MSPC}_{\text{exp}} = 19.2$

Table 4.10: MSPC - First Order Increase in Intake Pressure

	Sim 1	**Exp 1**	**Sim 2**	**Exp 2**
Duration	15	10	14	12
Smoothness	32.5	8.0	27.8	5.4
Knock	N/A	1.2	N/A	40.0
MSPC	47.5	19.2	41.8	57.4

respectively are similar between the experimental results and the simulation. The first order pressure increase initiated mode switch exhibits a faster switch from the SI IMEP level to the HCCI IMEP level than observed in the step increase in pressure initiated mode switches. Intermediate IMEP levels captured in the experimental results are not captured as well by the simulation because the simulation operates on the experimental spark profile, assuming that when the spark is activated SI combustion occurs and when the spark is deactivated HCCI combustion occurs. The apparent lag in the simulated IMEP and CA50 during the mode switch is the result of modeling the first 4 cycles after the mode switch as SI cycles because the experimental results indicated that the spark was activated for these cycles. The possibility of intermediate combustion phenomena such as SICI is not considered by the PMSM. The time response of the experimental results appears to be linear, while the time response of the simulated results appears to be first order, likely because the PMSM is known to over-predict the HCCI IMEP values.

Figures **??** and 4.24 show the mode switch with the highest MSPC from the first-order pressure increase tests. As can be seen, this run does not appear to vary considerably from the first test. Table 4.10 outlines the performance of each test with regards to the MSPC values.

The simulated results do not distinguish well between the different qualities of mode switches with respect to MSPC, but do exhibit slightly better MSPC values than observed in the step pressure increase tests. The MSPC value, useful when comparing experimental results, is only a good performance indicator for the

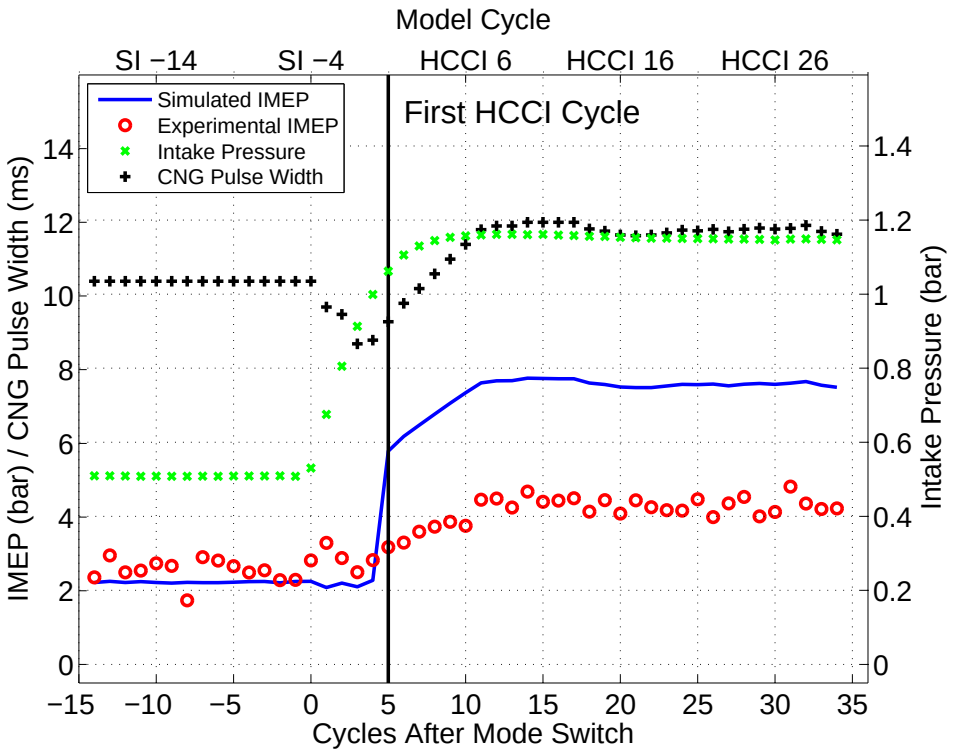

Figure 4.23: SI - HCCI Mode Switch - First Order Increase in Intake Pressure 2 - Cycle IMEP - $T_{\text{int}} = 389.15$ K, Small Intake Manifold. $\text{MSPC}_{\text{sim}} = 41.8$, $\text{MSPC}_{\text{exp}} = 57.4$

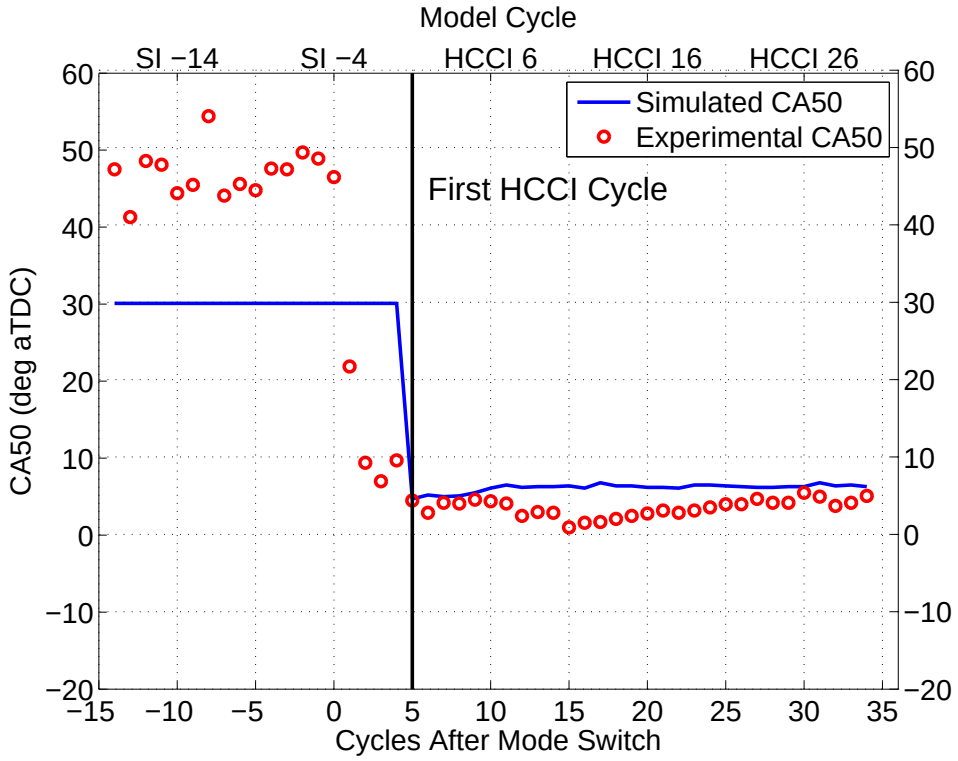

Figure 4.24: SI - HCCI Mode Switch - First Order Increase in Intake Pressure 2 - Cycle CA50 - $T_{\text{int}} = 389.15$ K, Small Intake Manifold. $\text{MSPC}_{\text{sim}} = 41.8$, $\text{MSPC}_{\text{exp}} = 57.4$

simulated results with respect to mode switch duration and smoothness. Since the PMSM does not consider cylinder knock, inhomogeneities, cylinder wall hot spots, fuel stratification, variations in engine speed, and pulsations during the scavenging processes, it is insensitive to many causes of cycle instabilities.

4.4.3 HCCI - SI Mode Switch

A mode switch from HCCI to SI mode is modeled and compared to experimental results for IMEP and CA50. The chosen mode switch profile is characterized by a rapid decrease in intake pressure from the level for steady state HCCI combustion to the level for steady state SI combustion. The experimental setup utilizes the smaller intake manifold, which allows the engine to quickly pump down the intake pressure, and high intake temperatures of approximately 413 K to enhance the stability of the HCCI combustion. Figure 4.25 shows the IMEP transition for the mode switch, and Figure 4.26 shows the CA50 transition. Operating data for the steady state cycles is contained in Tables B.8 and B.9 in Appendix B.

Figure 4.25 shows the mode switch as it progresses from medium load HCCI combustion to low load SI combustion. It is difficult to see that the simulated IMEP decreases in a straight line from the steady state HCCI value to the steady state SI value because of the high simulated IMEP in HCCI model. The simulated IMEP is too high due to the single zone model assumption. The shape of the IMEP transition and the success in the mode switch is similar in the simulations as in the experimental data.

Figure 4.26 shows the transition in CA50 from HCCI combustion to SI combustion. For both HCCI and SI modes the simulated results under-predict the CA50 value. In HCCI mode the under-prediction of the model for CA50 is likely a result of the longer combustion duration exhibited in the experimental results. The under-prediction of the SI cycles is attributed to the fault of using a Wiebe function

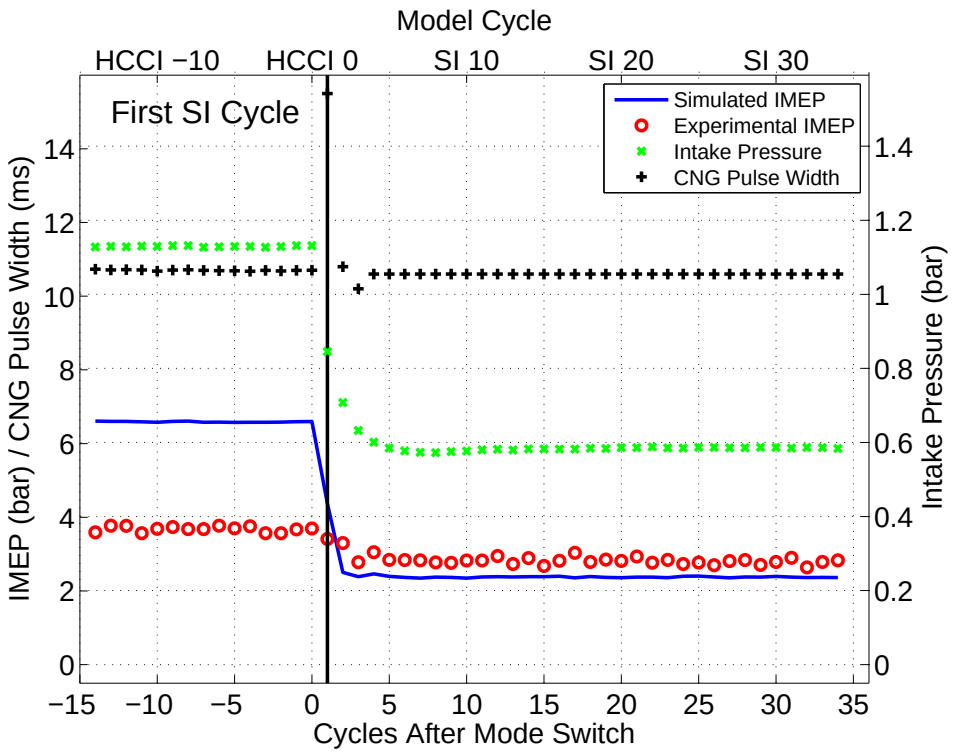

Figure 4.25: HCCI - SI Mode Switch - Step Decrease in Intake Pressure - Cycle IMEP - $T_{\text{int}} = 413.15$ K, Small Intake Manifold. $\text{MSPC}_{\text{sim}} = 2.0$, $\text{MSPC}_{\text{exp}} = 3.2$

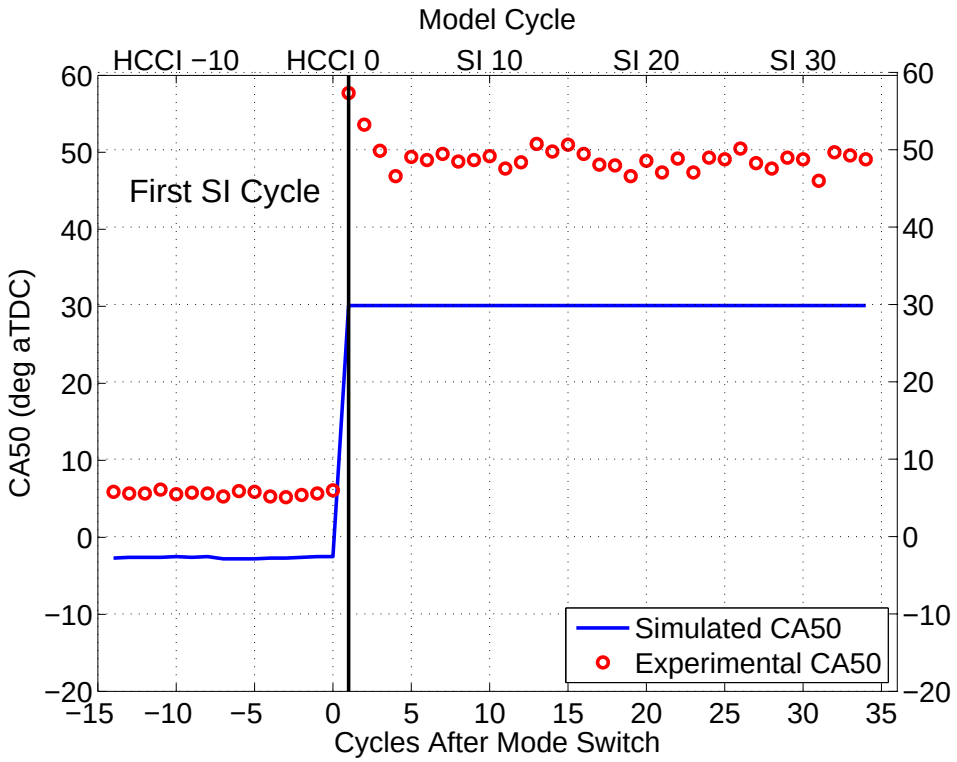

Figure 4.26: HCCI - SI Mode Switch - Step Decrease in Intake Pressure - Cycle CA50 - $T_{\text{int}} = 413.15$ K, Small Intake Manifold. $\text{MSPC}_{\text{sim}} = 2.0$, $\text{MSPC}_{\text{exp}} = 3.2$

Table 4.11: MSPC - HCCI - SI Mode Switch, Step Decrease in Intake Pressure

	Sim 1	**Exp 1**
Duration	2	3
Smoothness	0	0.2
Knock	N/A	0
MSPC	2.0	3.2

with fixed values of spark timing and combustion duration. For this SI operating point, the optimized values of spark timing and combustion duration are unable to capture properly the dynamics of the experimental system. CA50 time response is approximated by the simulation, but the lack of variability in the SI heat release function makes it so the model is unable to predict the late combustion cycles in the first SI cycles immediately following the mode switch. The first 3 cycles after the mode switch likely exhibit late combustion due to a longer combustion duration as a result of a lean AFR in these cycles (Heywood, 1988), used to avoid knock. If the SI combustion model were to be expanded to include multiple zones and thus capture the effects of AFR on combustion duration then it is possible that a more accurate response could be obtained.

Table 4.11 shows the MSPC values as determined for the simulated and experimental HCCI - SI mode switch. Simulated and experimental MSPC values are just more than 1 point apart, which is much closer than for the other mode switches. The relative value of MSPC to other mode switches reflects that this was an extremely successful mode switch according to the MSPC criteria.

4.4.4 Experimentally Optimized Mode Switch

An experimentally optimized mode switch is simulated. Experimentally this mode switch takes advantage of a fast first order pressure increase profile, a fueling profile optimized by hand, and a method of changing the fuel timing so that during SI combustion cycles the fuel is injected late resulting in fuel stratification and thus

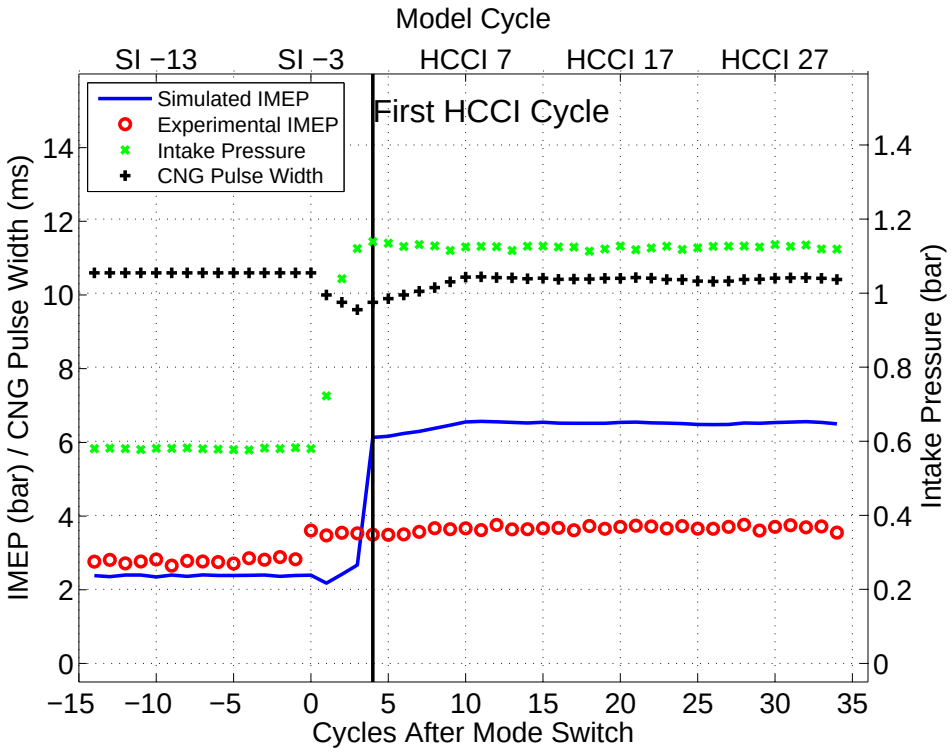

Figure 4.27: SI - HCCI Mode Switch - Experimentally Optimized Mode Switch - Cycle IMEP - $T_{\text{int}} = 403.15$ K, Small Intake Manifold

enhanced combustion stability. In HCCI cycles the fuel is injected early so that a homogeneous mixture can be achieved, promoting auto-ignition. This experimental data is outlined in the work of (Boddez, 2011). In the PMSM the intake mixture is assumed to be homogeneous, a consequence of having only a single zone, so capturing fuel stratification effects as a result of varied fuel injection timing is not possible. Figures 4.27 and 4.28 show how well the simulation captures a mode switch under these conditions. Steady state operating conditions for SI and HCCI cycles are listed in Tables B.10 and B.11 of Appendix B.

Figure 4.28 shows the difficulty that the model has in tracking CA50 for these tests. This discrepancy is attributed to a combination of higher intake temperatures, charge stratification, and variable fuel injection timing. The effects of fuel injection timing and charge stratification cannot be captured by the single zone models. The general shape of the simulated IMEP and CA50 time responses in

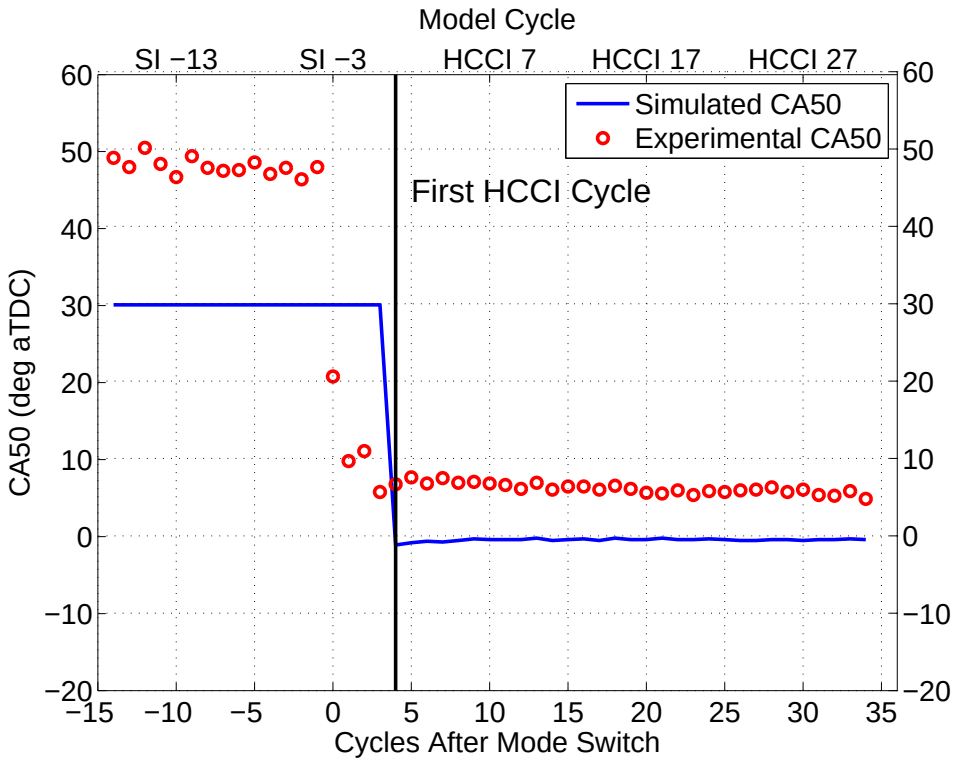

Figure 4.28: SI - HCCI Mode Switch - Experimentally Optimized Mode Switch - Cycle CA50 - $T_{\text{int}} = 403.15$ K, Small Intake Manifold

Table 4.12: MSPC - Experimentally Optimized Mode Switch

	Sim 1	**Exp 1**
Duration	6	1
Smoothness	11.5	0
Knock	N/A	0
MSPC	17.5	1

Figures 4.27 and 4.28 are similar to that of the experimental time responses with a three cycle delay. The apparent delay in the simulated IMEP and CA50 during the mode switch is the result of modeling the first 3 cycles after the mode switch as SI cycles because the experimental results indicated that the spark was activated for these cycles. It is possible that some form of spark assisted HCCI occurred in these cycles, as suggested in (Boddez, 2011); however, this form of combustion is not considered by the PMSM. Table 4.12 outlines the MSPC values for this mode switch test.

In the experimental test the fuel timing allows a mode switch to occur in 1 cycle resulting in an MSPC value of 1 for this test. While the simulated results are much higher than 1 at 17.5, the relative MSPC value for this test is much lower than in the previous tests where the simulated MSPC values are over 40 for each mode switch. Thus the simulation appears to be able to capture in an general sense the quality of the mode switch with regards to the parameters defined for MSPC in the work by (Boddez, 2011).

4.5 Parametrization and Validation Summary

The SI and HCCI models are tuned and shown to match well with experimental pressure traces and conditions at IVC and IVO. In most cases the predicted pressure traces remain within two standard deviations of the experimental values. The HCCI pressure trace tends to deviate from experimental results after ignition occurs,

because the use of a single zone model results in a simultaneous reaction throughout the combustion chamber and subsequently an extremely fast rate of pressure rise. This over-prediction in rate of pressure rise, and ultimately peak pressure, results in the IMEP values calculated for the HCCI cycles to be between 50 and 95 % higher than those observed experimentally. The full cycle simulated pressure traces are shown to match fairly well to experimental pressure traces of SI and HCCI cycles at two different sets of operating conditions.

Mode switches are simulated with the PMSM based on successful mode switch profiles from the experimental work of (Boddez, 2011). The PMSM takes approximately 20 minutes to simulate a 60 cycle mode switch, which meets the model objective of a 30 minute run time. The mode switch model is shown to be able to capture dynamics in IMEP and CA50 occurring through an SI - HCCI mode switch. This prediction is most accurate when simulating engine cycles based on the operating points for which the model was parameterized. These operating conditions are outlined in Tables B.4 and B.5 of Appendix B. The model's accuracy is lower at other operating points, particularly those points with significantly different intake air temperatures from those cycles for which the model is parameterized. The biggest difference between simulated mode switches and experimental results is seen in the simulation of SI CA50 values. Combustion timing is fixed through the choice of a constant spark time and combustion duration, so dynamics in SI CA50 values are not evident from the simulations. This poses a problem in predicting HCCI - SI mode switches, as dynamics in CA50 often occur in the early SI cycles following a mode switch.

The MSPC rating system developed by (Boddez, 2011) is investigated for use in rating mode switches simulated by the PMSM. The MSPC value is based on factors that describe mode switch duration, smoothness in IMEP, and knock levels. Knock levels are described by rate of pressure rise, and since the single zone HCCI

model in the PMSM is not able to accurately predict the rate of pressure rise for an HCCI cycle, this factor is not included in the model. The MSPC rating system when used for simulated mode switches is able to describe the relative difference in mode switch duration and smoothness in IMEP transition from one mode to the next in mode switches with different input conditions.

While it is difficult to precisely predict engine performance with the PMSM, it is important that the model is able to predict the shape of IMEP curves as well as early combustion cycles through its estimation of CA50. The PMSM does provide a platform for predicting combustion trends in an engine undergoing a mode switch within an operating range that is typically found on the experimental CFR engine, and thus could be used for optimization and investigation of additional actuators.

Chapter 5

Results and Discussion

5.1 Sensitivity Analysis

The sensitivities of key engine performance variables, IMEP and CA50, are investigated by varying model inputs and parameters for steady state SI, steady state HCCI, and mode switch HCCI operating conditions. Each of these operating conditions are outlined in detail in Appendix B. Sensitivities are computed as the slope of the model outputs with respect to each input variable and model parameter that is varied. Sensitivities can be evaluated using the equation $S_B^A = \frac{B}{A}\frac{\mathrm{d}A}{\mathrm{d}B}$, where S_B^A is the sensitivity of A with respect to B. These values are calculated and normalized around the operating conditions chosen for this study. Sensitivity analysis can provide information about the input variables to which the simulation is most sensitive and can help to show if the model is working properly.

Sensitivities of IMEP and CA50 to input variables and model parameters are evaluated. Input variables used in the PMSM include: intake air pressure, fueling rate, intake temperature, exhaust pressure, and residual temperature. Model parameters include: compression ratio, engine speed, spark timing, cylinder wall temperature, and combustion duration. Other model parameters are considered to be constant for all operating conditions. The sensitivities of inputs and parameters are evaluated by varying each independently by $\pm$ 20 % of the nominal operating

Table 5.1: Sensitivity of IMEP and CA50 in Steady State SI Operation with respect to Input Variables and Model Parameters. IMEP = 2.48 bar and CA50 = 390.1 CAD.

	Nominal Value	**Sensitivity of IMEP**	**Sensitivity of CA50**
Intake Pressure	53.3 kPa	0.192	0
Fuel Mass	13.3 mg	1.12	0
Intake Temperature	383 K	0.014	0
Exhaust Pressure	91.3 kPa	-0.366	0
Residual Temperature	699 K	-0.504	0
Compression Ratio	19	0.034	0
Engine Speed	700 rpm	0.099	0
Spark Timing	361 CAD	-5.30	0.481
Combustion Duration	60 CAD	-0.201	0.080
Wall Temperature	395 K	0.054	0

point value over 100 cycles. This range is chosen so that model performance with each input and parameter varied beyond normal engine operating conditions could be observed.

5.1.1 Model Sensitivity of Steady State SI Operation

Sensitivity of the PMSM about a steady state SI operating point for the CFR test engine is computed for the each of the inputs variables and model parameters discussed in section 5.1. The specific operating condition at which the sensitivity is calculated can be found in Table D.1 of Appendix B. Table 5.1 shows the sensitivity of IMEP and CA50 to variation in the input variables and model parameters.

Table 5.1 shows that the most influential input variables in the steady state spark ignition model are fuel mass and spark timing, and the most influential model parameter is spark timing. The fuel mass in the cylinder is important to IMEP as it directly influences the magnitude of the combustion heat release. There is a limit to the amount of fuel that will increase the IMEP. However, the chosen operating point is in the lean operating region and thus an increase in fuel can be

reasonably assumed to increase the IMEP. IMEP decreases when exhaust pressure increases because of pumping losses in trying to exhaust the cylinder mixture at the end of the cycle. Increases in residual temperature and exhaust pressure both result in a decreased IMEP because both are used as initial conditions at IVO and increases in these parameters result in less fresh mixture being inducted into the cylinder.

Spark timing is a very important model parameter in spark ignition engine cycles because the spark event controls the start of combustion and thus the location of the pressure increase with respect to the cylinder volume. The operating point that is considered has a spark timing of 361 CAD (TDC = 360 CAD), an earlier spark will result in the bulk of the heat release occurring closer to the minimum cylinder volume. The heat release when the cylinder has a smaller volume results in overall higher pressures in the cylinder than would be seen if the heat release occured later in the cycle when the cylinder volume is increasing. The higher overall pressure results in more work being done by the engine. Similar reasoning is used to explain the negative sensitivity of IMEP to combustion duration.

From Table 5.1 it is seen that CA50 in the spark ignition model at a steady state operating conditions is only affected by spark timing and combustion duration. Dependance of CA50 on these parameters is expected because the ignition timing, represented here by CA50, is specified by the initiation of the spark and the burn duration as defined in the model. Due to the influential nature of spark timing and combustion duration on IMEP and CA50 it is important that these terms be carefully defined for the operating condition as carried out in section 4.2.3.1.

5.1.2 Model Sensitivity of Steady State HCCI Operation

The sensitivity analysis of the PMSM at the steady state HCCI operating point was conducted in a similar fashion to the sensitivity analysis for the steady state SI

Table 5.2: Sensitivity of IMEP and CA50 in Steady State HCCI Operation with respect to Input Variables and Model Parameters. IMEP = 7.44 bar and CA50 = 368.7 CAD.

	Nominal Value	**Sensitivity of IMEP**	**Sensitivity of CA50**
Intake Pressure	120 kPa	0.364	-0.148
Fuel Mass	16.29 mg	1.02	-0.019
Intake Temperature	383 K	0.927	-0.973
Exhaust Pressure	91.3 kPa	-0.120	-0.013
Residual Temperature	640 K	-0.025	0.005
Compression Ratio	19	0.410	-0.383
Engine Speed	700 rpm	-0.095	0.045
Wall Temperature	383 K	0.059	-0.037

operating point. Operating parameters for this operating point are listed in Table B.13 of Appendix B. Table 5.2 shows the sensitivity of IMEP and CA50 to the input variables and model parameters for steady state HCCI combustion .

For this operating point IMEP is most sensitive to the mass of fuel and intake temperature as listed in Table 5.2. IMEP would not immediately be thought to have a positive sensitivity to intake temperature; however, at this operating point decreasing the intake temperature further can result in misfires or partial burn cycles in HCCI. For mode switching a balance needs to be struck for the intake temperature between SI and HCCI operation, because high intake temperatures result in auto-ignition, which is essential for operation in HCCI mode, but causes knock in SI mode. Due to the high sensitivity of IMEP to intake temperature it could be helpful to control mode switching cycles through the use of fast thermal management (FTM). IMEP also has a positive sensitivity to the mass of fuel as expected. Not apparent in this model is that a higher fuel to air ratio can result in earlier auto-ignition and unacceptably high rates of pressure rise that can damage the engine (Atkins, 2004), so on experimental engines fuel levels need to be limited to below practical knock limits whenever possible.

Intake pressure and compression ratio influence the IMEP in the HCCI combustion mode, but to a lesser extent than intake temperature and mass of fuel. A higher intake temperature will result in a higher pressure after compression, as will a higher compression ratio, pushing the cycle's peak pressure higher and consequently the IMEP. Particular care needs to be taken in a mode switch with both the compression ratio and the intake pressure values. Compression ratios and intake pressure that are too low can result in misfire and partial burn cycles.

CA50 for steady state HCCI, as determined by the single zone model, is most sensitive to intake temperature, compression ratio, and intake pressure. Combustion duration in a single zone chemical kinetics model of HCCI combustion can be assumed to have a small magnitude and is essentially constant for an operating condition such as this, so CA50 is an indicator of SOC as well. CA50 is indicated here in CAD, where TDC = 360 CAD, so the higher the value of CA50 the later the combustion occurs in the HCCI cycle. High intake temperature will result in earlier CA50 timing, because higher temperatures at IVC will result in higher temperatures after compression, decreasing the time to auto-ignition. High intake pressures and high compression ratios result in earlier CA50 timing because high pressures at IVC correlate again to higher temperatures after compression, thus increasing the probability of auto-ignition occurring. The CA50 has low positive sensitivity to residual temperature, which is not typically expected. This sensitivity is a result of using the assumption that input variables and model parameters are linearly independent of one another in the sensitivity analysis. Typically a higher residual temperature would also be associated with a higher wall temperature and result in early combustion timing. In the sensitivity analysis the wall temperature remains constant resulting in increased heat transfer caused by the higher residual temperatures and thus later combustion timing.

Output variables IMEP and CA50 are most sensitive to the input variables

Table 5.3: Sensitivity of IMEP and CA50 in HCCI Operation near Mode Switch with respect to Input Variables and Model Parameters. IMEP = 4.49 bar and CA50 = 373.3 CAD.

	Nominal Value	**Sensitivity of IMEP**	**Sensitivity of CA50**
Intake Pressure	90 kPa	0.448	-0.073
Fuel Mass	8.9 mg	0.575	0.226
Intake Temperature	383 K	2.26	-1.49
Exhaust Pressure	91.3 kPa	-0.106	-0.053
Residual Temperature	750 K	-0.068	0.018
Compression Ratio	19	3.171	-1.39
Engine Speed	700 rpm	-0.383	0.143
Wall Temperature	394 K	0.187	-0.087

chosen as actuators, which is desired, with the exception of the intake temperature. The assumption of constant intake temperature is valid for the CFR engine experimental setup due to the slow dynamics of the intake system; however, varying the intake temperature is shown to have significant effects on the engine performance.

5.1.3 Model Sensitivity of HCCI During Mode Switch Operation

Sensitivities of IMEP and CA50 for an HCCI combustion operating point during or near a mode switch, typically considered to be the least stable HCCI cycles, have been calculated with respect to the input variables and model parameters. Operating conditions for this HCCI point can be found in Table B.14 of Appendix B. Tabulated sensitivities for IMEP and CA50 are shown in Table 5.3.

Table 5.3 shows that the mode switch HCCI operating point IMEP has very similar sensitivities to the steady state HCCI operating point. The IMEP is most sensitive to compression ratio and intake temperature, with secondary sensitivities to intake pressure, mass of fuel, and engine speeds. An increase in sensitivities to compression ratio, intake temperature, and intake pressure is the result of the mode switch HCCI operating point lying closer to the misfire limit. If the intake temper-

ature, compression ratio, and intake pressure are decreased it becomes increasingly likely that the cylinder conditions will no longer be sufficient for auto-ignition and a misfire will occur. A misfire is defined for HCCI cycles in this study as a cycle where ignition does not occur.

Sensitivities for CA50 are slightly different than those calculated at the steady state HCCI operating point. The sensitivity to intake temperature, compression ratio, and fuel mass are greatly increased from the steady state case for CA50 because of the proximity of the mode switch operating point to the HCCI misfire limit. A decrease in intake temperature or an increase in fuel mass will both result in lower temperatures at IVC. Fuel is assumed to be injected at room temperature, so given the close proximity of this operating point to the misfire limit, the cooling that results from an increased mass of injected fuel will result in a lower temperature at IVC. HCCI combustion is extremely sensitive to pressure and temperature histories and thus a decreased temperature at IVC will result in later combustion timing and ultimately misfire. The cooling effect of adding natural gas fuel at room temperature is not as prominent as the evaporative cooling effect of liquid fuels; however, increased fuel amount can lead to decreased mixture temperature (Bi and Agrawal, 1998). The low positive sensitivity of CA50 to residual temperature exists for the HCCI mode switch operating point for the same reasons as stated above for the steady state HCCI operating point.

Sensitivity of IMEP and CA50 to intake temperature is even more significant in HCCI cycles that occur during a mode switch. While the assumption that intake temperature remains essentially constant from cycle to cycle is valid, the high sensitivities of both IMEP and CA50 suggest that controlling intake temperature could prove a useful method for mode switch optimization. Fast thermal management (FTM) is not an immediately practical solution to implementing HCCI in mobile engines such as automobile engines, but this technology could prove useful

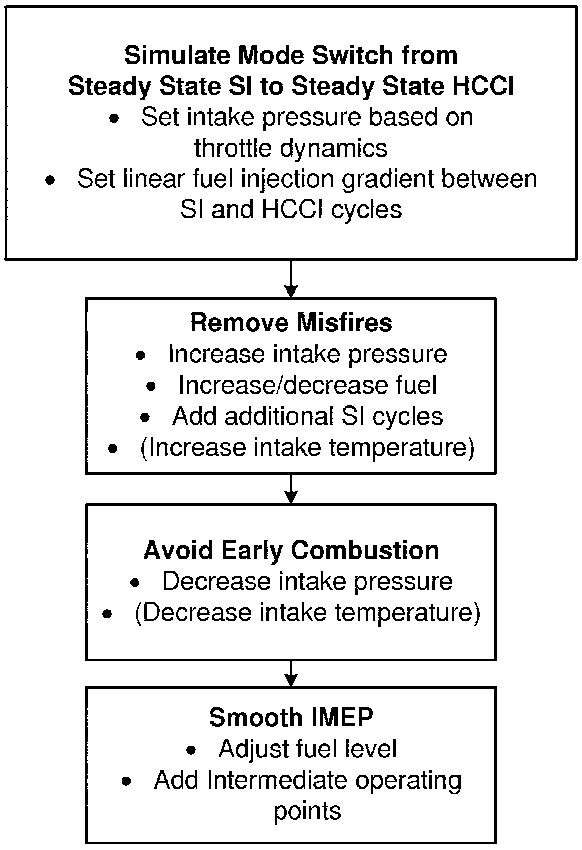

Figure 5.1: Process for Developing and Optimizing a Mode Switch Profile

in stationary engines (Yang et al., 2002; Haraldsson et al., 2004).

5.2 Mode Switching Optimization

Since the PMSM is useful for predicting the performance of an internal combustion engine undergoing a mode transition from SI to HCCI, it can be used to perform a mode switch optimization. The results of the optimized mode switch input profiles can be used as a starting point on the experimental engine to obtain a mode switch with the desired characteristics. The designer optimizing a mode switch uses a manual approach, utilizing physics-based knowledge for optimization, as outlined in Figure 5.1.

Optimization is done by manually varying individual parameters to maintain an understanding of the physical processes that are occurring as a result of the

changing simulation inputs. This procedure assumes only small coupling between inputs and variables, and can be used for a variety of actuators that are available for adjusting parameters. In some cases it may not be possible to achieve an ideal mode switch. Conventional actuators of intake pressure and fueling rate are used in this optimization. Due to the sensitivities of IMEP and CA50 to intake air temperatures, the effects of changing intake air temperature on mode switching are also investigated and used to further optimize a mode switch profile. Operating conditions from the stability analysis, tabulated in Tables D.1 and B.13 in Appendix B, are used as baseline steady state SI and HCCI operating conditions respectively in the optimization process.

5.2.1 Base Line Mode Switch - Step Increase in Intake Pressure

First introduced in the validation section of this study, the simplest mode switch from low load SI to medium load HCCI is to increase the intake pressure in a single step and turn off the spark. An increase in intake pressure results in a increase in the amount of fresh air supplied to the cylinder during the intake stroke, thus lowering the equivalence ratio of the cylinder mixture. At the same time, as is shown in the sensitivity section, an increase in intake pressure results in an overall increase in the initial cylinder temperature and pressure at IVC, advancing the ignition timing and allowing HCCI combustion to occur.

A mode switch from SI to HCCI, actuated by a step increase in intake pressure, is simulated to provide a base line from which to improve the quality of future mode switches. Figure 5.2 shows the IMEP, CA50, and inputs for the mode switch, while Figure 5.3 shows pressure of cycles during the mode switch.

According the MSPC scale (Boddez, 2011), the mode switch depicted in Figure 5.2 would score a value of 1, because it takes place in one cycle. However, the MSPC calculated with the simulation does not capture the effect of knock on these cycles.

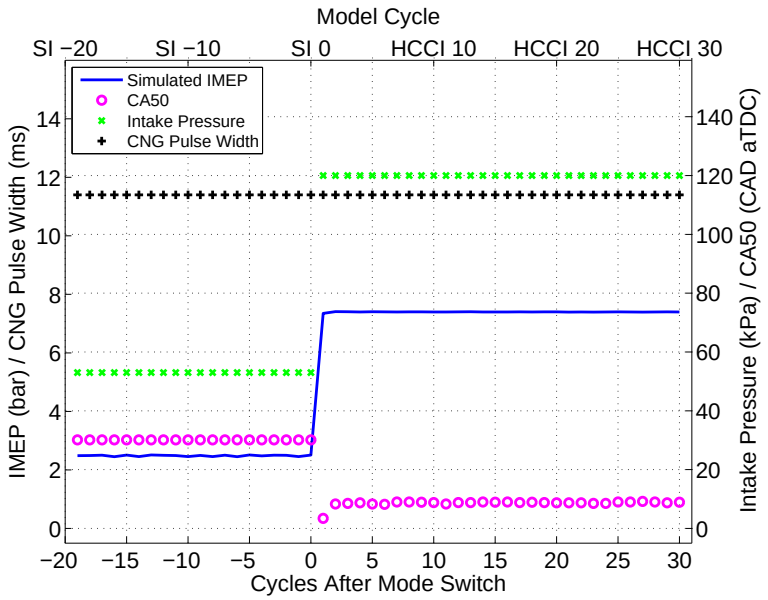

Figure 5.2: PMSM - Base Line Mode Switch from SI to HCCI Mode using Conventional Actuators of a Step Increase in Intake Pressure

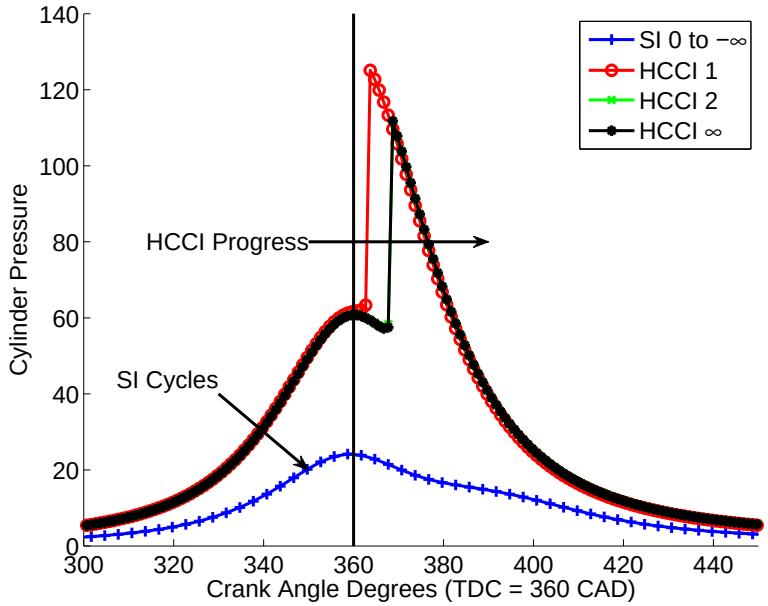

Figure 5.3: PMSM - Pressure Traces for Base Line Mode Switch from SI to HCCI Mode using Conventional Actuators of a Step Increase in Intake Pressure

Table 5.4: Exhaust Temperatures at EVO of SI and HCCI Cycles During Mode Switch

Cycle (Switch at 0)	T_{Residual}	T_{Wall}
SI -1	780 K	395.1 K
SI 0	753 K	395.0 K
HCCI 1	756 K	395.1 K
HCCI 2	627 K	394.0 K
HCCI 3	648 K	392.9 K

What is immediately obvious is that the first cycle after the mode switch has much earlier combustion timing then the subsequent cycles. HCCI operation in the CFR engine is limited by knock, therefore it could be reasonably assumed that cycles with ignition timing earlier than the steady state value for HCCI will experience engine knock in that cycle. Table 5.4 shows that early combustion in the first HCCI cycle is likely caused by high cylinder wall and exhaust temperatures from the previous SI cycle. (Shahbakhti et al., 2010) observed that exhaust temperatures in SI cycles are much higher than exhaust temperatures of HCCI cycles. The effect of residual exhaust gas temperature alone is shown in the sensitivity analysis to be less substantial than intake temperature and compression ratio. In this case residual temperature combined with the effects of a high cylinder wall temperature results in early ignition in the first HCCI cycle after the mode switch. It is possible that on a real operating engine local hot spots, such as a hot exhaust valve, could also cause this type of early combustion. Early combustion cycles are also observed in a study of mode switching by (Shaver et al., 2006).

Table 5.4 outlines the residual and wall temperatures for the spark ignition cycles leading up to the mode switch and the HCCI cycles immediately following the mode switch. Table 5.4 shows that the residual and cylinder wall temperatures for the first HCCI cycle (HCCI 1) are hotter than those of subsequent cycles and therefore early ignition is more likely in the first HCCI cycle. The difference in

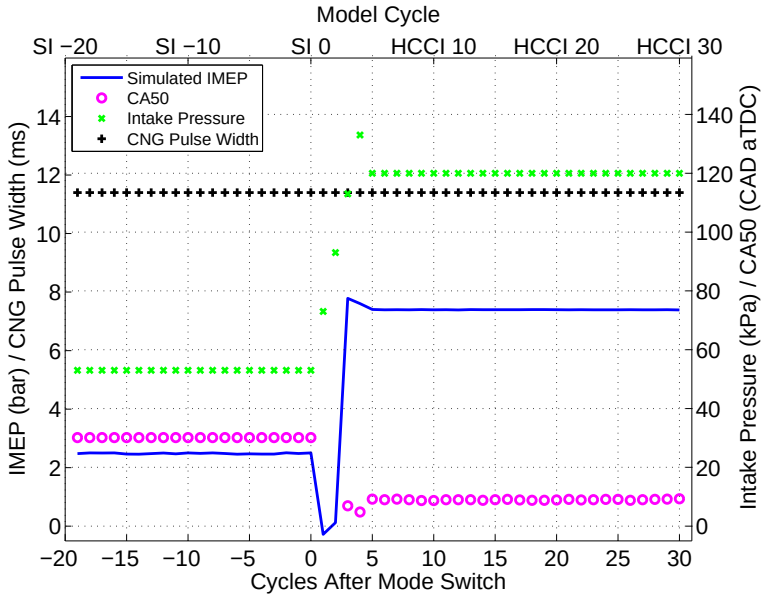

Figure 5.4: PMSM - Base Line Mode Switch from SI to HCCI Mode using Conventional Actuators of a Step increase in Intake Pressure for Slow Throttle Dynamics

residual and wall temperature between HCCI 2 and HCCI 3 is much smaller than the difference between HCCI 1 and HCCI 2 and thus very little difference is seen in CA50 timing. Very similar exhaust temperatures are observed in (Shahbakhti et al., 2010). The dynamics of the cylinder wall temperature result in the wall temperature changing over many more cycles than needed for the mode switch.

The same type of mode switch activation is shown again with the pressure actuator adjusted to represent slow throttle dynamics. Slow intake pressure adjustment would occur when using a large intake manifold volume compared to the displacement volume of the cylinder. Instead of the pressure being commanded to step from the pressure for SI to the pressure for HCCI in one cycle, it is assumed that the pressure changes linearly over 5 cycles with a slight overshoot of 10 kPa over the HCCI steady state value before settling at the set-point value. The IMEP, CA50, and pressure traces from the simulation of this mode switch are shown in Figures 5.4 and 5.5.

In this case the "quality" of the mode switch is much lower than that of the

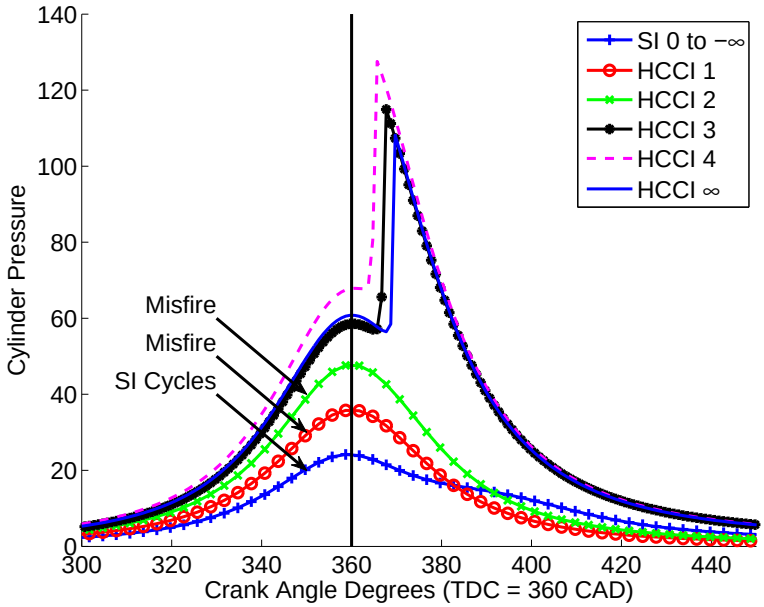

Figure 5.5: PMSM - Pressure Traces for Base Line Mode Switch from SI to HCCI Mode Using Conventional Actuators of a Step Increase in Intake Pressure for Slow Throttle Dynamics

first case, scoring a MSPC of 26.6. Misfires occur in the first two HCCI cycles and later cycles exhibit very early and unstable combustion. The intake pressure actuator is a fixed input, leaving fueling rate as the only control parameter when considering conventional actuators. Early combustion cycles seen in Figure 5.2 are not as evident in this case because the misfiring HCCI cycles result in lower residual and cylinder wall temperatures in the first successful HCCI cycle. Misfires are unacceptable for a successful mode switch, which requires a smooth transition in IMEP from SI to HCCI.

5.2.2 Mode Switching with Conventional Actuators

To improve upon the baseline mode switches presented above, the IMEP transition between the last steady SI cycle and the first steady HCCI cycle needs to be smoothed and early ignition cycles need to be avoided. According to the sensitivity analysis, the conventional actuator most able to rectify the combustion timing

problem is the intake pressure. If the intake pressure is lowered then the combustion timing will be retarded and early combustion can be avoided.

Optimization is performed as shown in Figure 5.1, varying the actuators individually so that the physics of the underlying process can be observed and maintained. Results of the iterations from the optimization process are shown for IMEP in Figure 5.6 and for CA50 in Figure 5.7. As there are no misfires, the intake pressure in the first HCCI cycle is reduced by 10 % to help retard the ignition timing. This reduction in intake pressure is not sufficient in reducing the ignition timing so a second simulation is run where the first HCCI cycle intake pressure is reduced by and additional 10 % from the target pressure for HCCI combustion. The 20 % reduction in intake pressure is sufficient at minimizing the early combustion timing in the first HCCI cycle, but to achieve a smooth transition in IMEP the intake pressure of the second HCCI cycle is reduced by 10 % from steady state value. Further simulation shows the ignition timing of these cycles to be later than the desired values. Reducing the fuel amount in these first cycles can serve the dual purpose of advancing the ignition timing and avoiding the possibility of knock in an experimental engine. Knock as a result of too much fuel in HCCI cycles following a mode switch has been observed in (Boddez, 2011; Shaver et al., 2006; Atkins, 2004).

The MSPC value of the base line mode switch is 1 and after the optimization process the MSPC has increased to 5.3. The MSPC value can be used as a measure of mode switch duration and smoothness in IMEP, but it is also necessary to look at the CA50 values when trying to establish the quality of the mode switch with regards to the possibility of knock occurring. Therefore MSPC is not always an appropriate measure for mode switch success of simulations by the PMSM. In the last iteration a suitable mode switch is established that lasts approximately 3 cycles. Cycle inputs and resulting IMEP and CA50 of the final iteration are shown

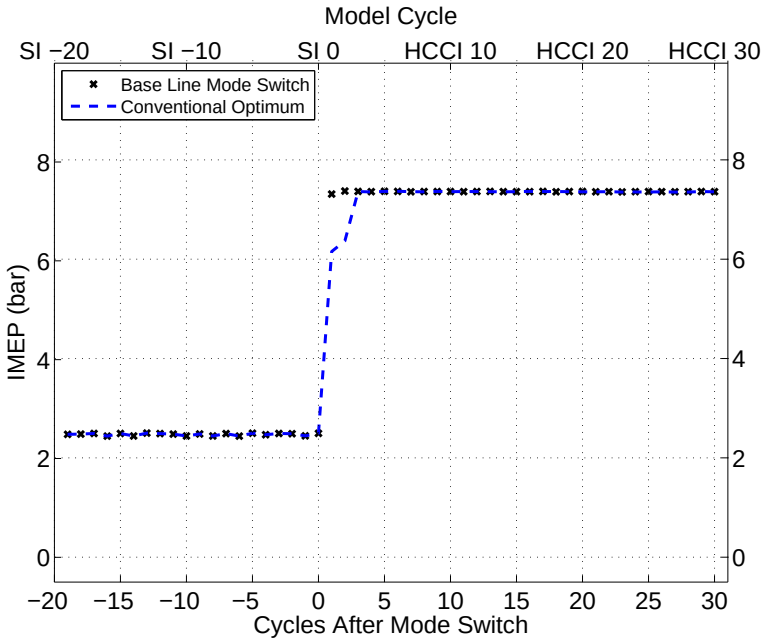

Figure 5.6: PMSM - IMEP of Optimized Mode Switch Compared to Base Line for the Small Intake Manifold System Controlled with Conventional Actuators

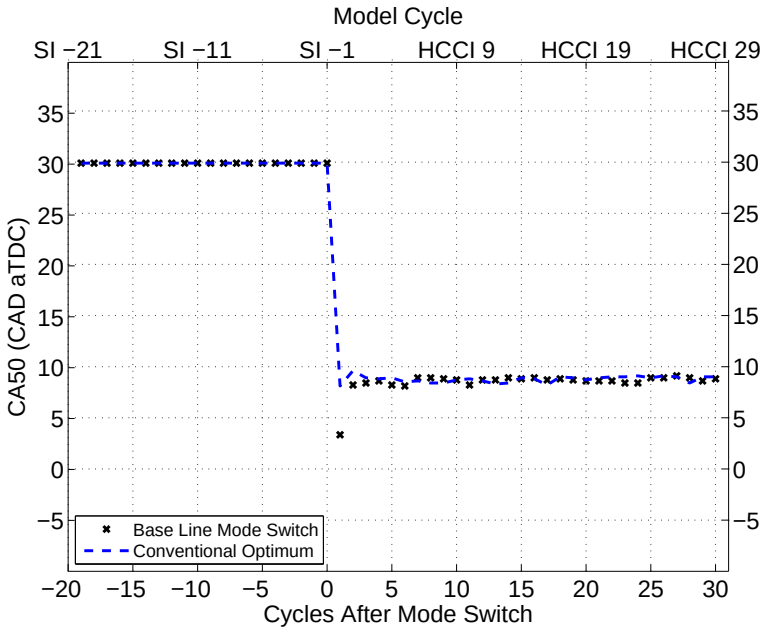

Figure 5.7: PMSM - CA50 of Optimized Mode Switch Compared to Base Line for the Small Intake Manifold System Controlled with Conventional Actuators

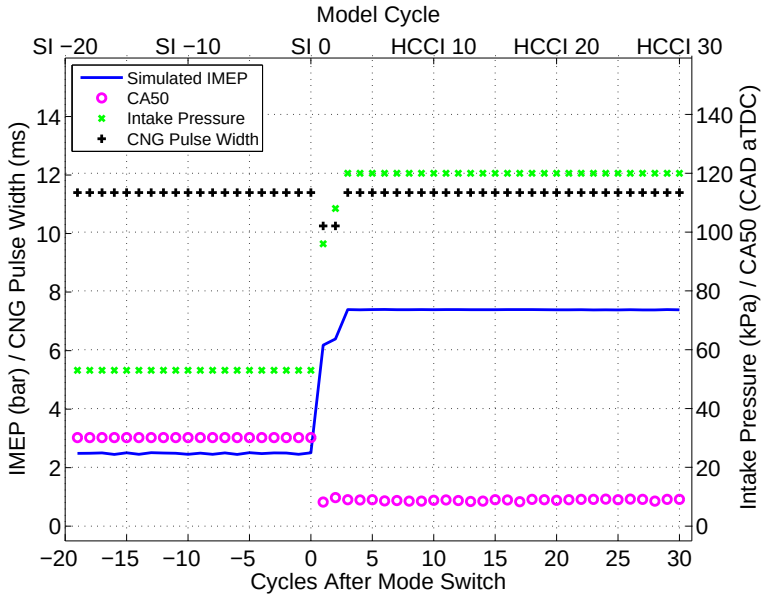

Figure 5.8: PMSM - Optimized Mode Switch from SI to HCCI Mode Using Conventional Actuators of Controlled Intake Pressure and Fueling Rate

in Figure 5.8 and the pressure traces are shown in Figure 5.9.

Optimization of the second base line mode switch is also performed, where the dynamics of the intake system restrict the speed at which the intake pressure can be adjusted. In this case the intake pressure profile is fixed and the only available actuator is the amount of fuel added to the system.

First the misfires that can be clearly seen in Figures 5.4 and 5.5 are eliminated. The first cycle following the mode switch does not have a high enough intake pressure for HCCI combustion to commence at the desired compression ratio and intake temperature, thus an additional SI cycle is added at higher intake pressure to avoid the misfire. The cost of adding an SI cycle at higher intake pressure is fluctuation in IMEP, a higher residual temperature and cylinder wall temperature, and as a result earlier combustion for the following HCCI cycle. Also the higher pressure SI cycle will likely have increased emissions due to high combustion temperatures and higher cylinder pressures. The fuel level for this SI cycle is decreased slightly to mitigate the increase in residual temperature and to avoid early combustion. Suc-

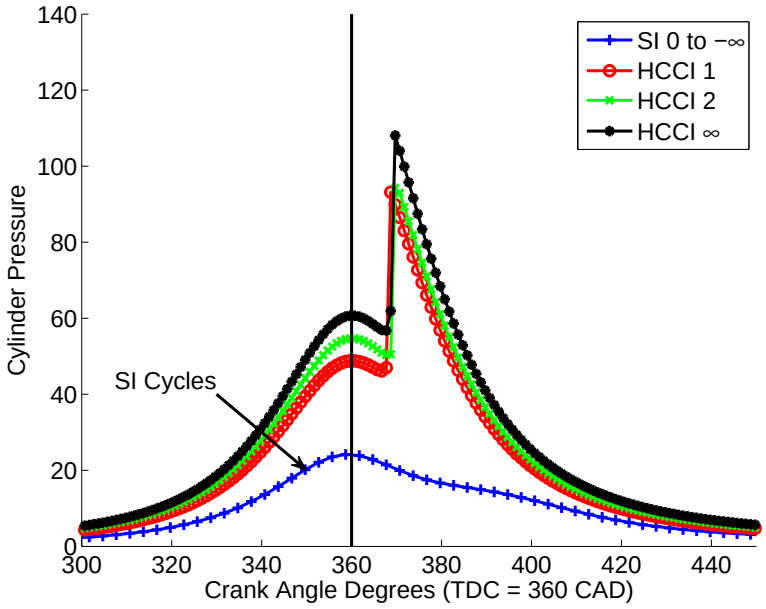

Figure 5.9: PMSM - Pressure Traces for Mode Switch from SI to HCCI Mode using Conventional Actuators of Controlled Intake Pressure and Fueling Rate

cessful HCCI combustion is achieved in the second cycle by reducing the amount of fuel, which advances combustion because of reduced cooling effect from additional fuel. The cycle with the overshoot in intake pressure is regulated by increasing the fuel amount slightly, resulting in the burn duration being slightly increased because of an increased fuel cooling effect. It is likely knock is avoided because the equivalence ratio is kept the same or lower than in previous cycles. The base line and optimized cycles are compared with regards to IMEP in Figure 5.10 and CA50 in Figure 5.11. An acceptable mode switch is achieved, although there is still a large variability in combustion timing and an extra SI cycle is necessary.

The MSPC value is greatly improved from the base line case to the optimized case because of the elimination of the misfire cycles. The MSPC value is improved from 26.6 for the base line case to 9.5 for the optimized case. The CA50 values still show a high level of fluctuation and early combustion timing in the first of the HCCI cycles. The optimized mode switch simulation output parameters are shown with the input values in Figure 5.12 and the pressure traces for the mode switch

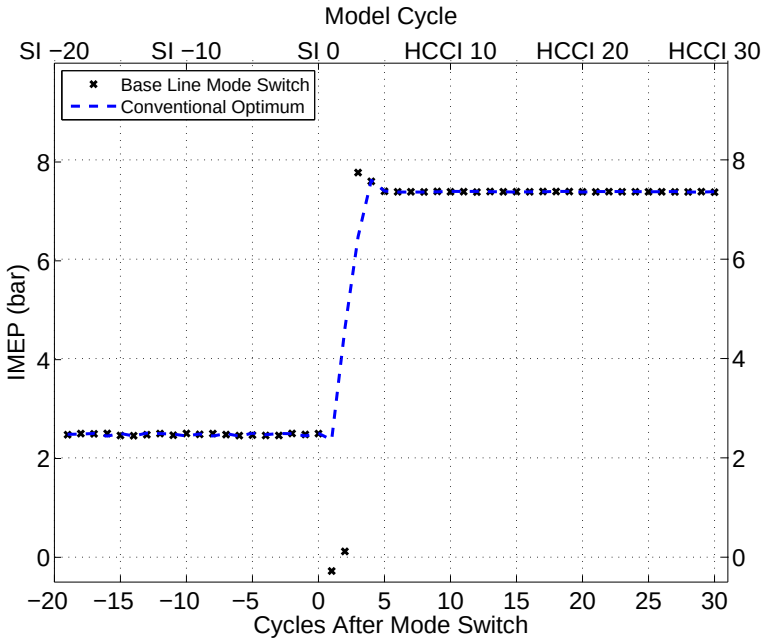

Figure 5.10: PMSM - IMEP of Optimized Mode Switch Compared to Base Line for the Large Intake Manifold System Controlled with Conventional Actuators

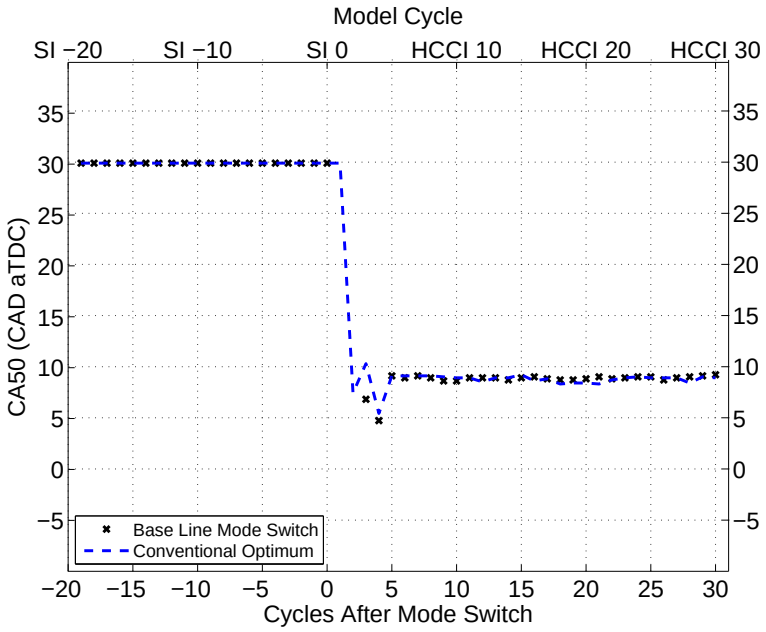

Figure 5.11: PMSM - CA50 of Optimized Mode Switch Compared to Base Line for the Large Intake Manifold System Controlled with Conventional Actuators

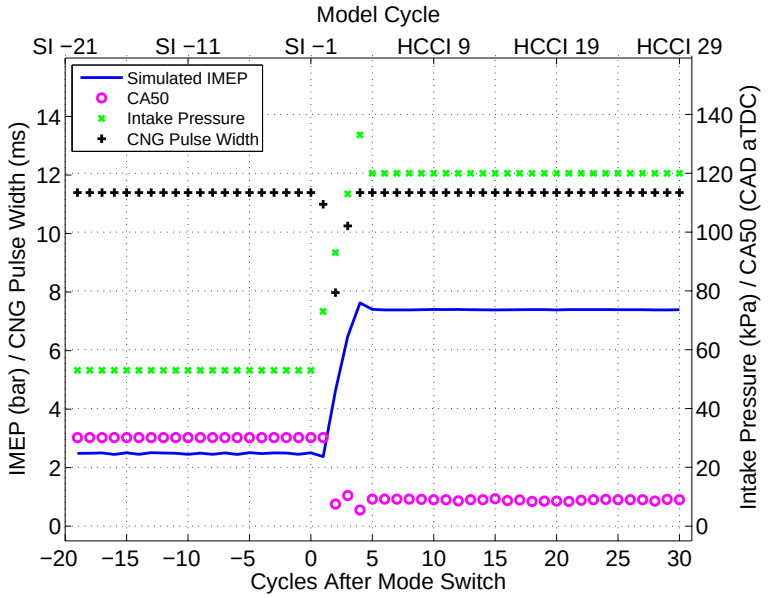

Figure 5.12: PMSM - Optimized Mode Switch from SI to HCCI Mode using Conventional Actuators of Controlled Intake Pressure and Fueling Rate for Slow Throttle Dynamics

are shown in Figure 5.13.

The misfires are eliminated and the mode switch is smoother with respect to the IMEP change. Much of the early combustion has also been eliminated and there is very little ability to improve the mode switch further with only conventional actuators.

5.2.3 Mode Switching with Variable Intake Temperature

The simulation can be used to test ideas that have not been experimentally implemented on the CFR engine. Problems with misfire limits and stability can be addressed by allowing intake temperature to be directly controlled on a cycle by cycle basis. Intake temperature was shown to have the largest influence on both CA50 and IMEP in HCCI cycles and as such is an important tool for control of mode switches from SI to HCCI combustion. Such technology exists, where two separate intake air streams, a hot stream and a cold stream, are mixed upstream of

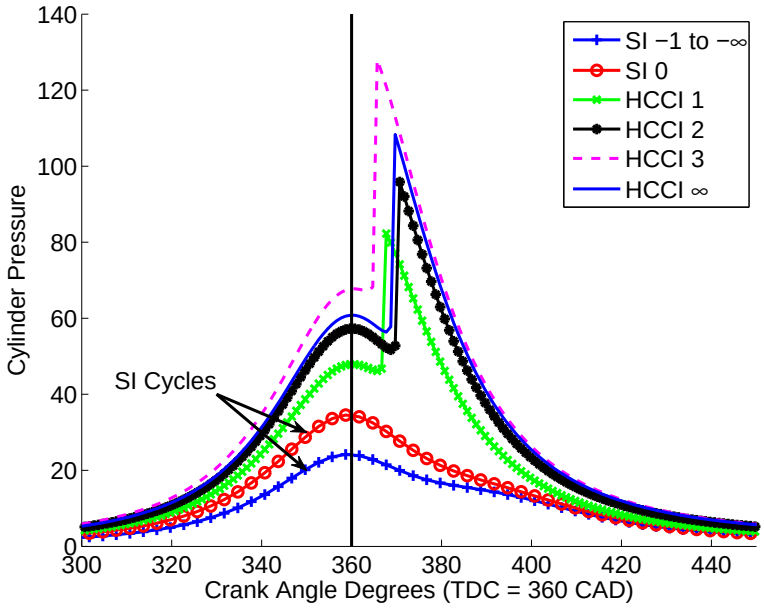

Figure 5.13: PMSM - Pressure Traces for Mode Switch from SI to HCCI Mode using Conventional Actuators of Controlled Intake Pressure and Fueling Rate for Slow Throttle Dynamics

the intake manifold to create an intake mixture of the desired intake temperature. This technology is called fast thermal management (FTM) and is discussed in more detail in chapter 2. The added benefit of such a technology is that it is possible to avoid knock and run SI combustion more efficiently at lower intake temperatures and then increase the intake temperature during a mode switch to avoid misfires in the HCCI cycles.

The baseline mode switch with the small intake and fast pressure adjustment is easily optimized using conventional actuators and therefore does not require the use of more advanced actuators such as intake air temperature. An acceptable response was obtained for the slow throttle response model using conventional actuators. To further optimize the mode switch the early combustion cycles and extra SI cycle after the mode switch can be improved. FTM allows the HCCI range to be extended to allow for suitable HCCI combustion in all of the cycles following the mode switch actuation. For the first HCCI cycle the intake air temperature

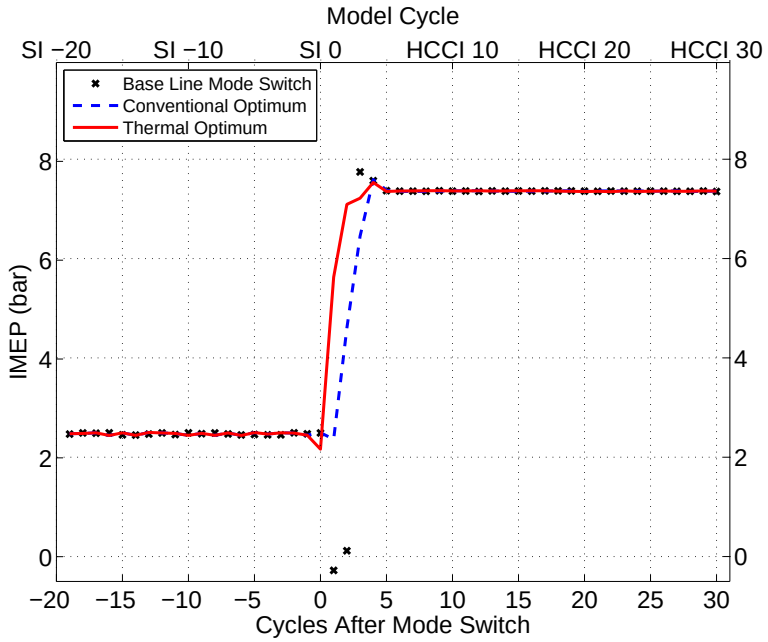

Figure 5.14: PMSM - IMEP of Optimized Mode Switch Compared to Base Line and Conventional Actuator Optimization for the Large Intake Manifold System Controlled with Conventional Actuators and Intake Temperature

is immediately increased from 110 °C to 130 °C in order to facilitate early combustion in the first cycle. In the following cycles the temperature is reduced to avoid early combustion and then further reduced for the HCCI cycle with pressure overshoot, after which steady state HCCI operation continues at the steady state intake temperature of 110 °C. The results of the optimum mode switch are shown in terms of IMEP in Figure 5.14 and CA50 in Figure 5.15. This method assumes that intake temperature could be changed by as much as 20 °C accurately from cycle to cycle.

The MSPC value is reduced from a value of 26.6 for the base line mode switch, to 9.5 with conventional actuators, and to 3.0 using FTM. In this case intake temperature is used as the primary basis for eliminating misfires and controlling early combustion, while fuel level is reserved for smoothing the IMEP transition. The optimal mode switch obtained through the use of conventional actuators is denoted “Conventional Optimum” and is shown along with the optimum mode

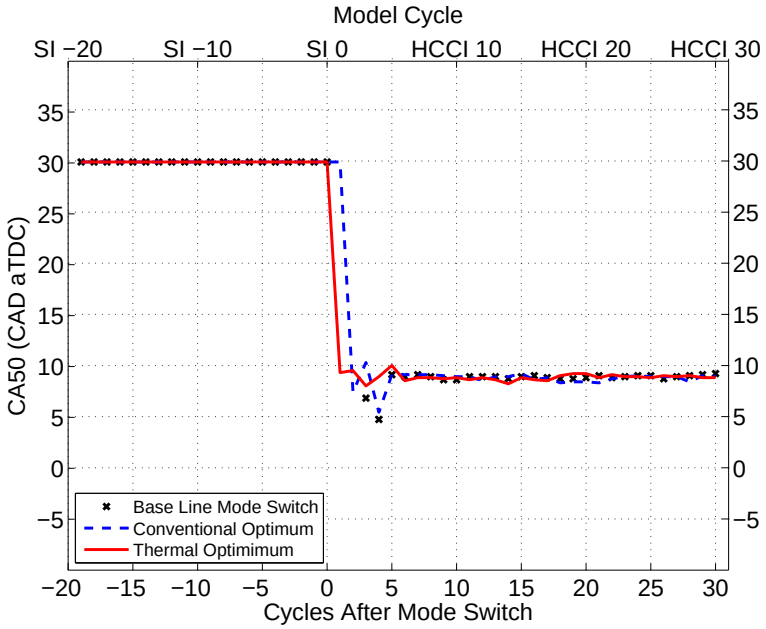

Figure 5.15: PMSM - CA50 of Optimized Mode Switch Compared to Base Line and Conventional Actuator Optimization for the Large Intake Manifold System Controlled with Conventional Actuators and Intake Temperature

switch achieved using FTM denoted "Thermal Optimum" in Figure 5.16. The pressure traces of the optimal mode switch achieved using FTM are shown in Figure 5.17.

As can be seen in Figures 5.16 and 5.17 the mode switch has been improved from the baseline case using just conventional actuators and is improved further by allowing intake air temperature to be adjusted.

5.3 Results and Discussion Summary

Sensitivities of IMEP and CA50 to model inputs and parameters are calculated for three operating points using the PMSM: steady state SI, steady state HCCI, and HCCI during a mode switch. The information gained from the sensitivity analysis is used to perform a manual optimization to improve two basic mode switch scenarios using only the conventional actuators of intake pressure and fuel injection rate. Further improvement of the mode switches is demonstrated using

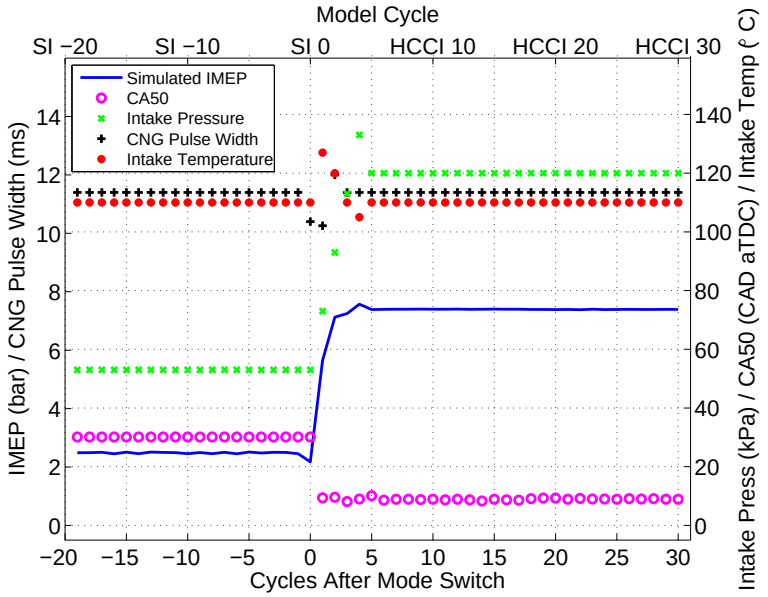

Figure 5.16: PMSM - Optimized Mode Switch from SI to HCCI Mode using Conventional Actuators of Controlled Intake Pressure and Fueling Rate for Slow Throttle Dynamics

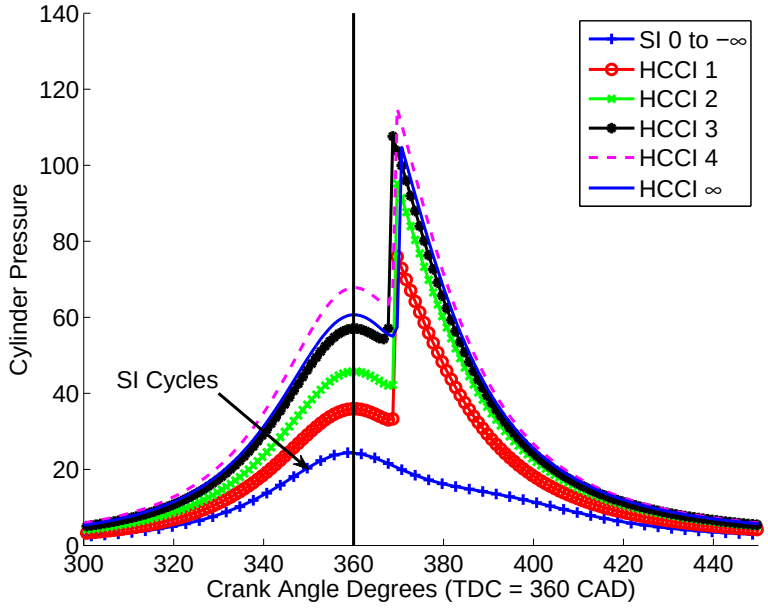

Figure 5.17: PMSM - Pressure Trace for Mode Switch from SI to HCCI Mode using Conventional Actuators of Controlled Intake Pressure and Fueling Rate for Slow Throttle Dynamics

fast thermal management as an additional actuator.

The results of this sensitivity analysis are shown in Tables 5.1, 5.2, and 5.3. At the steady state SI operating point IMEP is shown to be most sensitive to fuel mass (1.12) and spark timing (-5.30) and CA50 is shown to be only sensitive to spark timing (0.48) and combustion duration (0.08). IMEP at the steady state HCCI operating point is most sensitive to fuel mass (1.02) and intake temperature (0.927) and at the same operating point CA50 is most sensitive to intake temperature (-0.97) and compression ratio (-0.38). Sensitivities of IMEP and CA50 for HCCI during a mode switch are slightly different than at steady state. During a mode switch IMEP is most sensitive to intake temperature (2.26) and compression ratio (3.17) and CA50 is also most sensitive to intake temperature (-1.49) and compression ratio (-1.39).

Manual mode switching optimization is performed for two mode switching scenarios; one representing a fast intake throttle response and one representing a fixed slow intake throttle response. The objectives of the optimization are to: eliminate misfire cycles, achieve stable HCCI combustion in as few cycles as possible, achieve a smooth transition in IMEP between modes, and minimize early combustion. The CFR engine is knock limited so HCCI with early ignition timing relative to the steady state operating point will likely exhibit engine knock. Conventional input parameters of intake pressure (kPa) and fuel injector pulse width (ms) are considered for the optimization as they are direct inputs for the experimental CFR engine. To adapt the PMSM for optimization of a generic engine, AFR or equivalence ratio can be used as an input instead of fuel injector pulse width. These values can be calculated from the intake equations presented in Chapter 3.

Using conventional actuators of intake air pressure and fueling rate the baseline mode switches are optimized for the above objectives; demonstrated in Figures 5.6, 5.7, 5.10 and 5.11. The mode switch with fast intake throttle response is easily

optimized by varying intake air pressure and fueling rate during the mode switch. An acceptable mode switch is also achieved for the mode switch with a fixed slow intake throttle response.

The sensitivity analysis indicates that intake temperature has a significant effect on performance variables IMEP and CA50. By allowing intake temperature to be varied on a cycle to cycle basis the mode switch with a fixed slow intake throttle response is further improved; shown in Figures 5.14 and 5.15.

Chapter 6

Conclusions

The objective of this work is to develop a physics-based numerical model of an internal combustion engine that simulates switching between spark ignition (SI) and homogeneous charge compression ignition (HCCI) combustion modes, which can be used as a tool to understand and optimize mode switches. A model execution time fast enough to simulate 60 - 100 cycle mode switches within 30 minutes is required so that mode switch optimization and sensitivity can be calculated within a reasonable amount of time. The physics-based mode switch model (PMSM) achieves a mode switch simulation time under 30 minutes. The PMSM captures trends in the mode switching performance criteria (MSPC) developed by (Boddez, 2011) when compared to experimental data, IMEP and CA50, during a mode switch. The PMSM is then used to develop new mode switching strategies and establish the suitability of existing experimental mode switch strategies.

- A physics-based mode switch model (PMSM) that combines SI and HCCI engine models is developed and models the processes occurring during a mode switch in an internal combustion engine from SI to HCCI combustion modes. This model meets a self imposed computational time constraint of 30 minutes.

- The SI combustion mode is modeled as a single zone thermodynamic model. Combustion heat release is modeled as a single step reaction from reactants

to products with fixed spark timing and combustion duration described by a Wiebe function. Heat transfer is modeled with a modified Woschni correlation (Woschni, 1967) and ties into a cycle by cycle cylinder wall temperature model.

- The HCCI combustion mode is modeled as a single zone with detailed chemical kinetics that proceed according to the GRI-Mech 3.0 reaction mechanism. The bulk of the HCCI model is similar in form to the SI model and is capable of predicting HCCI combustion timing. Heat transfer is also modeled with a modified Woschni correlation that ties into the cylinder wall temperature model.

- The PMSM is validated with experimental mode switch data from a CFR test engine setup and is shown to be able to estimate the shape and timing of IMEP and CA50 SI - HCCI mode switch responses for the operating conditions considered. The PMSM experiences limitations in accurately predicting rate of pressure rise, peak pressure, and combustion duration for HCCI cycles. Engine knock is not considered by the PMSM.

- A sensitivity analysis of the PMSM shows that steady state SI combustion IMEP is most sensitive to fuel mass and spark timing and CA50 is only influenced by the selection of spark timing and combustion duration.

- Steady state HCCI combustion IMEP is most sensitive to fuel mass and intake temperature while CA50 is most sensitive to intake temperature and compression ratio. An analysis of the sensitivities of an HCCI cycle at the operating condition of an HCCI cycle during a mode switch shows IMEP and CA50 to be most sensitive to intake temperature and compression ratio.

- Insight from the sensitivity analysis and PMSM simulation results allows for

the optimization of a mode switch with conventional actuators. It is found that by reducing intake pressure and fuel mass slightly in the first HCCI cycles acceptable mode switches in terms of short duration, smooth IMEP transition, and stable combustion timing are achieved. Acceptable mode switches are also achieved in mode switch scenarios where the intake pressure profile is fixed, allowing adjustment of only fuel mass and spark activation.

- Due to high sensitivities of the PMSM HCCI cycle IMEP and CA50 values to intake temperature the PMSM is used to further improve a mode switch using conventional actuators and fast thermal management (FTM). By allowing intake temperature to be adjusted on a cycle by cycle basis, slightly more acceptable mode switches in terms of IMEP smoothness and CA50 combustion timing stability are achieved.

6.1 Future Research

- In the future this model can be used to develop optimized mode switch profiles that can be applied to the experimental CFR engine in practice.

- Fast thermal management could be investigated as a method for optimizing mode switches on the CFR engine and could be particularly interesting for engines where a slow intake manifold pressure response means the intake manifold pressure can only be changed over several cycles.

- The PMSM cam be adapted for optimization of a generic engine, using AFR or equivalence ratio as inputs instead of fuel injector pulse width.

Bibliography

AlbertaGasPrices.com (2011). Historical price charts.

Aleiferis, P. G., Charalambides, A. G., Hardalupas, Y., Taylor, A. M. K. P., and Urata, Y. (2005). Modeling and Experiments of HCCI Engine Combustion with Charge Stratification and Internal EGR. SAE paper 2005-01-3725, Imperial College London and Honda R&D CO., Ltd.

Amelio, M., Belli, M., and Danieli, G. A. (1986). A Multidimensional Performance Model of a Spark Ignition Engine Characterized by a Single Step Reaction to Equilibrium. *Combustion Science and Technology*, 45:p.p 115–128.

Atkins, M. J. (2004). Experimental Examination of the Effects of Fuel Octane and Diluent on HCCI Combustion. Master's thesis, University of Alberta.

Atkins, M. J. and Koch, C. R. (2005). The Effect of Fuel Octane and Diluent on Homogeneous Charge Compression Ignition Combustion. *Journal of Automobile Engineering*, 219(D07604):665 – 675.

Bade Shrestha, S. O. and Karim, G. A. (1999). A Predictive Model for Gas Fueled Spark Ignition Engine Applications. SAE paper 1999-01-3482, University of Calgary.

Berntsson, A. W. and Denbratt, I. (2007a). HCCI Combustion Using Charge Stratification for Combustion Control. SAE paper 2007-01-0210, Chalmers University of Technology.

Berntsson, A. W. and Denbratt, I. (2007b). Optical Study of HCCI Combustion using NVO and an SI Stratified Charge. SAE paper 2007-24-0012, Chalmers University of Technology.

Bi, H. and Agrawal, A. K. (1998). Study of Autoignition of Natural Gas in Diesel Environments Using Computational Fluid Dynamics with Detailed Chemical Kinetics. *Combustion and Flame*, 113:289–302.

Boddez, J. (2011). Conventional Actuation for SI-HCCI-SI Mode-Switching with Quantitative Evaluation. Master's thesis, University of Alberta.

Burcat, A. and McBride, B. J. (1993). 1994 Ideal Gas Thermodynamic Data for Combustion and Air- Pollution Use. Technion Report TAE 697, Technion.

Cairns, A. and Blaxill, H. (2005). The Effects of Combined Internal and External Exhaust Gas Recirculation on Gasoline Controlled Auto-Ignition. SAE paper 2005-01-0133, Cosworth Technology Ltd.

Canada, E. (2011). National Inventory Report - Greenhouse Gas Sources and Sinks in Canada 1990 - 2009. Technical report, Government of Canada.

Cengel, Y. A. and Boles, M. A. (2006). *Thermodynamics - An Engineering Approach*. McGraw-Hill, Inc.

Chang, J., Gueralp, O., Filipi, Z., Assanis, D., Kuo, T.-W., Najt, P., and Rask, R. (2004). New Heat Transfer Correlation for an HCCI Engine Derived from Measurements of Instantaneous Surface Heat Flux. In *Powertrain & Fluid Systems Conference & Exhibition*, number 2004-01-2996. University of Michigan and GM Research and Development Centre.

Chen, T., Xie, H., Ye, W., Li, Z., and Zhao, H. (2011). Continuous Load Adjust-

ment Strategy of Gasoline HCCI-SI Engine Fully Controlled by Exhaust Gas. SAE paper 2011-01-1408, Tianjin University and Brunel University.

Chevalier, A., Mueller, M., and Hendricks, E. (2000). On the Validity of Mean Value Engine Models During Transient Operation. SAE paper 2000-01-1261, Ford Motor Co. and Delphi Automotive System and Technical University of Denmark.

Cho, H. M. and He, B.-Q. (2007). Spark Ignition Natural Gas Engines - A Review. *Energy Conversion and Management*, 48:608–618.

Christensen, M. and Johansson, B. (1998). Influence of Mixture Quality on Homogeneous Charge Compression Ignition. SAE paper 982454, Lund Institute of Technology.

Christensen, M. and Johansson, B. (1999). Homogeneous Charge Compression Ignition with Water Injection. SAE paper 1999-01-0182, Division of Combustion Engines, Lund Institute of Technology.

Christensen, M. and Johansson, B. (2000). Supercharged Homogeneous Charge Compression Ignition (HCCI) with Exhaust Gas Recirculation and Pilot Fuel. SAE paper 2000-01-1835, Lund Institute of Technology.

Coppin, T., Grondin, O., Le Solliec, G., Rambault, L., and Maamri, N. (2010). Control-Oriented Mean-Value Model of a Fuel-Flexible Turbocharged Spark Ignition Engine. SAE paper 2010-01-0937, IFP and LAII, University of Poitiers.

Dahl, D., Denbratt, I., and Koopmans, L. (2008). An Evaluation of Different Combustion Strategies for SI Engines in a Multi-Mode Combustion Engine. SAE paper 2008-01-0426, Chalmers University of Technology and Volvo Car Corporation.

Dec, J. E. and Sjoberg, M. (2003). A Parametric Study of HCCI Combustion - the Sources of Emissions at Low Loads and the Effects of GDI Fuel Injection. SAE paper 2003-01-0752, Sandia National Laboratories.

Dec, J. E. and Sjoberg, M. (2004). Isolating the Effects of Fuel Chemistry on Combustion Phasing in an HCCI Engine and the Potential of Fuel Stratification for Ignition Control. SAE paper 2004-01-0557, Sandia National Laboratories.

Etheridge, J., Mosbach, S., Kraft, M., Wu, H., and Collings, N. (2010a). A Detailed Chemistry Simulation of the SI-HCCI Transition. SAE paper 2010-01-0574, University of Cambridge and Cambustion Ltd.

Etheridge, J., Mosbach, S., Kraft, M., Wu, H., and Collings, N. (2010b). A Fast Detailed-Chemistry Modelling Approach for Simulating the SI-HCCI Transition. SAE paper 2010-01-1241, University of Cambridge and Cambustion Ltd.

Fekete, N. P., Nester, U., Gruden, I., and Powell, J. D. (1995). Model-Based Air-Fuel Ratio Control of a Lean Multi-Cylinder Engine. SAE paper 950846, Stanford University and Daimler-Benz AG.

Gong, W., Bell, S. R., Micklow, G. J., Fiveland, S. B., and Willi, M. (2002). Using Pilot Diesel Injection in a Natural Gas Fueled HCCI Engine. SAE paper 2002-01-2866, The University of Alabama and Caterpillar Inc.

Government of Alberta (2011). Monthly reference price calculations.

Handford, D. I. (2009). Direct Injection Assisted HCCI Combustion of Natural Gas. Master's thesis, University of Alberta.

Haraldsson, G., Tunestal, P., Johansson, B., and Hyvoenen, J. (2004). HCCI Closed-Loop Combustion Control using Fast Thermal Management. SAE paper 2004-01-0943, Lund Institute of Technology and Fiat-GM Powertrain Sweden.

Helmantel, A. and Denbratt, I. (2004). HCCI Operation of a Passenger Car Common Rail DI Diesel Engine with Early Injection of Conventional Diesel Fuel. SAE paper 2004-01-0935, Chalmers University of Technology.

Hendricks, E. (1989). The Analysis of Mean Value Engine Models. SAE paper 890563, The Technical University of Denmark.

Hendricks, E. and Vesterholm, T. (1992). The Analysis of Mean Value SI Engine Models. SAE paper 920682, Technical University of Denmark.

Heywood, J. B. (1988). *Internal Combustion Engine Fundamentals*. McGraw-Hill, Inc.

Hosseini, V. (2008). *Reformer Gas Application in HCCI Combustion Engine*. PhD thesis, University of Alberta.

Hosseini, V. and Checkel, M. D. (2006). Using Reformer Gas to Enhance HCCI Combustion of CNG in a CFR Engine. SAE paper 2006-01-3247, University of Alberta.

Hosseini, V. and Checkel, M. D. (2007a). Effect of Reformer Gas on HCCI Combustion - Part I: High Octane Fuels. SAE paper 2007-01-0208, University of Alberta.

Hosseini, V. and Checkel, M. D. (2007b). Effect of Reformer Gas on HCCI Combustion - Part II: Low Octane Fuels. SAE paper 2007-01-0206, University of Alberta.

Hosseini, V. and Checkel, M. D. (2008). Reformer Gas Composition Effect on HCCI Combustion of n-Heptane, iso-Octane, and Natural Gas. SAE paper 2008-01-0049, University of Alberta.

Incropera, F. P. and DeWitt, D. P. (2002). *Heat and Mass Transfer*. John Wiley & Sons.

Jun, D. and Lida, N. (2004). A Study of High Combustion Efficiency and Low CO Emission in an Natural Gas HCCI Engine. SAE paper 2004-01-1974, KEIO University.

Kakuya, H., Yamaoka, S., Kumano, K., and Sato, S. (2008). Investigation of a SI-HCCI Combustion Switching Control Method in a Multi-Cylinder Gasoline Engine. SAE paper 2008-01-0792, Hitachi Research Laboratory, Hitachi, Ltd.

Kawasaki, K., Takegoshi, A., Yamane, K., Ohtsubo, H., Nakazono, T., and Yamauchi, K. (2006). Combustion Improvement and Control for a Natural Gas Engine by the Internal EGR by Means of Intake-Valve Pilot-Opening. SAE paper 2006-01-0208, The University of Shiga Prefecture and Yanmar CO., Ltd.

Kirchen, P., Shahbakhti, M., and Koch, C. R. (2007). A Skeletal Kinetic Mechanism for PRF Combustion in HCCI Engines. *Combustion Science and Technology*, 179:1058–1083.

Kongsereeparp, P. (2008). *Chemical Kinetic Based Simulation for an HCCI Engine and its Combustion*. PhD thesis, University of Alberta.

Kongsereeparp, P. and Checkel, M. D. (2008a). Environmental, Thermodynamic and Chemical Factor Effects on Heptane- and CNG-Fueled HCCI Combustion with Various Mixture Compositions. SAE paper 2008-01-0038, University of Alberta.

Kongsereeparp, P. and Checkel, M. D. (2008b). Study of Reformer Gas Effects on n-Heptane HCCI Combustion Using a Chemical Kinetic Mechanism Optimized by Genetic Algorithm. SAE paper 2008-01-0039, The University of Alberta.

Kuzuyama, H., Machida, M., Akihama, K., Ingrain, K., and Ueda, M. (2007). A Study on Natural Gas Fueled Homogeneous Charge Compression Ignition Engine - Expanding the Operating Range and Combustion Mode Switching. SAE paper 2007-01-0176, Toyota Industries Corporation and Toyota Central R&D Labs., Inc.

Lavy, J., Dabadie, J.-C., Angelberger, C., Duret, P., Willand, J., Juretzka, A., Schaeflein, J., Ma, T., Yvane, L., Satre, A., Schulz, C., Kraemer, H., Zhao, H., and Damiano, L. (2000). Innovative Ultra-Low NOx Controlled Auto-Ignition Combustion Process for Gasoline Engines: the 4-SPACE Project. SAE paper 2000-01-1837, IFP, Daimler Chrysler, Ford, PSA Peugeot Citroen, PCI - Heidelberg University, Brunel University.

Law, D., Kemp, D., Allen, J., Kirkpatrick, G., and Copland, T. (2000). Controlled Combustion in an IC-Engine with a Fully Variable Valve Train. SAE paper 2000-01-0251, Lotus Engineering Ltd.

Lupul, R. (2008). Steady State and Transient Characterization of a HCCI Engine with Varying Octane Fuel. M.Sc. thesis, University of Alberta.

McBride, B. J., Gordon, S., and Reno, M. A. (1993). Coefficients for Calculating Thermodynamic and Transport Properties of Individual Species. NASA TM 4513, NASA.

Milovanovic, N., Blundell, D., Gedge, S., and Turner, J. (2005). SI-HCCI-SI Mode Transition at Different Engine Operating Conditions. SAE paper 2005-01-0156, Lotus Engineering.

Milovanovic, N., Chen, R., and Turner, J. (2004). Influence of the Variable Valve Timing Strategy on the Control of a Homogeneous Charge Compression (HCCI)

Engine. SAE paper 2004-01-1899, Loughborough University and Lotus Engineering.

Morimoto, S. S., Kawabata, Y., Sakurai, T., and Amano, T. (2001). Operating Characteristics of a Natural Gas-Fired Homogeneous Charge Compression Ignition Engine (Performance Improvement Using EGR). SAE paper 2001-01-1034, Tokyo Gas Co., Ltd.

Najt, P. M. and Foster, D. E. (1983). Compression-Ignited Homogeneous Charge Combustion. SAE paper 830264, University of Wisconsin-Madison.

Ohyama, Y. (2000). Engine Control using Combustion Model. SAE paper 2000-01-0198, Hitachi Car Engineering CO., Ltd.

Olsson, J.-O., Erlandsson, O., and Johansson, B. (2000). Experiments and Simulation of a Six-Cylinder Homogeneous Charge Compression Ignition (HCCI) Engine. SAE paper 2000-01-2867, Lund Institute of Technology.

Olsson, J.-O., Tunestal, P., Johansson, B., Fiveland, S. B., Agama, R., Willi, M., and Assanis, D. (2002). Compression Ratio Influence on Maximum Load of a Natural Gas Fueled HCCI Engine. SAE paper 2002-01-0111, Lund Institute of Technology and Caterpillar Inc. and University of Michigan.

Onishi, S., Jo, S. H., Shoda, K., Jo, P. D., and Kato, S. (1979). Active Thermo-Atmosphere Combustion (ATAC) - A New Combustion Process for Internal Combustion Engines. SAE paper 790501, Nippon Clean Energy Research Institute Co., Ltd.

Ramos, J. I. (1989). *Internal Combustion Engine Modeling*. Hemisphere Publishing Corporation.

Ristinen, R. A. and Kraushaar, J. P. (2006). *Energy and the Environment, 2nd Edition*. John Wiley.

Roelle, M. J., Ravi, N., Jungkunz, A. F., and Gerdes, J. C. (2006). A Dynamic Model of Recompression HCCI Combustion Including Cylinder Wall Temperature. In *Proceedings of IMECE2006 2006 ASME International Mechanical Engineering Congress and Exposition*, number IMECE2006-15125 in 2006 ASME International Mechanical Engineering Congress and Exposition, Chicago, Illinois, USA.

Roelle, M. J., Shaver, G. M., and Gerdes, J. C. (2004). Tackling the Transition: A Multi-Mode Combustion Model of SI and HCCI for Mode Transition Control. In *Proceedings of IMECE04 2004 ASME International Mechanical Engineering Congress and Exposition*, number IMECE2004 - 62188. ASME.

Saanum, I., Bysveen, M., Tunestal, P., and Trajkovic, S. (2008). HCCI Combustion of Natural Gas and Hydrogen Enriched Natural Gas - Combustion Control by Early Direct Injection of Diesel Oil and RME. SAE paper 2008-01-1657, Norwegian University of Science and Technology and Lund University.

Shahbakhti, M., Ghazimirsaied, A., and Koch, C. R. (2010). Experimental Study of Exhaust Temperature Variation in a Homogeneous Charge Compression Ignition Engine. *Proceedings of the Institution of Mechanical Engineers, Park D: Journal of Automobile Engineering*, 224:1177–1197.

Shahbakhti, M. and Koch, C. R. (2010). Physics Based Control Oriented Model for HCCI Combustion Timing. *Journal of Dynamic Systems, Measurement, and Control*, 132(2):021010.

Shaver, G. M., Roelle, M. J., and Gerdes, J. C. (2006). Modeling Cycle-to-Cycle

Dynamics and Mode Transition in HCCI Engines with Variable Valve Actuation. *Control Engineering Practice*, 14:213–222.

Shibata, G., Oyama, K., Urushihara, T., and Nakano, T. (2004). The Effect of Fuel Properties on Low and High Temperature Heat Release and Resulting Performance of an HCCI Engine. SAE paper 2004-01-0553, Central Technical Research Laboratory, Nippon Oil Corporation and Nissan Research Center, Nissan Motor Co., Ltd.

Smith, G. P., Golden, D. M., Frenklach, M., Moriarty, N. W., Eiteneer, B., Goldenberg, M., Bowman, C. T., Hanson, R. K., Song, S., Gardiner, William C., J., Lissianski, V. V., and Qin, Z. (1999). GRI-Mech 3.0.

Soyhan, H. S., Yasar, H., Walmsley, H., Head, B., Kalghatgi, G. T., and Sorusbay, C. (2009). Evaluation of Heat Transfer Correleations for HCCI Engine Modeling. *Applied Thermal Engineering*, 29:541–549.

Stanglmaier, R. H. and Roberts, C. E. (1999). Homogeneous Charge Compression Ignition (HCCI): Benefits, Compromises, and Future Engine Applications. SAE paper 1999-01-3682, Southwest Research Institute.

Stanglmaier, R. H., Ryan III, T. W., and Souder, J. S. (2001). HCCI Operation of a Dual-Fuel Natural Gas Engine for Improved Fuel Efficiency and Ultra-Low NOx Emissions at Low to Moderate Engine Loads. SAE paper 2001-01-1897, Engine Research Department, Southwest Research Institute.

Stone, R. (1999). *Introduction to Internal Combustion Engines*. SAE International.

Stralin, P., Wahlin, F., and Angstrom, H.-E. (2003). Effects of Injection Timing on the Conditions at Top Dead Center for Direct Injected HCCI. SAE paper 2003-01-3219, Scania CV AB/KTH and KTH.

Strandh, P., Bengtsson, J., Johansson, R., Tunestal, P., and Johansson, B. (2004). Cycle-to-Cycle Control of a Dual-Fuel HCCI Engine. SAE paper 2004-01-0941, Lund Institute of Technology.

Su, H., Mosbach, S., Kraft, M., Bhave, A., Kook, S., and Bae, C. (2007). Two-Stage Fuel Direct Injection in a Diesel Fueled HCCI Engine. SAE paper 2007-01-1880, University of Cambridge and Reaction Engineering Solutions Ltd. and Korea Advanced Institute of Science and Technology (KAIST).

Tian, G., Wang, Z., Ge, Q., Wang, J., and Shuai, S. (2007). Mode Switch of SI-HCCI Combustion on a GDI Engine. SAE paper 2007-01-0195, State Key Laboratory of Automotive Safety and Energy, Tsinghua University.

Tominaga, R., Morimoto, S., Kawabata, Y., Matsuo, S., and Amano, T. (2004). Effects of Heterogeneous EGR on the Natural Gas Fueled HCCI Engine using Experiments, CFD and Detailed Kinetics. SAE paper 2004-01-0945, Tokyo Gas Co., Ltd.

Tzanetakis, T., Singh, P., Chen, J.-T., and Thomson, M. J. (2010). Knock Limit Prediction via Multi-Zone Modeling of a Primary Reference Fuel HCCI Engine. *International Journal of Vehicle Design*, 54:47 – 72.

Urata, Y., Awasaks, M., Takanashi, J., Kakinuma, T., Hakozaki, T., and Umemoto, A. (2004). A Study of Gasoline-Fueled HCCI Engine Equipped with an Electromagnetic Valve Train. SAE paper 2004-01-1898, Honda R&D CO., Ltd.

Urushihara, T., Hiraya, K., Kakuhou, A., and Itoh, T. (2003). Expansion of HCCI Operating Region by the Combination of Direct Fuel Injection, Negative Valve Overlap and Internal Fuel Reformation. SAE paper 2003-01-0749, Nissan Motor Co., Ltd.

Wagner, U., Anca, R., Velji, A., and Spicher, U. (2003). An Experimental Study of Homogeneous Charge Compression Ignition (HCCI) with Various Compression Ratios, Intake Air Temperatures and Fuels with Port and Direct Fuel Injection. SAE paper 2003-01-2293, Institute for Reciprocating Engines, University Karlsruhe.

Wang, Z., Wang, J., Shuai, S., He, X., Xu, F., Yang, D., and Ma, X. (2009). Research on Spark Induced Compression Ignition (SICI). SAE paper 2009-01-0132, State Key Laboratory of Automotive Safety and Energy, Tsinghua University.

Wang, Z., Wang, J.-X., Shuai, S., and Zhang, F. (2004). Numerical Simulation of HCCI Engine with Multi-Stage Gasoline Direct Injection using 3D-CFD with Detailed Chemistry. SAE paper 2004-01-0563, State Key Laboratory of Automotive Safety and Energy, Tsinghua University.

Wang, Z., Wang, J. X., Shual, S. J., and Ma, Q. J. (2005). Effects of Spark Ignition and Stratified Charge on Gasoline HCCI Combustion With Direct Injection. SAE paper 2005-01-0137, State Key Laboratory of Automotive Safety and Energy, Tsinghua University.

Waukesha CFR (2003). *Waukesha CFR Operation and Maintenance Manual*. Dresser Waukesha, Waukesha, Wisconsin 53188, second edition.

Wilhelmsson, C., Tunestal, P., and Johansson, B. (2007). Operation Strategy of a Dual Fuel HCCI Engine with VGT. SAE paper 2007-01-1855, Lund University.

Woschni, G. (1967). A Universally Applicable Equation for the Instantaneous Coefficient in the Internal Combustion Engine. SAE paper 670931, Maschinenfabrik, Augsburg - Nuernberg AG.

Wu, H., Collings, N., Regitz, S., Etheridge, J., and Kraft, M. (2010). Experimental

Investigation of a Control Method for SI-HCCI-SI Transition in a Multi-Cylinder Gasoline Engine. SAE paper 2010-01-1245, University of Cambridge.

Xu, H., Liu, M., Gharahbaghi, S., Richardson, S., Wyszynski, M. L., and Megaritis, T. (2005). Modeling of HCCI Engines: Comparison of Single-Zone, Multi-Zone and Test Data. SAE paper 2005-01-2123, Jaguar Cars Ltd. and The University of Birmingham.

Yang, J., Culp, T., and Kenney, T. (2002). Development of a Gasoline Engine System Using HCCI Technology - The Concept and the Test Results. SAE paper 2002-01-2832, Ford Motor Co.

Yao, M., Zheng, Z., and Liu, H. (2009). Progress and Recent Trends in Homogeneous Charge Compression Ignition (HCCI) Engines. *Progress in Energy and Combustion Science*, 35:398–437.

Yap, D., Megaritis, A., Wyszynski, M. L., and Xu, H. (2004). Residual Gas Trapping for Natural Gas HCCI. SAE paper 2004-01-1973, University of Birmingham and Jaguar Cars Ltd.

Appendix A

Derivations

The subject of this appendix is the detailed derivation of the differential temperature equation for the intake stroke thermodynamics described in section 3, equation 3.14. (Heywood, 1988) presents the rate form of the first law of thermodynamics for an open system describing the thermodynamics for the intake stroke of an engine cycle. The rate for of the first las of thermodynamics for an open system is

$$\dot{T}_{\text{cyl}} = \frac{B}{A}\left[\frac{\dot{m}_{\text{cyl}}}{m_{\text{cyl}}}\left(1 - \frac{h_{\text{cyl}}}{B}\right) - \frac{\dot{V}_{\text{cyl}}}{V_{\text{cyl}}} - \frac{C}{B}\dot{\phi} + \frac{1}{Bm_{\text{cyl}}}\left(\dot{m}_{\text{int}}h_{\text{int}} - \dot{m}_{\text{exh}}h_{\text{exh}} - \dot{Q}_{\text{wall}}\right)\right] \tag{A.1}$$

$$A = \frac{\partial h_{\text{cyl}}}{\partial T_{\text{cyl}}} + \frac{\frac{\partial \rho_{\text{cyl}}}{\partial T_{\text{cyl}}}}{\frac{\partial \rho_{\text{cyl}}}{\partial P_{\text{cyl}}}}\left(\frac{1}{\rho_{\text{cyl}}} - \frac{\partial h_{\text{cyl}}}{\partial P_{\text{cyl}}}\right)$$

$$B = \frac{\left(1 - \rho_{\text{cyl}}\left(\frac{\partial h_{\text{cyl}}}{\partial P_{\text{cyl}}}\right)\right)}{\frac{\partial \rho_{\text{cyl}}}{\partial P_{\text{cyl}}}}$$

$$C = \frac{\partial h_{\text{cyl}}}{\partial \phi} + \frac{\frac{\partial \rho_{\text{cyl}}}{\partial \phi}}{\frac{\partial \rho_{\text{cyl}}}{\partial P_{\text{cyl}}}}\left(\frac{1}{\rho_{\text{cyl}}} - \frac{\partial h_{\text{cyl}}}{\partial P_{\text{cyl}}}\right)$$

It is assumed that the intake to the cylinder is only through the intake valve (no flow into or out of the exhaust valve), thus $\dot{m}_{\text{exh}} = 0$ and that term drops out. The opposite is true for the exhaust stroke, where exhaust gases flow through the

exhaust valve only, eliminating the $\dot{m}_{\text{int}}$ term. Also, it can be assumed that during the intake stroke the cylinder pressure does not change significantly and therefore the cylinder enthalpy is not a function of pressure for this process. The above equations can be written as

$$\dot{T}_{\text{cyl}} = \frac{B}{A}\left[\frac{\dot{m}_{\text{cyl}}}{m_{\text{cyl}}}\left(1 - \frac{h_{\text{cyl}}}{B}\right) - \frac{\dot{V}_{\text{cyl}}}{V_{\text{cyl}}} - \frac{C}{B}\dot{\phi} + \frac{1}{Bm_{\text{cyl}}}\left(\dot{m}_{\text{int}}h_{\text{int}} - \dot{Q}_{\text{wall}}\right)\right] \tag{A.2a}$$

$$A = \frac{\partial h_{\text{cyl}}}{\partial T_{\text{cyl}}} + \frac{\frac{\partial \rho_{\text{cyl}}}{\partial T_{\text{cyl}}}}{\frac{\partial \rho_{\text{cyl}}}{\partial P_{\text{cyl}}}}\left(\frac{1}{\rho_{\text{cyl}}}\right) \tag{A.2b}$$

$$B = \frac{1}{\frac{\partial \rho_{\text{cyl}}}{\partial P_{\text{cyl}}}} \tag{A.2c}$$

$$C = \frac{\partial h_{\text{cyl}}}{\partial \phi} + \frac{\frac{\partial \rho_{\text{cyl}}}{\partial \phi}}{\frac{\partial \rho_{\text{cyl}}}{\partial P_{\text{cyl}}}}\left(\frac{1}{\rho_{\text{cyl}}}\right) \tag{A.2d}$$

The ideal gas law is used to find terms in equations A.2b, A.2c, and A.2d in the following:

$$\frac{\partial \rho_{\text{cyl}}}{\partial P_{\text{cyl}}} = \frac{1}{R_{\text{cyl}}T\text{cyl}} \tag{A.3}$$

$$\frac{\partial \rho_{\text{cyl}}}{\partial T_{\text{cyl}}} = \frac{-P_{\text{cyl}}}{R_{\text{cyl}}T_{\text{cyl}}^2} \tag{A.4}$$

The definition of the cylinder mixture enthalpy provides an additional term, which is

$$h = \sum_{k=1}^{K} y_k \left(h_{f,k}^o + \int_{T_o}^{T} c_{\text{p},k}\,\text{dT}\right) \tag{A.5}$$

By allowing $c_{\text{p,cyl}}$ to describe the average specific heat for the mixture at temperature T_{cyl} and taking the derivative of the enthalpy with respect to temperature,

the partial derivative of equation A.5 can be shown as

$$\frac{\partial h_{\text{cyl}}}{\partial T_{\text{cyl}}} = c_{\text{p,cyl}} \tag{A.6}$$

To further describe the temperature rate equation we define y_{f} as the mass fraction of fuel in the cylinder mixture and y_{a} as the mass fraction of air in the cylinder mixture. The relationships

$$y_{\text{f}} + y_{\text{a}} = \sum_{k=1}^{K} y_k \tag{A.7}$$

$$y_{\text{f}} + y_{\text{a}} = 1 \tag{A.8}$$

$$y_{\text{a}} = 1 - y_{\text{f}} \tag{A.9}$$

$$\dot{y}_{\text{f}} + \dot{y}_{\text{a}} = \sum_{k=1}^{K} \dot{y}_k \tag{A.10}$$

$$\dot{y}_{\text{a}} = -\dot{y}_{\text{f}} \tag{A.11}$$

hold true for these variables. Using the above mass fractions, the equations for equivalence ratio and its rate form can be written as

$$\phi = \frac{\frac{y_{\text{f}}}{y_{\text{a}}}}{\left(\frac{y_{\text{f}}}{y_{\text{a}}}\right)_{\text{s}}} \tag{A.12}$$

$$\phi = \frac{\frac{y_{\text{f}}}{1-y_{\text{f}}}}{\left(\frac{y_{\text{f}}}{y_{\text{a}}}\right)_{\text{s}}} \tag{A.13}$$

Letting the constant $\text{F/A}_{\text{s}} = \left(\frac{y_{\text{f}}}{y_{\text{a}}}\right)_{\text{s}}$ the differential form of Equation A.12 can

be written as

$$\dot{\phi} = \frac{\frac{\dot{y}_\mathrm{f}}{(1-y_\mathrm{f})^2}}{\mathrm{F/A_s}} \tag{A.14}$$

Now the term in equation A.2d is manipulated as

$$\frac{\partial h_\mathrm{cyl}}{\partial \phi}\dot{\phi} = \left(\frac{\partial h_\mathrm{cyl}}{\partial y_\mathrm{f}}\right)\left(\frac{\partial y_\mathrm{f}}{\partial \phi}\right)\dot{\phi} \tag{A.15a}$$

where,

$$\frac{\partial h_\mathrm{cyl}}{\partial y_\mathrm{f}} = \frac{\partial}{\partial y_\mathrm{f}}\left(\sum_{k=1}^{K} y_k h_k\right) \tag{A.15b}$$

$$\frac{\partial h_\mathrm{cyl}}{\partial y_\mathrm{f}} = \frac{\partial}{\partial y_\mathrm{f}}\left(y_\mathrm{f}\sum_{j=1}^{J} y_j h_j + y_\mathrm{a}\sum_{m=1}^{M} y_m h_m\right) \tag{A.15c}$$

where y_j is the mass fraction of species j in the fuel and y_m is the mass fraction of species m in air. This equation can be further simplified as

$$\frac{\partial h_\mathrm{cyl}}{\partial y_\mathrm{f}} = \frac{\partial}{\partial y_\mathrm{f}}\left(y_\mathrm{f}h_\mathrm{f} + (1-y_\mathrm{f})h_\mathrm{a}\right) \tag{A.15d}$$

$$\frac{\partial h_\mathrm{cyl}}{\partial y_\mathrm{f}} = h_\mathrm{f} - h_\mathrm{a} \tag{A.15e}$$

where

$$\frac{\partial y_\mathrm{f}}{\partial \phi} = \frac{\partial}{\partial \phi}\frac{\mathrm{F/A_s}\phi}{(1+\mathrm{F/A_s}\phi)} \tag{A.15f}$$

$$\frac{\partial y_\mathrm{f}}{\partial \phi} = \frac{\mathrm{F/A_s}}{(1+\mathrm{F/A_s}\phi)^2} \tag{A.15g}$$

$$\frac{\partial y_\mathrm{f}}{\partial \phi} = \mathrm{F/A_s}\left(1-y_\mathrm{f}\right)^2 \tag{A.15h}$$

Equations A.15e, A.15h, and A.14 are combined in A.15a to get,

$$\frac{\partial h_{\mathrm{cyl}}}{\partial \phi}\dot{\phi} = (h_f - h_a)\left(\mathrm{F/A_s}\,(1-y_{\mathrm{f}})^2\right)\frac{\frac{\dot{y}_{\mathrm{f}}}{(1-y_{\mathrm{f}})^2}}{\mathrm{F/A_s}} \tag{A.15i}$$

$$\frac{\partial h_{\mathrm{cyl}}}{\partial \phi}\dot{\phi} = \dot{y}_{\mathrm{f}}\,(h_{\mathrm{f}} - h_{\mathrm{a}}) \tag{A.15j}$$

$$\frac{\partial h_{\mathrm{cyl}}}{\partial \phi}\dot{\phi} = (\dot{y}_{\mathrm{f}} h_{\mathrm{f}} + (-\dot{y}_{\mathrm{f}})h_{\mathrm{a}}) \tag{A.15k}$$

$$\frac{\partial h_{\mathrm{cyl}}}{\partial \phi}\dot{\phi} = \sum_{k=1}^{K} \dot{y}_k h_k \tag{A.15l}$$

The final term of equation A.2d can now be derived by subbing in equation A.3. This final term becomes,

$$\frac{\frac{\partial \rho_{\mathrm{cyl}}}{\partial \phi}}{\frac{\partial \rho_{\mathrm{cyl}}}{\partial P_{\mathrm{cyl}}}} = R_{\mathrm{cyl}} T_{\mathrm{cyl}} \left(\frac{\partial \rho_{\mathrm{cyl}}}{\partial \phi}\right)\left(\frac{1}{\rho_{\mathrm{cyl}}}\right) \tag{A.16a}$$

where,

$$\frac{\partial \rho_{\mathrm{cyl}}}{\partial \phi} = \left(\frac{\partial \rho_{\mathrm{cyl}}}{\partial y_{\mathrm{f}}}\right)\left(\frac{\partial y_{\mathrm{f}}}{\partial \phi}\right) \tag{A.16b}$$

and

$$\frac{\partial \rho_{\mathrm{cyl}}}{\partial y_{\mathrm{f}}} = \frac{\partial}{\partial y_{\mathrm{f}}} \sum_{k=1}^{K} y_k \rho_k \tag{A.16c}$$

$$\frac{\partial \rho_{\mathrm{cyl}}}{\partial y_{\mathrm{f}}} = \frac{\partial}{\partial y_{\mathrm{f}}} \left(y_{\mathrm{f}} \sum_{j=1}^{J} y_j \rho_j + y_a \sum_{m=1}^{M} y_m \rho_m \right) \tag{A.16d}$$

$$\frac{\partial \rho_{\mathrm{cyl}}}{\partial y_{\mathrm{f}}} = \frac{\partial}{\partial y_{\mathrm{f}}} \left(y_{\mathrm{f}} \rho_{\mathrm{f}} + (1 - y_{\mathrm{f}}) \rho_{\mathrm{a}} \right) \tag{A.16e}$$

$$\frac{\partial \rho_{\mathrm{cyl}}}{\partial y_{\mathrm{f}}} = \rho_{\mathrm{f}} - \rho_{\mathrm{a}} \tag{A.16f}$$

Equations A.15h, A.16b, and A.16f are combined into equation A.16a to yield,

$$\frac{\frac{\partial \rho_{\mathrm{cyl}}}{\partial \phi}}{\frac{\partial \rho_{\mathrm{cyl}}}{\partial P_{\mathrm{cyl}}}} = R_{\mathrm{cyl}} T_{\mathrm{cyl}} \left(\frac{\partial \rho_{\mathrm{cyl}}}{\partial y_{\mathrm{f}}}\right) \left(\frac{\partial y_{\mathrm{f}}}{\partial \phi}\right) \tag{A.16g}$$

$$\frac{\frac{\partial \rho_{\mathrm{cyl}}}{\partial \phi}}{\frac{\partial \rho_{\mathrm{cyl}}}{\partial P_{\mathrm{cyl}}}} = R_{\mathrm{cyl}} T_{\mathrm{cyl}} \left(\rho_{\mathrm{f}} - \rho_{\mathrm{a}}\right) \left(\mathrm{F}/\mathrm{A_s}\left(1 - y_{\mathrm{f}}\right)^2\right) \tag{A.16h}$$

Multiplying the term by $\dot{\phi}$ yields,

$$\frac{\frac{\partial \rho_{\mathrm{cyl}}}{\partial \phi}}{\frac{\partial \rho_{\mathrm{cyl}}}{\partial P_{\mathrm{cyl}}}} \left(\frac{1}{\rho_{\mathrm{cyl}}}\right) \dot{\phi} = R_{\mathrm{cyl}} T_{\mathrm{cyl}} \left(\rho_{\mathrm{f}} - \rho_{\mathrm{a}}\right) \left(\mathrm{F}/\mathrm{A_s}\left(1 - y_{\mathrm{f}}\right)^2\right) \left(\frac{1}{\rho_{\mathrm{cyl}}}\right) \dot{\phi} \tag{A.16i}$$

$$\frac{\frac{\partial \rho_{\mathrm{cyl}}}{\partial \phi}}{\frac{\partial \rho_{\mathrm{cyl}}}{\partial P_{\mathrm{cyl}}}} \left(\frac{1}{\rho_{\mathrm{cyl}}}\right) \dot{\phi} = R_{\mathrm{cyl}} T_{\mathrm{cyl}} \left(\rho_{\mathrm{f}} - \rho_{\mathrm{a}}\right) \left(\mathrm{F}/\mathrm{A_s}\left(1 - y_{\mathrm{f}}\right)^2\right) \frac{\frac{\dot{y}_{\mathrm{f}}}{(1-y_{\mathrm{f}})^2}}{\mathrm{F}/\mathrm{A_s}} \left(\frac{1}{\rho_{\mathrm{cyl}}}\right) \tag{A.16j}$$

$$\frac{\frac{\partial \rho_{\mathrm{cyl}}}{\partial \phi}}{\frac{\partial \rho_{\mathrm{cyl}}}{\partial P_{\mathrm{cyl}}}} \left(\frac{1}{\rho_{\mathrm{cyl}}}\right) \dot{\phi} = R_{\mathrm{cyl}} T_{\mathrm{cyl}} \left(\dot{y}_{\mathrm{f}} \rho_{\mathrm{f}} - \dot{y}_{\mathrm{f}} \rho_{\mathrm{a}}\right) \left(\frac{1}{\rho_{\mathrm{cyl}}}\right) \tag{A.16k}$$

$$\frac{\frac{\partial \rho_{\mathrm{cyl}}}{\partial \phi}}{\frac{\partial \rho_{\mathrm{cyl}}}{\partial P_{\mathrm{cyl}}}} \left(\frac{1}{\rho_{\mathrm{cyl}}}\right) \dot{\phi} = R_{\mathrm{cyl}} T_{\mathrm{cyl}} \left(\sum_{k=1}^{K} \dot{y}_k y_k\right) \tag{A.16l}$$

Now, equations A.2b, A.2c, A.2d, and their terms that are derived above, are combined into equation A.2a to create,

$$\begin{aligned} \dot{T}_{\mathrm{cyl}} \left(c_{\mathrm{p,cyl}} - \frac{\mathrm{P_{cyl}}}{\rho_{\mathrm{cyl}} T_{\mathrm{cyl}}}\right) \;=\; & \frac{R_{\mathrm{cyl}} T_{\mathrm{cyl}} \dot{m}_{\mathrm{cyl}}}{m_{\mathrm{cyl}}} \left(1 - \frac{h_{\mathrm{cyl}}}{R_{\mathrm{cyl}} T_{\mathrm{cyl}}}\right) - \frac{R_{\mathrm{cyl}} T_{\mathrm{cyl}} \dot{V}_{\mathrm{cyl}}}{V_{\mathrm{cyl}}} \\ & - \left(\sum_{k=1}^{K} \dot{y}_k h_k + R_{\mathrm{cyl}} T_{\mathrm{cyl}} \left(\sum_{k=1}^{K} \dot{y}_k y_k\right)\right) \\ & + \frac{1}{m_{\mathrm{cyl}}} \left(\dot{m}_{\mathrm{cyl}} h_{\mathrm{int}} - \dot{Q}_{\mathrm{wall}}\right) \end{aligned} \tag{A.17}$$

$$\begin{aligned}\dot{T}_{\mathrm{cyl}} &= \frac{1}{c_{\mathrm{p,cyl}} - R_{\mathrm{cyl}}}[\frac{-\dot{m}_{\mathrm{cyl}}}{m_{\mathrm{cyl}}}\left(h_{\mathrm{cyl}} - R_{\mathrm{cyl}}T_{\mathrm{cyl}}\right) \\ &\quad - \left(\sum_{k=1}^{K}\dot{y}_k h_k + R_{\mathrm{cyl}}T_{\mathrm{cyl}}\left(\sum_{k=1}^{K}\dot{y}_k y_k\right)\right) + \\ &\quad \frac{1}{m_{\mathrm{cyl}}}\left(-P_{cyl}\dot{V}_{\mathrm{cyl}} + \dot{m}_{\mathrm{cyl}}h_{\mathrm{int}} - \dot{Q}_{\mathrm{wall}}\right)]\end{aligned} \tag{A.18}$$

which appears in the model summary as equation 3.14 for the intake process. A very similar equation is used for the exhaust process, but additional terms can be eliminated as the composition of the cylinder gases during the exhaust stroke is assumed to be fixed. In reality a small amount of dissociation would occur during the exhaust stroke, but this change is likely to be small in comparison to the change in composition seen during the intake as a result of fresh intake air mixing with the exhaust gas residual.

Appendix B

Operating Conditions

The main operating conditions used for the development, validation, and simulation of the PMSM are selected based on experimental observations and literature values. Data used for the validation of this model comes from tests conducted in conjunction with the work of Boddez (Boddez, 2011). Operating conditions are selected for tests at steady state SI and HCCI operation for both large and small intake manifold configurations. The following tables outline the experimental and physical parameters used for the modeling of the combustion cycles.

B.1 Engine and Fuel Parameters

Table B.1 outlines engine operating parameters that are kept constant throughout the simulations. Table B.2 breaks down the natural gas fuel composition of the fuel used in the experimental CFR engine as indicated in (Kongsereeparp, 2008) and table B.3 shows the composition of air used in the models.

B.2 Operating Conditions for Validation

This section contains variable input values and operating conditions from steady state SI and HCCI cycles that are used in the simulation of engine cycles for the model validation section of this thesis.

Table B.1: Constant Engine Geometry and Parameters

Parameter	**Value**
T_{cool}	373.15 K
T_{fuel}	296.85 K
External EGR	0%
Compression Ratio	19
Bore	8.26 cm
Stroke	11.43 cm
Connecting Rod	25.40 cm

Table B.2: Model Natural Gas Fuel Composition

Species	**Mole Fraction**
CH_4	0.965
C_2H_6	0.019
CO_2	0.008
N_2	0.008

Table B.3: Model Air Composition

Species	**Mole Fraction**
O_2	0.210
N_2	0.790

Table B.4: Steady State SI Operating Conditions with Large Intake Manifold Configuration for Validation - Step Increase in Pressure Mode Switch Initiation

Parameter	**Value**	**Initial Condition**
P_{int}	0.53 bar	
T_{int}	383.15 K	
P_{exh}	0.913 bar	
P_{ivo}	0.913 bar	x
T_{exh}	698.75 K	x
T_{wall}	395 K	x
T_{residual}	698.75 K	x
Fuel Pulse Width	11.4 ms	
Engine Speed	700 rpm	

Table B.5: Steady State HCCI Operating Conditions with Large Intake Manifold Configuration for Validation - Step Increase in Pressure Mode Switch Initiation

Parameter	**Value**	**Initial Condition**
P_{int}	1.20 bar	
T_{int}	383.15 K	
P_{exh}	0.913 bar	
P_{ivo}	0.913 bar	x
T_{exh}	698.75 K	x
T_{wall}	395 K	x
T_{residual}	698.75 K	x
Fuel Pulse Width	11.4 ms	
Engine Speed	700 rpm	

Table B.4 and B.5 contain the steady state operating conditions for SI and HCCI modes respectively. These operating conditions are taken from the data set for the mode switch using a step increase in intake pressure for its actuation method. The large manifold configuration is used for these data points. These operating conditions are based on data from March 17, 2010 - Run 19.

Table B.6 and B.7 contain the steady state operating conditions for SI and HCCI modes respectively. These operating conditions are taken from the data set for the mode switch using a linear increase in intake pressure for its actuation method. The small manifold configuration is used for these data points. These

Table B.6: Steady State SI Operating Conditions with Small Intake Manifold Configuration for Validation - First Order Increase in Pressure Mode Switch Initiation

Parameter	**Value**	**Initial Condition**
P_{int}	0.510 bar	
T_{int}	389.15 K	
P_{exh}	0.909 bar	
P_{ivo}	0.909 bar	x
T_{exh}	736 K	x
T_{wall}	395 K	x
T_{residual}	736 K	x
Fuel Pulse Width	10.4 ms	
Engine Speed	700 rpm	

Table B.7: Steady State HCCI Operating Conditions with Small Intake Manifold Configuration - First Order Increase in Pressure Mode Switch Initiation

Parameter	**Value**	**Initial Condition**
P_{int}	1.15 bar	
T_{int}	389.15 K	
P_{exh}	0.909 bar	
P_{ivo}	0.909 bar	x
T_{exh}	573 K	x
T_{wall}	395 K	x
T_{residual}	573 K	x
Fuel Pulse Width	11.9 ms	
Engine Speed	700 rpm	

operating conditions are based on data from August 9, 2010 - Run 33.

Table B.8 and B.9 contain the steady state operating conditions for SI and HCCI modes respectively. These operating conditions are taken from the data set for the mode switch from HCCI to SI using a step decrease in intake pressure for its actuation method. The small manifold configuration is used for these data points. These operating conditions are based on data from September 28, 2010 - Run 22.

Table B.10 and B.11 contain the steady state operating conditions for SI and HCCI modes respectively. These operating conditions are taken from the data set for the mode switch using the optimized actuation method. The small manifold

Table B.8: Steady State SI Operating Conditions with Small Intake Manifold Configuration for Validation - HCCI - SI Mode Switch

Parameter	**Value**	**Initial Condition**
P_{int}	0.70 bar	
T_{int}	413 K	
P_{exh}	0.909 bar	
P_{ivo}	0.909 bar	x
T_{exh}	691 K	x
T_{wall}	395 K	x
T_{residual}	691 K	x
Fuel Pulse Width	10.6 ms	
Engine Speed	700 rpm	

Table B.9: Steady State HCCI Operating Conditions with Small Intake Manifold Configuration for Validation - HCCI - SI Mode Switch

Parameter	**Value**	**Initial Condition**
P_{int}	1.15 bar	
T_{int}	413 K	
P_{exh}	0.914 bar	
P_{ivo}	0.914 bar	x
T_{exh}	494 K	x
T_{wall}	395 K	x
T_{residual}	494 K	x
Fuel Pulse Width	10.7 ms	
Engine Speed	700 rpm	

Table B.10: Steady State SI Operating Conditions with Small Intake Manifold Configuration for Validation - Optimized Mode Switch Initiation with Fuel Injection Timing

Parameter	**Value**	**Initial Condition**
P_{int}	0.58 bar	
T_{int}	403.15 K	
P_{exh}	0.915 bar	
P_{ivo}	0.915 bar	x
T_{exh}	745 K	x
T_{wall}	395 K	x
T_{residual}	745 K	x
Fuel Pulse Width	10.6 ms	
Engine Speed	700 rpm	

Table B.11: Steady State HCCI Operating Conditions with Small Intake Manifold Configuration for Validation - Optimized Mode Switch Initiation with Fuel Injection Timing

Parameter	**Value**	**Initial Condition**
P_{int}	1.13 bar	
T_{int}	403.15 K	
P_{exh}	0.915 bar	
P_{ivo}	0.915 bar	x
T_{exh}	563 K	x
T_{wall}	395 K	x
T_{residual}	563 K	x
Fuel Pulse Width	10.5 ms	
Engine Speed	700 rpm	

configuration is used for these data points. These operating conditions are based on data from September 24, 2010 - Run 63.

B.3 Operating Conditions for Results

The following tables, D.1, B.13, and B.14 outline the conditions used for the sensitivity analysis in the results section of this thesis. Tables D.1 and B.14 contain steady state operating conditions for SI and HCCI operating modes respectively. Table B.13 contains approximate operating conditions for an HCCI cycle occurring

Table B.12: Steady State SI Operating Conditions with Large Intake Manifold Configuration

Parameter	**Value**	**Initial Condition**
P_{int}	0.53 bar	
T_{int}	383.15 K	
P_{exh}	0.913 bar	
P_{ivo}	0.913 bar	x
T_{exh}	698.75 K	x
T_{wall}	395 K	x
T_{residual}	698.75 K	x
Fuel Pulse Width	11.4 ms	
Spark Timing	-1 CAD bTDC	
Combustion Duration	60 CAD	
Engine Speed	700 rpm	

Table B.13: Steady State HCCI Operating Conditions with Large Intake Manifold Configuration

Parameter	**Value**	**Initial Condition**
P_{int}	1.20 bar	
T_{int}	383.15 K	
P_{exh}	0.913 bar	
P_{ivo}	0.913 bar	x
T_{exh}	640 K	x
T_{wall}	383 K	x
T_{residual}	640 K	x
Fuel Pulse Width	11.4 ms	
Engine Speed	700 rpm	

during a mode switch used in the sensitivity analysis. The steady state operating conditions outline in tables D.1 and B.14 are also used as the initial and target conditions during the optimization process in the results section.

Table B.14: Near Mode Switch HCCI Operating Conditions with Large Intake Manifold Configuration

Parameter	**Value**	**Initial Condition**
P_{int}	0.90 bar	
T_{int}	383.15 K	
P_{exh}	0.913 bar	
P_{ivo}	0.913 bar	x
T_{exh}	750 K	x
T_{wall}	394 K	x
T_{residual}	750 K	x
Fuel Pulse Width	8.0 ms	
Engine Speed	700 rpm	

Appendix C

Model Parameters

This appendix outlines the model parameters that are used as part of the simulation presented in this thesis.

Table C.1: Model Parameters for HCCI and SI Intake and Exhaust Models

Parameter	**Value**	**Source**	**Comments**
η_v	0.95	Tuned	Large Manifold SI Mode
η_v	0.75	Tuned	Small Manifold SI Mode
η_v	0.80	Tuned	HCCI Mode
f	0.5		Intake Valve Area Coefficient
f	1		Exhaust Valve Area Coefficient
D_v	3.44 cm	Measured	Valve Diameter

Table C.2: Discharge Coefficients for Intake and Exhaust Valve Flows as Determined on a Flow Bench

Valve Lift (L_v(cm))	**Discharge Coefficient (C_D)**	**Valve Lift (L_v(cm))**	**Discharge Coefficient (C_D)**
0	0.541429	0.111111	0.567422
0.00362319	0.542857	0.120756	0.580459
0.0137681	0.551429	0.13221	0.597051
0.026087	0.562857	0.141855	0.616014
0.0369565	0.574286	0.1515	0.630236
0.0471014	0.584286	0.159939	0.644458
0.049021	0.586385	0.168981	0.65868
0.0592689	0.599422	0.176215	0.637347
0.0646943	0.607718	0.183449	0.616014
0.0701196	0.617199	0.190683	0.598236
0.0755449	0.626681	0.199725	0.582829
0.0797647	0.634977	0.206356	0.567422
0.0845872	0.644458	0.21359	0.552015
0.0906154	0.65631	0.225043	0.537793
0.0936294	0.637347	0.235291	0.5212
0.0978492	0.605347	0.246745	0.504608
0.10026	0.581644	0.255184	0.493941
0.102672	0.559126	0.262418	0.48446
Continued	→	0.267843	0.477349

Table C.3: Model Parameters for HCCI and SI Heat Transfer Models

Parameter	**Value**	**Source**	**Comments**
α	129.944	(Woschni, 1967)	SI Heat Transfer
α	64.972	Tuned - 0.5 × (Woschni, 1967)	HCCI Heat Transfer - Compression
α	259.888	Tuned - 2 × (Woschni, 1967)	HCCI Heat Transfer - Expansion
c_1	2.28	(Ramos, 1989)	Woschni Coefficient
c_2	0	(Ramos, 1989)	Woschni Coefficient - Compression
c_2	0.00324	(Ramos, 1989)	Woschni Coefficient - Combustion & Expansion

Table C.4: Model Parameters for HCCI Cylinder Temperature Model

Parameter	**Value**	**Source**	**Comments**
τ	34	(Kongsereeparp, 2008)	Inverse Time Scale of Relative Temperature Rise
Γ	0	(Kongsereeparp, 2008)	Cylinder Temperature Coefficient, $T_{cyl} > T_{int}$
Γ	1	(Kongsereeparp, 2008)	Cylinder Temperature Coefficient, $T_{cyl} \leq T_{int}$

Table C.5: Model Parameters for SI Wiebe Function

Parameter	**Value**	**Source**	**Comments**
a	5	(Ramos, 1989; Stone, 1999)	Wiebe Function Coefficient
m	2	(Ramos, 1989; Stone, 1999)	Wiebe Function Coefficient
θ_{spark}	1 CAD aTDC	Tuned	Wiebe Function Parameter
t_{spark}	0.0860 s	Tuned	
$\Delta\theta_{\text{b}}$	60 CAD	Tuned	Wiebe Function Parameter

Table C.6: Model Parameters for Wall Temperature Model

Parameter	**Value**	**Source**	**Comments**
k_{w}	60.5 W/mK	(Incropera and DeWitt, 2002)	Cylinder Wall Thermal Conductivity
L_{w}	0.792 cm	(Waukesha CFR, 2003)	Cylinder Wall Thickness
$c_{\text{p,w}}$	434 J/kgK	(Incropera and DeWitt, 2002)	Cylinder Wall Heat Capacity
ρ_{w}	7854 kg/m^3	(Incropera and DeWitt, 2002)	Cylinder Wall Density - Plain Carbon Steel

Appendix D

Simulation Functions

Several M-files have been developed as part of this study. The following list outlines function names, parent functions/files, and the purpose of each file. In the case that a function has multiple parent functions only one of those parent functions is listed.

Table D.1: Simulation MATLAB® Functions

File Name	Parent Function	Description
File Name	**Parent Function**	**Description**
AveThermoCalc_v4sz.m	ODE_SIEngine_v6sz.m	Compute bulk thermodynamic properties from mixture composition
Calculation_SZM_Switch.m	dyn_engine_sim.m	Simulate the single zone HCCI cycle
cgsconversion.m	Engine_Model_v7sz.m	Convert pressures from MPa to dyne/cm^2
CombSZM_calculation_switch.m	Calculation_SZM_Switch.m	Simulate compression, combustion, and expansion for HCCI cycle
CylWallTemp.m	dynamic_conditions.m	Calculate the next cycle's cylinder wall temperature
DataExtraction.m	dyn_engine_sim.m	Place simulation results in vectors arranged by cycle
DataPlot.m	dyn_engine_sim.m	Produce simulation validation plots

Continued on next page

Table D.1 – continued from previous page

File Name	Parent Function	Description
dyn_engine_sim.m	None	Main file for running mode switch simulations
dynamic_conditions.m	dyn_engine_sim.m	Determine initial conditions of next cycle based on results of current cycle
energycontent_order.m	Calculation_SZM_Switch.m	Determines order of fuel species based on energy content
equilibrium_constant.m	kin_calculation.m	Calculates the equilibrium rate constant
Engine_Model_v9sz.m	dyn_engine_sim.m	Simulate the single zone SI cycle
Exhaust_calculation_switch.m	Calculation_SZM_Switch.m	Simulate the exhaust stroke for HCCI cycle
ExpDataCalc.m	dyn_engine_sim.m	Calculate engine performance values based on experimental data

Continued on next page

Table D.1 – continued from previous page

File Name	Parent Function	Description
ExpDataExtract.m	dyn_engine_sim.m	Extract experimental data from data files
HV_Switch.m	Engine_Model_v9sz.m	Calculate the lower heating value based on fuel composition
HeatTrans_SI_v2.m	ODE_SIEngine_v6sz.m	Calculate heat transfer to cylinder walls for SI cycle
HeatTrans_SZM_switch.m	ODE_SZM_switch.m	Calculate heat transfer to cylinder walls for HCCI cycle
Intake_calculation_switch.m	Calculation_SZM_Switch.m	Simulate the intake stroke for HCCI cycle
kin_calculation.m	ODE_SZM_Switch.m	Determines the chemical reaction rate constants
MassflowCal.m	Intake_calculation_switch.m	Determines the instantaneous mass flow rate through intake valve

Continued on next page

Table D.1 – continued from previous page

File Name	Parent Function	Description
MassflowCalExh.m	Exhaust_calculation_switch.m	Determines the instantaneous mass flow rate through exhaust valve
mspc.m	dyn_engine_sim.m	Calculates the MSPC value of input data
ODE_Exhaust_SI.m	Engine_Model_v9sz.m	SI exhaust model ODE function
ODE_Intake_SI.m	Engine_Model_v9sz.m	SI intake model ODE function
ODE_SIEngine_v6sz.m	Engine_Model_v9sz.m	SI compression, combustion, and expansion model ODE function
ODE_SZM_frozen_switch.m	CombSZM_calculation_Switch.m	HCCI compression model with frozen chemistry ODE function
ODE_SZM_switch.m	CombSZM_calculation_Switch.m	HCCI compression, combustion, and expansion model with active chemistry ODE function
ODE_exhaust_switch.m	Exhaust_calculation_switch.m	HCCI exhaust model ODE function

Continued on next page

Table D.1 – continued from previous page

File Name	Parent Function	Description
ODE_intake_intake.m	Intake_calculation_switch.m	HCCI intake model ODE function
q_generator.m	ODE_SZM_switch.m	Determines the chemical reaction rates
reading.m	Reading_SZM_Chem.m	Reads the chemical mechanism file and returns reaction constants
ReadingAlgor.m	ReadingInputFileSparkIgnition.m	Algorithm for reading input files
ReadingInputFileSparkIgnition.m	dyn_engine_sim.m	Extract information from input file
ReadingSetupFileSparkIgnition.m	dyn_engine_sim.m	Engine setup information from input file
Reading_SZM_Chem.m	dyn_engine_sim.m	Extract information from the chemical mechanism
Reading_SZM_Compostion.m	dyn_engine_sim.m	Determine mixture composition related information
Reading_SZM_IntialConditions.m	dyn_engine_sim.m	Extract the initial conditions

Continued on next page

Table D.1 – continued from previous page

File Name	Parent Function	Description
Results_Plots.m	None	Plot the results from mode switch simulations
SZMRecordData_Switch.m	CombSZM_calculation_switch.m	Extracts data from simulation results passed to solvers
SensitivityPlots.m	None	Plots output parameters against input parameters for sensitivity analysis
Sensitivity_Calculations.m	None	Calculates and plots sensitivity values
sensitivity_conditions.m	dyn_engine_sim.m	Determines next cycle inputs for sensitivity analysis
SimulationResults.m	dyn_engine_sim.m	Calculates engine performance parameters from simulation
Simulation_Plots.m	None	Plots results of mode switch simulations

Continued on next page

Table D.1 – continued from previous page

File Name	Parent Function	Description
thermo_data.m	Engine_Model_v9sz.m	Returns thermodynamic data for species based on NASA polynomials
thermo_reading.m	Reading_SZM_chem.m	Reads the thermodynamic file for the chemical mechanism
validation.m	dyn_engine_sim.m	Stores data used for model validation
volume_fn.m	ODE_SZM_switch.m	Calculates instantaneous volume and rate of change in volume